Reconfigurable Shapes and Assemblies of Anisotropic Particles

by

Jaewon Yoon

A dissertation submitted in partial fulfillment
of the requirements for the degree of
Doctor of Philosophy
(Macromolecular Science and Engineering)
in The University of Michigan
2013

Doctoral Committee:

Professor Joerg Lahann, Chair
Professor Ronald G. Larson
Professor Michael J. Solomon
Professor Shuichi Takayama

ACKNOWLEDGEMENTS

I would like to express my deepest gratitude to my advisor, Professor Joerg Lahann, for providing me the opportunity to learn and work in a wonderful research environment during my PhD. His encouragement, guidance and support enabled me to develop an understanding of the research and gave me strength to pursue my studies during these years. I am honored to have been his student and deeply grateful for all I have learned from him. I would also like to convey my warm and sincere thanks to my committee members, Professor Ronald G. Larson, Professor Michael J. Solomon, and Professor Shuichi Takayama, for their valuable support and advice during the course of my work.

A significant amount of the work documented in this dissertation was conducted jointly with our group members, and I wish to thank all my colleagues for their help and discussion in improving my dissertation. I am forever grateful for Dr. Kyung-Jin Lee for his great ideas and motivating approach to research. I would like to thank Tom Eyster for conducting the cell experiments and the valuable discussions. I also wish to thank Dr. Sangyeul Hwang for collaborating magnetic particle-based experiments, and Dr. Sampa Saha, Dr. Hakan Durmaz for synthesizing the functionalized polymers. I would like to express my gratitude to the Tuteja group for the great research. Dr. Arun Kota has been a major help for the surface energy analysis.

Over the years, I have had the opportunity to work with different postdoctoral associates and PhD students in the Lahann group, and I would like to thank the past

group members: Dr. Sangyeul Hwang, Dr. Dong Woo Lim, Dr. Kyung-Jin Lee, Dr. Tae-Hong Park, Dr. Sampa Saha, Dr. Aftin Ross, Dr. Srijanani Bhaskar, Dr. Suparna Mandal, Dr. Yaseen Elkasabi, and Dr. Himabindu Nandivada. I gratefully acknowledge all of them for the help they have given me. They had always been willing to listen or advise as necessary.

I also wish to express my love and gratitude to all my beloved current group members, Sahar Rahmani, Asish Misra, Jake Jordahl, Tom Eyster, Xiaopei Deng, Kenneth Cheng, Ramya Kumar, Stacy Ramcharan, Nathan Jones, Dr. Hakan Durmaz, and Dr. Kathleen McEnnis for giving me friendly environment during the course of my studies. I would like to especially thank Sahar Rahmani and Asish Misra, who were not just co-workers but my friends and family for all the years I was far from home. Their encouragement and care with exceptional kindness and understanding will not be forgotten. I would like to express my gratitude to the Lahann group members in Karlsruhe Institute of Technology, Germany for the knowledge and expertise I have benefited from them. I would also like to thank core facilities, Microscopy and Image Analysis Lab (MIL) and Electron Microbeam Analysis Laboratory (EMAL), at the University of Michigan for teaching me the microscopy techniques.

Finally, I am thankful to all my friends at University of Michigan. I would also like to thank my parents, my sister, and my brother for their continuous support and encouragement they have provided me over the years, without which this journey would not have been possible for me.

TABLE OF CONTENTS

LIST OF FIGURES

LIST OF TABLES

ABSTRACT

This dissertation describes dynamically reconfigurable particles that can undergo permanent or reversible changes in sizes and shapes depending on the surrounding environment. Electrohydrodynamic co-jetting provides the key for the successful design of highly integrated structures with pre-defined shapes and stimuli-responsive properties. Unlike shape memory polymers where delicate synthesis is required to tailor molecular segments, the new type of particle systems exhibit complex adaptive properties simply by introducing conventional polymers. The separate control of each compartment with different polymers that have dissimilar functionalities and properties, the EHD co-jetting allows complex particles with anisotropic shapes, surfaces, and compartments.

Throughout the chapters, each research explores the design, fabrication and application of various particle systems. These include 1) a shape-shifting process that can simply control the shape of either the entire particles or individual compartments, 2) amphiphilic Janus particles with surfactant-like properties, 3) bio-integrated actuators that can selectively guide cardiomyocytes and generate autonomous bending by the beating of the cells, and 4) bicolor-coded magnetic particles for reversible color-switching devices. Moreover, fundamental studies of the chemical, physical, and mechanical properties of each system are discussed, and the evaluation of the potential applications is reported. Consequently, the present work suggests a potential uses of diverse anisotropic particles in biomimetic systems, optical displays, catalysts, drug delivery, and sensing applications.

CHAPTER 1

Introduction

The material in this chapter has been adapted with minor modifications from the following published articles:

(1) J. Yoon*, K. J. Lee*, J. Lahann, "Multifunctional polymer particles with distinct compartments", *Journal of Materials Chemistry* **2011**, 21, 8502.

(2) K. J. Lee*, J. Yoon*, J. Lahann, "Recent Advances with Anisotropic Particles", *Current Opinion in Colloid & Interface Science* **2011**, 16, 195.

(3) K. J. Lee*, J. Yoon*, S. Rahmani, S. Hwang, S. Bhaskar, S. Mitragotri, J. Lahann, *Proceedings of the National Academy of Sciences* **2012**, 109, 16057.

*co-first author

1.1. Anisotropic Particles

In recent years, the areas of anisotropic materials have gained a great interest and have become inevitable in many applications. In fact, nature provides many examples of non-spherical structures with multicomposition that possess different functionalities,[1,2] and for this reason, the development of anisotropic particles is required to mimic biomolecules in various size, shape, and function. Moreover, further advances in material

system impose requirements for dual or multiple surface properties that are due to orthogonal chemical functionalities, such as hydrophobic/hydrophilic, acidic/basic, conductive/non-conductive or adhesive/repellent.[3] These particles could provide a new class of materials that can be useful for multicomponent carriers for drug delivery,[4,5] imaging,[6,7] sensors,[6,8] dual color-switching device,[9,10] and potential building blocks for three dimensional self-assembled structures.[11-14] Although it is still a fundamental challenge to develop higher complexity in particle fabrication, a broad range of methods have been demonstrated to imply anisotropic features, such as shape, outer surface, and inner architecture of particles (Figure 1-1).[15-19] Anisotropic shapes and selective surface modification combined with compartmentalized particles will develop new strategies for smart materials, and in this aspect, chemical, physical, and biological properties can be manipulated for desired applications.

1.2. Current Trends in Synthesis of Anisotropic Particles

To address intrinsic limitations associated with isotropic particles, a number of design strategies have attempted the development of novel synthetic routes toward anisotropic particles.[18-21] Several techniques to control particle shape, surface, and compartmentalization are displayed in Figure 1-2. The materials used for particle synthesis can be diverse and include inorganic materials, polymers, biomolecules, and low-molecular weight additives.[22-25] Diversification of materials has been accompanied by a growing trend towards precisely controlled particles with respect to size, shape, and topography.[26-29]

1.2.1. Non-spherical Particles

As previously outlined in a number of excellent reviews,[11,20,30-33] shape is one of the essential properties of particles, and thus, a broad range of investigations has been focused on the fabrication of non-spherical particles. Preparation of asymmetric micro- and nanoparticles, such as rods, disks, fibers, tubes, dumbbell-shapes, acorn-shapes, sheets and ellipsoids, have been realized by a myriad of different fabrication processes.[20,31-33] Among these approaches, stretching,[26,34,35] micromolding,[8,36,37] microfluidic approaches,[38] and methods using seeded polymerization[39-41] have been particularly successful in creating pre-determined particle shapes. Many of these fabrication methods have been adopted from other areas of materials processing. For instance, particle replication templates[36] or photolithographic approaches[38] were adopted from conventional microfabrication processes to design microparticles with distinct morphologies.

Using a particle stretching method, Ho et al. prepared monodisperse elliptical particles through embedment of polystyrene (PS) particles into polyvinyl alcohol (PVA) thin films.[34] The particle loaded films were first heated above their glass transition temperature and then mechanically stretched (Figure 1-2B, top).[34] This approach was further developed to design over 20 complex shapes by Mitragotri and coworkers.[26] Furthermore, they have investigated the effect of ellipsoids on endocytosis and intracellular distribution of the particles in endothelial cells.[42] More recently, Pushkar et al. reported the assembly of stretched particles into three-dimensional structures. These relatively simple stretching methods offer the potential for scalability and are typically applicable to particle sizes above 200 nm.[27]

Based on a novel micromolding process, DeSimone and coworkers developed another promising approach towards non-spherical particles, for which they coined the term "particle replication in nonwetting template" or PRINT.[36] Unlike traditional imprint lithography, this method uses fluorinated perfluoropolyether (PFPE) elastomer in the form of a reusable nonwetting mold (Figure 1-B, bottom). This detail is important as it eliminates the need for harsh etching procedures to remove unnecessary materials. Due to the compatibility of the PRINT process with biocompatible polymers, a wide range of applications in the areas of drug delivery and medical imaging may be contemplated.[43-46] Other possible strategies for designing non-spherical particles include microfluidic techniques. Doyle and coworkers demonstrated that the simple processing of photocurable polymers in microchannels can form different structures of particles.[38,47] Both microchannel geometry and flow rates were found to be critical in fabricating different structures. In subsequent work, this technique has been broadened to generate a wide range of shapes. Moreover, Weitz group pioneered the droplet-based microfluidics to create highly monodisperse non-spherical shapes of particles.[48]

Besides the above-mentioned fabrication methods, seeded polymerization has often been considered a prime candidate for generating non-spherical particles. When seed particles are swollen in the presence of polymerizable monomer, dumbbell-like particles can be generated due to polymerization-induced phase separation. Sheu et al. have successfully synthesized uniform dumbbell-shaped polystyrene (PS) latex particles through seeded polymerization.[39] This early work demonstrated the potential for fabricating non-spherical particles in a controlled manner. Similarly, Weitz and coworkers have since shown that particle shapes can be effectively tuned by varying

either the crosslinking density or the degree of phase separation between the seed polymers and the newly made polymers.[40,41] While the range of shapes that can be generated with this approach is rather limited, the technique further allows for the chemical variation of the seeded compartments by simply changing the type of monomer used during seeded polymerization.

1.2.2. Patchy Particles

The formation of surface patterns on the particles can yield anisotropic surface features.[31,32,49] These particles, often referred to as "patchy" particles, are of special interest in a number of different areas including self-assembly,[11] photonic materials,[50] and drug delivery.[21] Among the most direct ways to produce "patchy" particles is the selective surface modification of isotropic micro/nanoparticles.[51-53] First, target particles are assembled onto substrate and then partially entrapped by a matrix. The exposed particle area is subsequently treated by physical and chemical methods, such as sputtering, polymerization, and plasma functionalization. After surface treatment, the sacrificial matrix is removed and Janus particles can be harvested. These particles still consist of one single component, but display different surface areas, as illustrated in Figure 1-2C. In the early years, microparticles were assembled on two-dimensional surfaces. This work was initially conducted using inorganic particles. Casagrande et al. first reported partial protection of microspheres with cellulose and sequential decoration with hydrophobic silanes.[54] In addition, Bao's group prepared silica microsphere arrays and spin-coated photoresist film onto the particle arrays.[55] Through reactive ion etching, the silica surface was partially exposed and Au or Ti was decorated onto silica particles, resulting in

chemically anisotropic particles. Since then, numerous researchers have developed efficient methods for particle trapping and selective chemical modification.[52,53,56-58] Because pre-existing micro/nanoparticles including commercially available silica or PS particles can be selectively modified, this approach offers a versatile, potentially economical and quite general route toward "patchy" particles. In some cases, a second surface modification step has been added, and dual functionalized microparticles can then be produced.[52,59] While these methods represent highly innovative approaches toward Janus particles, they are also associated with a number of intrinsic limitations. Because these approaches rely on 2D modification of preformed monolayers of microparticle, the yields are typically low and only a few milligrams of Janus particles can be produced in one batch. In an attempt to address this limitation, Kuo and coworkers reported preparation of larger amounts of Janus particles by the incorporation of microparticles into electro-spun fibers instead of 2D films.[60]

Beyond these efforts, there have been inventive ways to enhance throughput even further by using sacrificial layers in a 3D architecture. One promising example uses so-called "pickering emulsions" for the preparation of Janus particles. The use of pickering emulsions was initially motivated by the concept of "colloidosomes", which are formed by nanoparticles self-assembled at the liquid–liquid interface.[61] To restrict the surface modification only to the surface area exposed to one liquid phase, the pickering emulsion approach requires delicate thermodynamic control of the interface. However, the overall thermodynamic equilibrium is highly sensitive to the introduction of foreign materials into the system. Therefore, the preparation of colloidosomes has been an important challenge in its own right. Granick's group has pioneered this area of interfacial science,

which ultimately resulted in a diverse range of Janus particles.[62-65] They used organic wax as the oil phase to prepare colloidosomal clusters of microparticles. At high temperatures, the wax was dispersed in water and acted as a liquid. In this state, the microparticle colloidosomes nucleated around the liquid wax phase. Upon decreasing temperature, the wax phase was solidified, and the microparticles were partially locked into the wax phase exposing only a certain part of their surface to the surrounding. In this state, various surface chemical functionalizations can now be applied to the 3D colloidosomes clusters to prepare Janus micro/nanoparticles. In addition to a range of solvent-based modification methods, the Granick group recently illustrated the preparation of Janus particles by solvent-free synthesis based on microparticles fixed on the wax.[63] Similarly, Perro et al. also reported similar results but employed silica nanoparticles with smaller diameter.[66] While the use of pickering emulsions lends itself to the mass production of chemically anisotropic particles, it is particularly difficult to change in the delicate liquid/liquid thermodynamic equilibrium, which is required to form colloidosomes.[67] Therefore, only a limited range of particles has been shown to be compatible with this approach and further expansion of this technique to a diverse set of micro- and nanoparticles remains a dawning task at this point.

In addition to the matrix entrapping method, there have been several other methods reported for preparing "patchy" particles via selective surface modifications including printing with predefined masks[68,69] and glancing angle sputtering.[70-72]

1.2.3. Anisotropic Compartmentalization

Although anisotropic surface control of particles can offer interesting properties with importance to a range of applications, there are intrinsic limitations to control the physical properties of each half compartment by just modifying the surface. When particles with multifunctional properties in terms of both chemical and physical properties are needed, precise control of particle compartmentalization has to be realized. For example, in some cases, two or more therapeutic agents may need to be administered in a specific order and with defined and independent release kinetics. Additionally, when particles contain compartments with different functions, particles that can reconfigure in response to environmental changes may be prepared.

At the most fundamental level, block copolymers, which are comprised of polymer segments displaying dissimilar properties, can self-assemble into nanoparticles with defined compartmentalization.[73-78] The self-assembly of block copolymers leads to a range of different nanoparticle architectures featuring parallel lamellar, concentric lamellar, Janus-like, and tennis-ball-like structures.[79,80] Based on Monte Carlo simulations of the phase separation behavior of diblock copolymers self-assembled into nanospheres, a wide range of morphologies can be predicted as a function of nanoparticle size, equilibrium period of distinct lamellae, and interaction with the boundaries.[75] On the other hand, the majority of research on anisotropic block-copolymer nanoparticles has relied on blending of block copolymers.[32,81-85] Recent experimental and theoretical progress has broadened our understanding of compartmentalized particles created from block-copolymers. However, in terms of polymer accessibility and processability, several limitations and challenges still exist. In practice, the scope of multicompartmental

particles available through block copolymer self-assembly is limited to a relatively narrow range of materials and the synthesis of block-copolymers is associated with a substantial cost. Furthermore, incorporation of functional additives (i.e., drugs, inorganic nanoparticles, or macromolecules) into individual compartments remains challenging using this method. Some of these limitations are offset by the fact that the size of multicompartmental particles based on block-copolymers is typically below 100 nm. Thus, more investigations are needed to produce determinable multicompartmental colloidal particles based on well-controlled block copolymers.

Another pathway to make compartmentalized particles is induced by phase separation. The development of heterogeneous particles through phase separation is based on the immiscible nature of two materials. The common method for introducing new compartments in a particle requires polymerization of monomers within a premade seed particle. Other methods rely on emulsification of a heterogeneous material suspension in an immiscible medium. Once the droplets are prepared, phase separation can take place during solvent evaporation or in response to an external field. Seeded polymerization involves swelling of a crosslinked seed particle due to absorption of monomer that is subsequently polymerized. The resulting polymer is no longer soluble in the seed particle and segregates from the template particle, which then allows for the formation of small bulbs on the surface of the seed particle.[39] As recent efforts demonstrated the precise control over the position and the size of newly made polymer protusions, this approach has been increasingly used for broadening the diversity of particle shapes as well as surface chemistry.[86,87] Although one of the main advantages of the phase separation method is that particles can be prepared by facile and cost-effective

syntheses using batch production, the particle population tends to be heterogeneous with significant batch-to-batch variability. Thus, subsequent separation methods are often required to isolate particles based on the overall size, shape, or magnetic loading. Aside from the seeded polymerization, there are several approaches to induce phase separation during the particle synthesis, such as solvent evaporation, temperature, and the use of external fields.[88-90]

An alternative approach for the fabrication of compartmentalized particles is based on the fusion of pre-existing particles into larger assemblies. The assembly of particles typically involves attractive interactions between the surfaces of particles, such as electrostatic or covalent interactions,[91] or relies on the removal of a depletant, such as polymer or nanoparticles, when the gap between colloids is physically closed.[92] Particle fusion has been used in the past to weld pre-arranged sets of particles together. The particle pre-arrangement can be achieved by a variety of templates including droplets or microstructured templates.[93] Unlike methods that rely on direct particle interactions, a template can facilitate arrangement and engagement of particles with various sizes and shapes. Alternatively, particle fusion may be achieved by exposure to elevated temperatures above the glass transition, where polymer particles can be permanently fused together. Several other studies have been reported that focused on the development of novel methods to form complex particles through temperature induced fusion.[94-97] A potential advantage of this approach is the ability to obtain reproducible shapes with a diverse set of functionalities, since pre-existing particles can be combined. Thus, designing more complex morphologies is feasible, but will require a deeper understanding of the fundamental mechanisms that drive interfacial particle interactions.

Potential limitations of the particle fusion method include low throughput and high cost, if lithographically fabricated templates are used.

In principle, the strategies mentioned above are mostly based on self-assembly of pre-defined building blocks, and thus require delicate thermodynamic adjustment. Today, it is still challenging to establish a broad and versatile toolbox to produce well-defined multifunctional anisotropic particles in larger quantities. Moreover, particles prepared by thermodynamically driven processes mostly result in round shapes. However, recent studies regarding the influence of asymmetrically shaped colloidal particles on biological applications, such as drug delivery, lead to recognition of the importance of non-spherical particles.

Among techniques for fabrication of asymmetrically shaped colloidal particles, lithographic and template based methods are used most frequently.[43,98,99] Generally, multiple soft-lithographical steps can be used in series to produce polymeric particles with complex shapes and anisotropy. However, difficulties may arise from the separation of the particles from the matrix. DeSimone et al. developed an exceptionally creative pathway to solve this problem and introduced ''PRINT'' which uses a non-wetting mold (fluorinated template).[36] The molds have no chemical or physical affinity with the desired product and thus allow for facile separation of the product from the mold. Step-wise filling of a non-wetting template with different polymer solutions can result in multicompartmental particles.[43] In order to prevent coalescence and delamination of individual compartments, the first layer is only partially cured before introducing the second layer allowing for interfacial diffusion between the layers. Only after step-wise filling, both layers are completely cured by UV irradiation. This method provides great

flexibility in producing non-spherical particles. However, the range of internal architectures is more limited, as compartmentalization is achieved in one direction only due to step-by-step build up. Lastly, there is still a significant limitation on the materials that have been processed with this method.

Current microfluidic approaches can by-and-large be divided into droplet-based methods,[100-102] and photolithographic processing using laminar flow of miscible fluids (Figure 1-2D, left).[38,103] In droplet-based systems, immiscible fluids are used to form inner architectures. Nisisako et al. demonstrated electric responsive bicolor particles by incorporating two pigments (carbon black and titania) in different particle hemispheres.[9] The acrylic base monomers were then thermally polymerized after combining the two flows through a Y-junction channel.[9] Similarly, Nie et al. produced bi- and triphasic polyurethane microparticles by photopolymerization,[104] and Shepherd et al. reported the encapsulation of silica colloids in Janus hydrogel microparticles.[105] Moreover, double emulsion systems including water-in-oil-in-water (W–O–W) or oil-in-water-in-oil (O–W–O) systems, can be adapted for microfluidic processing.[102,106,107] Conventional double emulsion methods offer only limited control over the monodispersity of particles. To solve this problem, Weitz and coworkers introduced microchannels to fabricate well-controlled emulsion droplets by co-flow of immiscible fluids.[108,109] Extending the conventional microfluidic techniques with photolithography has allowed for design and fabrication of anisotropic particles. Beyond the fabrication of distinct shapes using photolithographic masks,[110] material scientists have started to manipulate the inner architectures of particles as well. For instance, Doyle and co-workers produced Janus particles through two different streams containing photo-curable poly(ethylene glycol)

diacrylate (PEGDA), lithographically printed in unique morphologies, and widened the technology to pursue anisotropic shapes of two- and three-dimensional anisotropy.[111] In addition, they introduced the fabrication of multi-level channels to enable three dimensional configurations,[103] as stacked layers of fluids were used to produce inner compartments in y- and z-direction.[112] Progress towards the design of microfluidic synthesis has permitted the fabrication of highly uniform particles using continuous production schemes. Furthermore, the use of photolithographic techniques can result in more complex geometries with sharp edges. The microfluidic technique provides a promising route towards compartmentalized particles, however, due to the relatively large size of fluidic channels, the resultant particles are typically rather large. In addition, there is currently a narrow choice of materials available and further progress will require substantial diversification of the type of materials that can be processed in this way. Thus, materials chemistry as well as the design of appropriate processing devices can be expected to be the focus of future research.

Another technique for preparing anisotropic microparticles is electrohydrodynamic (EHD) co-jetting (Figure 1-2D, right). The terms electrospraying and electrospinning designate technologies for fabrication of polymeric nano-/micro-particles and fibers by applying high electrical voltage to polymeric solutions.[113-115] Control of the properties of the polymer solutions (concentration, viscosity and conductivity) as well as the flow configuration can provide a wide range of compartmentalized particles with different shapes, compositions, and compartmentalizations.[116,117] To date, core/shell structures are the most abundant examples of compartmentalized particles prepared by electrified jetting.[118-120] However, the limitations of these particles are in their ability to possess

multiple surface functionalities because the core is fully covered by the outer shell. EHD co-jetting extensively investigated in our group creates side-by-side or pie-shaped multicompartmental structures so that it enables the obtained particles and fibers to possess different surface functions as well as bulk properties.[121-127] Such EHD co-jetting process will be discussed more in detail in the next section.

1.3.   Electrohydrodynamic Co-Jetting

As the anisotropy became critical in their influence on structure properties, electrified jetting (which can be named as 'electrospinning' or 'electrospraying' depending on whether the polymer forms fibers or particles) has proven to be an efficient method to produce polymeric fibers or particles with diameters in the range of nanometers to micrometers.[114,128-130] Briefly, a high voltage is applied to a conductive capillary needle that connects polymer solutions. A charged polymer jet is ejected, when the charge imbalance exceeds the surface tension of the polymer solution.[114] When the jet stream is driven by the electrostatic force, solvent evaporates, and polymeric fibers or particles are formed on the grounded collector.[113] Similar to this conventional electrified jetting technique, but unique in its ability to control particle geometries, EHD co-jetting has gained much attention in our group.

The schematic of the EHD co-jetting is introduced in Figure 1-3. The key feature of this method is that instead of using a single capillary, two or more capillaries with different polymer solutions are pumped through the system at a laminar flow rate.[121] As shown in Figure 1-4, a wide range of functional polymers can be fabricated in a

multicompartmentalized structure by this simple, rapid and cost-effective method.[116,121,123,125,131-135] Diverse shapes of bicompartmental building blocks, such as disk-, spindle shapes, or red blood cell-mimicking particles have been observed, when the flow rate and concentration of the jetting solutions were controlled within tight limits.[116,117,131] When inorganic materials, such as gold nanoparticles or magnetite nanocrystals, are introduced into one jetting solution, novel composite materials can be realized.[133,134] Similarly, microfibers having multicompartmental architectures can be prepared,[134] and subsequent cryosectioning can yield multicompartmental microcylinders.[123] In addition, selective surface modification of individual compartments is possible[136] and can result in directed interactions between particles, surfaces, and cells.[124,137] Its characteristic merits allow the EHD co-jetting technique to be diversely employed to prospective applications in drug delivery carrier, catalyst, imaging, optical device, and actuator.[125-127,135,138] However, there is still a limited understanding of the theoretical framework of EHD co-jetting, and a number of interesting issues will need to be addressed in terms of material diversity, generalization and geometry of products. Improved understanding of the complicated processes that are involved in EHD co-jetting will further guide the preparation of different compartmentalized particles and may enable the use of these particles for a number of future applications.

1.4. Importance of Reconfigurability

As more diverse synthetic pathways to build anisotropic particles are being investigated than ever before, a lot of research groups are now exploring more unique and

complex particles for potential stimuli-responsive system. In fact, nano- and microstructures in nature have meaningful information that allows us to design novel types of adaptive particles. Therefore, one of the essential features to consider is the particles' reconfigurability. Reconfigurable particles have ability to change their shapes or functions in response to specific stimuli such as temperature, pH, light, or solvent. Such particles are expected to undergo shape-shifting, actuation, or assembly/disassembly behavior based on their environmental changes.

One of the essential success criteria of living organisms has been the evolution of processes for actuating organ movement.[1,139,140] In plants, for instance, organ actuation is often not achieved by metabolically driven processes, but through exploitation of hierarchical geometrical architectures with critical functional feature sizes at the micron and nanometer scale.[140] Examples of shape reconfiguration without metabolic activity include the hydration-mediated opening of pine cones[141] and ice plant seeds,[142] or the catapult mechanism in fern spores.[140] In these cases, changes in the humidity level induce interfacial stresses that result in defined mechanical reconfigurations, such as opening of a spore capsule. A particularly sophisticated adaptive system can be found in Venus flytraps, where the snap-bucking instabilities that lead to millisecond closure of the trapping organ have been linked to convex–concave reconfigurations in the organ wall.[143] While these and other adaptive material systems have been hallmarks of nature, they have not yet been systematically realized in synthetic colloidal materials. Synthetic analogues of nature's particles are needed that can spontaneously and reversibly adapt characteristic properties, such as shape, size, or curvature in response to defined external stimuli.[139,144-148] Therefore, the focus of this work is in dynamic control and assemblies of particles

with unique anisotropic architectures. With the series of experiments for various applications which will be discussed in the following chapters, we expect to propose new areas of reconfigurable and adaptive system.

1.5. Objectives of this Study

The major objectives of this dissertation are to develop new types of anisotropic particles through EHD co-jetting for various future applications. This involves selection of appropriate polymers for each conceptual design, full understanding of their chemical, physical, or mechanical properties, characterization of the obtained particle systems, and evaluation of their performances. Based on different application strategies, the following aims were established (Figure 1-5).

Aim I. To develop new synthetic route for anisotropic particles by unique process called 'shape-shifting'. This would not only be investigating novel fabrication technique, but also open up the next generation particles with smart functions such as 'reconfigurability'.

Aim II. To fabricate amphiphilic particles by EHD co-jetting, and demonstrate the suitabiilty of the particles as future emulsion stabilizers. The surfactant-like characteristic of particles would be studied based on their self-assembly behavior at liquid-liquid interfaces.

Aim III. To design biohybrid polymer actuators driven by motion of cells. This could be achieved through the fabrication of anisotropic microcylinders, which have capability of recruiting cardiomyocytes selectively in certain direction.

Aim IV. To investigate the applicability of EHD co-jetting in particle-based optical display. Bicolor-coded magnetic particles could be a good candidate for this application, and the manipulation of particle motion would be studied with external magnetic field.

1.6. Figures and Tables
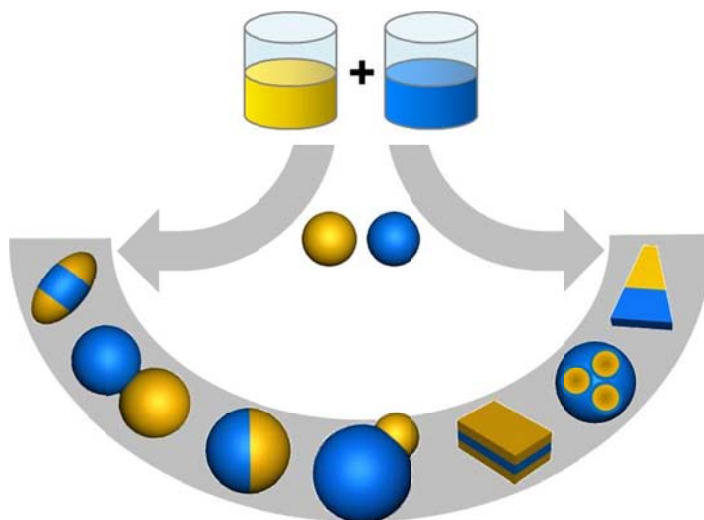
Figure 1-1. Illustrations of the transition from isotropic to anisotropic particles.
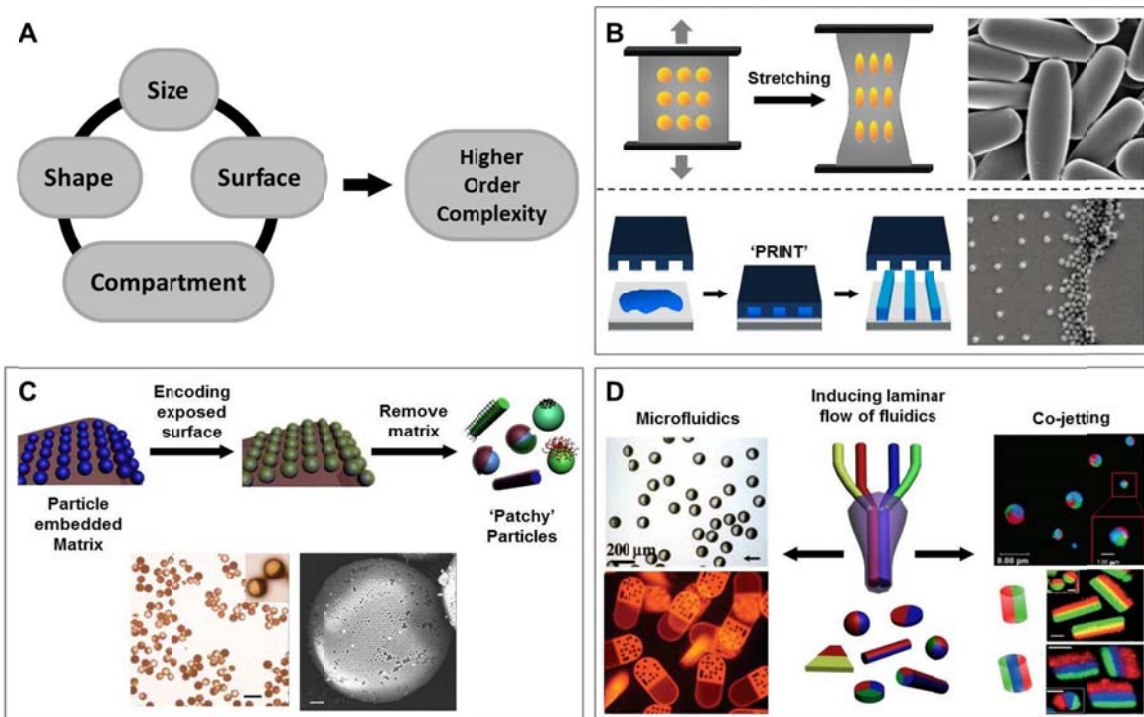
Figure 1-2. Several techniques to control particles with higher order complexity. (A) Schematic showing the importance of size, shape, surface, and compartment on building anisotropic particles. (B, C, D) Examples of synthetic routes for non-spherical particles, patchy particles, and compartmentalized particles, respectively. Adapted from refs. (B),[26,36] (C),[58,63] (D).[10,123,149,150]
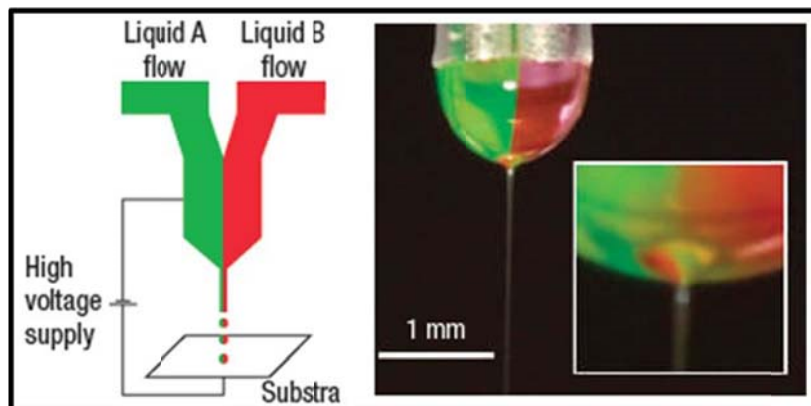
Figure 1-3. Side-by-side EHD co-jetting through dual capillaries. (A) Typical experimental setup of EHD co-jetting system. (B) Photograph of a bicompartmental Taylor cone with a stable jet stream. The inset is the zoomed-in image of the jet ejection point. Adapted from ref.[121]
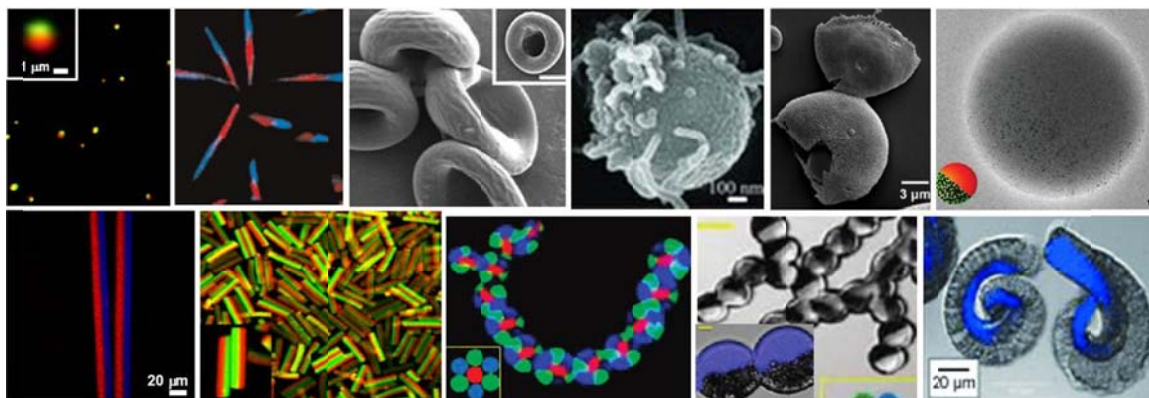
Figure 1-4. Wide ranges of anisotropic particles that can be fabricated through EHD co-jetting. Top row (left to right): bicompartmental spheres, bicompartmental rods, red-blood cell-mimicking particles, bicompartmental particles having selective growth of carbon nanotubes, half-moon shaped particles, and bicompartmental particles with selective encapsulation of gold nanoparticles. Bottom row (left to right): bicompartmental fibers, bicompartmental cylinders, cross-sectional view of 7-compartmental fibers, bicompartmental fibers with magnetite nanocrystals in half compartment, and surface-initiated atom-transfer radical polymerized (ATRP) microcylinders. Adapted from Refs.[116,123,125,131-135]
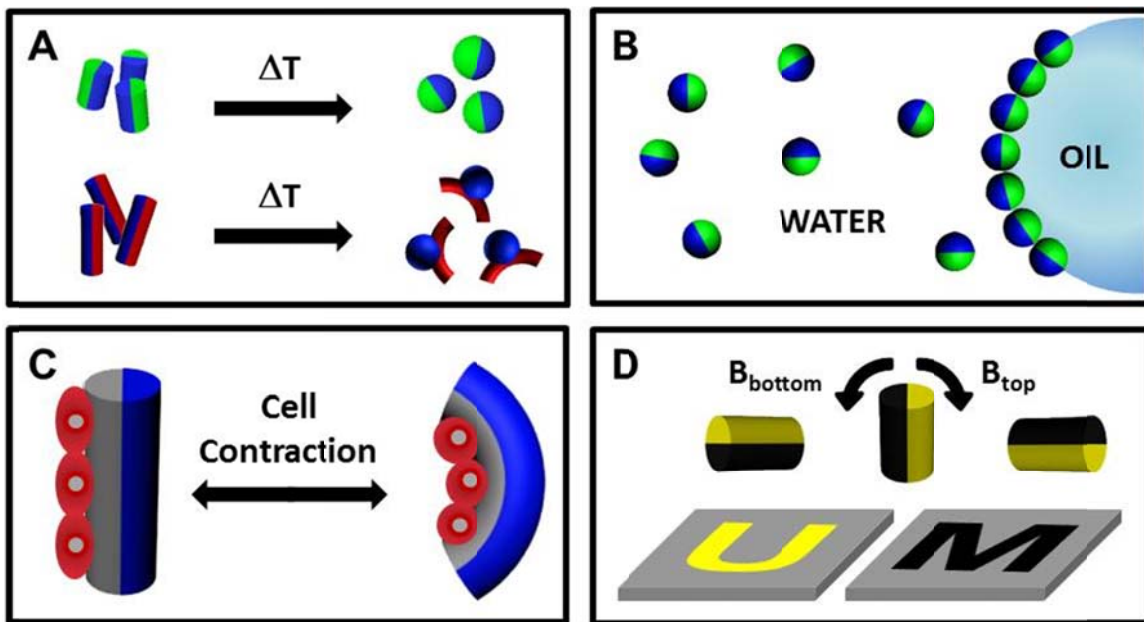
Figure 1-5. Schematic illustrations of specific aims for this study. (A) Shape-shifting of microcylinders. (B) Self-assembly of amphiphilic particles at liquid-liquid interfaces. (C) Cell-based biohybrid actuators. (D) Magnetic particle-based optical displays.

1.7. Reference

1.   Young, K. D. The Selective Value of Bacterial Shape. *Microbiology and Molecular Biology Reviews* **2006**, 70, 660-703.
2.   Cabeen, M. T.; Jacobs-Wagner, C. Bacterial Cell Shape. *Nat Rev Micro* **2005**, 3, 601-610.
3.   Luzinov, I.; Minko, S.; Tsukruk, V. V. Adaptive and Responsive Surfaces through Controlled Reorganization of Interfacial Polymer Layers. *Progress in Polymer Science* **2004**, 29, 635-698.
4.   Champion, J. A.; Katare, Y. K.; Mitragotri, S. Particle Shape: A New Design Parameter for Micro- and Nanoscale Drug Delivery Carriers. *Journal of Controlled Release* **2007**, 121, 3-9.
5.   Moon, J. J.; Huang, B.; Irvine, D. J. Engineering Nano- and Microparticles to Tune Immunity. *Advanced Materials* **2012**, 24, 3724-3746.
6.   Cederquist, K. B.; Dean, S. L.; Keating, C. D. Encoded Anisotropic Particles for Multiplexed Bioanalysis. *Wiley Interdisciplinary Reviews: Nanomedicine and Nanobiotechnology* **2010**, 2, 578-600.
7.   Depalo, N.; Carrieri, P.; Comparelli, R.; Striccoli, M.; Agostiano, A.; Bertinetti, L.; Innocenti, C.; Sangregorio, C.; Curri, M. L. Biofunctionalization of Anisotropic Nanocrystalline Semiconductor–Magnetic Heterostructures. *Langmuir* **2011**, 27, 6962-6970.
8.   Jung, S.; Yi, H. Fabrication of Chitosan-Poly(Ethylene Glycol) Hybrid Hydrogel Microparticles Via Replica Molding and Its Application toward Facile Conjugation of Biomolecules. *Langmuir* **2012**, 28, 17061-17070.
9.   Nisisako, T.; Torii, T.; Takahashi, T.; Takizawa, Y. Synthesis of Monodisperse Bicolored Janus Particles with Electrical Anisotropy Using a Microfluidic Co-Flow System. *Advanced Materials* **2006**, 18, 1152-1156.
10.   Kim, S.-H.; Sim, J. Y.; Lim, J.-M.; Yang, S.-M. Magnetoresponsive Microparticles with Nanoscopic Surface Structures for Remote-Controlled Locomotion. *Angewandte Chemie International Edition* **2010**, 49, 3786-3790.
11.   Glotzer, S. C.; Solomon, M. J. Anisotropy of Building Blocks and Their Assembly into Complex Structures. *Nat Mater* **2007**, 6, 557-562.
12.   Fejer, S. N.; Chakrabarti, D.; Wales, D. J. Self-Assembly of Anisotropic Particles. *Soft Matter* **2011**, 7, 3553-3564.
13.   Galisteo-López, J. F.; Ibisate, M.; Sapienza, R.; Froufe-Pérez, L. S.; Blanco, Á.; López, C. Self-Assembled Photonic Structures. *Advanced Materials* **2011**, 23, 30-69.
14.   Morgan, J. W. R.; Chakrabarti, D.; Dorsaz, N.; Wales, D. J. Designing a Bernal Spiral from Patchy Colloids. *ACS Nano* **2013**, 7, 1246-1256.
15.   Crespy, D.; Staff, R. H.; Becker, T.; Landfester, K. Chemical Routes toward Multicompartment Colloids. *Macromolecular Chemistry and Physics* **2012**, 213, 1183-1189.
16.   Polarz, S. Shape Matters: Anisotropy of the Morphology of Inorganic Colloidal Particles – Synthesis and Function. *Advanced Functional Materials* **2011**, 21, 3214-3230.
17.   Niu, Z.; He, J.; Russell, T. P.; Wang, Q. Synthesis of Nano/Microstructures at Fluid Interfaces. *Angewandte Chemie International Edition* **2010**, 49, 10052-10066.
18.   Yoon, J.; Lee, K. J.; Lahann, J. Multifunctional Polymer Particles with Distinct Compartments. *Journal of Materials Chemistry* **2011**, 21, 8502-8510.

19.   Lee, K. J.; Yoon, J.; Lahann, J. Recent Advances with Anisotropic Particles. *Current Opinion in Colloid & Interface Science* **2011**, 16, 195-202.

20.   Yang, S.-M.; Kim, S.-H.; Lim, J.-M.; Yi, G.-R. Synthesis and Assembly of Structured Colloidal Particles. *Journal of Materials Chemistry* **2008**, 18, 2177-2190.

21.   Pawar, A. B.; Kretzschmar, I. Fabrication, Assembly, and Application of Patchy Particles. *Macromolecular Rapid Communications* **2010**, 31, 150-168.

22.   Agrawal, M.; Gupta, S.; Stamm, M. Recent Developments in Fabrication and Applications of Colloid Based Composite Particles. *Journal of Materials Chemistry* **2011**, 21, 615-627.

23.   Kraus, T.; Malaquin, L.; Schmid, H.; Riess, W.; Spencer, N. D.; Wolf, H. Nanoparticle Printing with Single-Particle Resolution. *Nat Nano* **2007**, 2, 570-576.

24.   Landfester, K. Miniemulsion Polymerization and the Structure of Polymer and Hybrid Nanoparticles. *Angewandte Chemie International Edition* **2009**, 48, 4488-4507.

25.   Johnston, A. P. R.; Such, G. K.; Ng, S. L.; Caruso, F. Challenges Facing Colloidal Delivery Systems: From Synthesis to the Clinic. *Current Opinion in Colloid & Interface Science* **2011**, 16, 171-181.

26.   Champion, J. A.; Katare, Y. K.; Mitragotri, S. Making Polymeric Micro- and Nanoparticles of Complex Shapes. *Proceedings of the National Academy of Sciences* **2007**, 104, 11901-11904.

27.   Lele, P. P.; Furst, E. M. Assemble-and-Stretch Method for Creating Two- and Three-Dimensional Structures of Anisotropic Particles. *Langmuir* **2009**, 25, 8875-8878.

28.   Misra, A.; Urban, M. W. Acorn-Shape Polymeric Nano-Colloids: Synthesis and Self-Assembled Films. *Macromolecular Rapid Communications* **2010**, 31, 119-127.

29.   Haghgooie, R.; Toner, M.; Doyle, P. S. Squishy Non-Spherical Hydrogel Microparticles. *Macromolecular Rapid Communications* **2010**, 31, 128-134.

30.   Mitragotri, S.; Lahann, J. Physical Approaches to Biomaterial Design. *Nat Mater* **2009**, 8, 15-23.

31.   Wurm, F.; Kilbinger, A. F. M. Polymeric Janus Particles. *Angewandte Chemie International Edition* **2009**, 48, 8412-8421.

32.   Walther, A.; Muller, A. H. E. Janus Particles. *Soft Matter* **2008**, 4, 663-668.

33.   Perro, A.; Reculusa, S.; Ravaine, S.; Bourgeat-Lami, E.; Duguet, E. Design and Synthesis of Janus Micro- and Nanoparticles. *Journal of Materials Chemistry* **2005**, 15, 3745-3760.

34.   Ho, C. C.; Ottewill, R. H.; Keller, A.; Odell, J. A. Monodisperse Ellipsoidal Polystyrene Latex Particles: Preparation and Characterisation. *Polymer International* **1993**, 30, 207-211.

35.   Shah, A. A.; Kang, H.; Kohlstedt, K. L.; Ahn, K. H.; Glotzer, S. C.; Monroe, C. W.; Solomon, M. J. Liquid Crystal Order in Colloidal Suspensions of Spheroidal Particles by Direct Current Electric Field Assembly. *Small* **2012**, 8, 1551-1562.

36.   Rolland, J. P.; Maynor, B. W.; Euliss, L. E.; Exner, A. E.; Denison, G. M.; DeSimone, J. M. Direct Fabrication and Harvesting of Monodisperse, Shape-Specific Nanobiomaterials. *Journal of the American Chemical Society* **2005**, 127, 10096-10100.

37.   Wang, Y.; Byrne, J. D.; Napier, M. E.; DeSimone, J. M. Engineering Nanomedicines Using Stimuli-Responsive Biomaterials. *Advanced Drug Delivery Reviews* **2012**, 64, 1021-1030.

38.   Dendukuri, D.; Tsoi, K.; Hatton, T. A.; Doyle, P. S. Controlled Synthesis of Nonspherical Microparticles Using Microfluidics. *Langmuir* **2005**, 21, 2113-2116.

39.   Sheu, H. R.; El-Aasser, M. S.; Vanderhoff, J. W. Phase Separation in Polystyrene Latex Interpenetrating Polymer Networks. *Journal of Polymer Science Part A: Polymer Chemistry* **1990**, 28, 629-651.

40.   Kim, J.-W.; Larsen, R. J.; Weitz, D. A. Synthesis of Nonspherical Colloidal Particles with Anisotropic Properties. *Journal of the American Chemical Society* **2006**, 128, 14374-14377.

41.   Kim, J. W.; Larsen, R. J.; Weitz, D. A. Uniform Nonspherical Colloidal Particles with Tunable Shapes. *Advanced Materials* **2007**, 19, 2005-2009.

42.   Yoo, J.-W.; Doshi, N.; Mitragotri, S. Endocytosis and Intracellular Distribution of Plga Particles in Endothelial Cells: Effect of Particle Geometry. *Macromolecular Rapid Communications* **2010**, 31, 142-148.

43.   Perry, J. L.; Herlihy, K. P.; Napier, M. E.; DeSimone, J. M. Print: A Novel Platform toward Shape and Size Specific Nanoparticle Theranostics. *Accounts of Chemical Research* **2011**, 44, 990-998.

44.   Petros, R. A.; DeSimone, J. M. Strategies in the Design of Nanoparticles for Therapeutic Applications. *Nat Rev Drug Discov* **2010**, 9, 615-627.

45.   Merkel, T. J.; Jones, S. W.; Herlihy, K. P.; Kersey, F. R.; Shields, A. R.; Napier, M.; Luft, J. C.; Wu, H.; Zamboni, W. C.; Wang, A. Z.*; et al.* Using Mechanobiological Mimicry of Red Blood Cells to Extend Circulation Times of Hydrogel Microparticles. *Proceedings of the National Academy of Sciences* **2011**, 108, 586-591.

46.   Parrott, M. C.; Luft, J. C.; Byrne, J. D.; Fain, J. H.; Napier, M. E.; DeSimone, J. M. Tunable Bifunctional Silyl Ether Cross-Linkers for the Design of Acid-Sensitive Biomaterials. *Journal of the American Chemical Society* **2010**, 132, 17928-17932.

47.   Dendukuri, D.; Hatton, T. A.; Doyle, P. S. Synthesis and Self-Assembly of Amphiphilic Polymeric Microparticles. *Langmuir* **2006**, 23, 4669-4674.

48.   Shum, H. C.; Abate, A. R.; Lee, D.; Studart, A. R.; Wang, B.; Chen, C.-H.; Thiele, J.; Shah, R. K.; Krummel, A.; Weitz, D. A. Droplet Microfluidics for Fabrication of Non-Spherical Particles. *Macromolecular Rapid Communications* **2010**, 31, 108-118.

49.   Jiang, S.; Chen, Q.; Tripathy, M.; Luijten, E.; Schweizer, K. S.; Granick, S. Janus Particle Synthesis and Assembly. *Advanced Materials* **2010**, 22, 1060-1071.

50.   Hosein, I. D.; Ghebrebrhan, M.; Joannopoulos, J. D.; Liddell, C. M. Dimer Shape Anisotropy: A Nonspherical Colloidal Approach to Omnidirectonal Photonic Band Gaps. *Langmuir : the ACS journal of surfaces and colloids* **2010**, 26, 2151-2159.

51.   Ling, X. Y.; Phang, I. Y.; Acikgoz, C.; Yilmaz, M. D.; Hempenius, M. A.; Vancso, G. J.; Huskens, J. Janus Particles with Controllable Patchiness and Their Chemical Functionalization and Supramolecular Assembly. *Angewandte Chemie International Edition* **2009**, 48, 7677-7682.

52.   McConnell, M. D.; Kraeutler, M. J.; Yang, S.; Composto, R. J. Patchy and Multiregion Janus Particles with Tunable Optical Properties. *Nano Letters* **2010**, 10, 603-609.

53.   Anderson, K. D.; Luo, M.; Jakubiak, R.; Naik, R. R.; Bunning, T. J.; Tsukruk, V. V. Robust Plasma Polymerized-Titania/Silica Janus Microparticles. *Chemistry of Materials* **2010**, 22, 3259-3264.

54.   Casagrande, C. Janus Beads-Realization and 1st Observation of Interfacial Properties. *C. R. Acad. Sci., Ser. II* **1988**, 306.

55.   Bao, Z.; Chen, L.; Weldon, M.; Chandross, E.; Cherniavskaya, O.; Dai, Y.; Tok, J. B. H. Toward Controllable Self-Assembly of Microstructures: Selective Functionalization and Fabrication of Patterned Spheres. *Chemistry of Materials* **2002**, 14, 24-26.

56.   Paunov, V. N.; Cayre, O. J. Supraparticles and "Janus" Particles Fabricated by Replication of Particle Monolayers at Liquid Surfaces Using a Gel Trapping Technique. *Advanced Materials* **2004**, 16, 788-791.

57.   Ling, X. Y.; Phang, I. Y.; Acikgoz, C.; Deniz Yilmaz, M.; Hempenius, M. A.; Julius Vancso, G.; Huskens, J. Janus Particles with Controllable Patchiness and Their Chemical Functionalization and Supramolecular Assembly. *Angewandte Chemie - International Edition* **2009**, 48, 7677-7682.

58.   Liu, L.; Ren, M.; Yang, W. Preparation of Polymeric Janus Particles by Directional Uv-Induced Reactions. *Langmuir* **2009**, 25, 11048-11053.

59.   Erb, R. M.; Jenness, N. J.; Clark, R. L.; Yellen, B. B. Towards Holonomic Control of Janus Particles in Optomagnetic Traps. *Advanced Materials* **2009**, 21, 4825-4829.

60.   Ho, C. C.; Chen, W. S.; Shie, T. Y.; Lin, J. N.; Kuo, C. Novel Fabrication of Janus Particles from the Surfaces of Electrospun Polymer Fibers. *Langmuir* **2008**, 24, 5663-5666.

61.   Lin, Y.; Skaff, H.; Emrick, T.; Dinsmore, A. D.; Russell, T. P. Nanoparticle Assembly and Transport at Liquid-Liquid Interfaces. *Science* **2003**, 299, 226-229.

62.   Hong, L.; Jiang, S.; Granick, S. Simple Method to Produce Janus Colloidal Particles in Large Quantity. *Langmuir* **2006**, 22, 9495-9499.

63.   Jiang, S.; Schultz, M. J.; Chen, Q.; Moore, J. S.; Granick, S. Solvent-Free Synthesis of Janus Colloidal Particles. *Langmuir* **2008**, 24, 10073-10077.

64.   Chen, Q.; Bae, S. C.; Granick, S. Directed Self-Assembly of a Colloidal Kagome Lattice. *Nature* **2011**, 469, 381-384.

65.   Yan, J.; Bloom, M.; Bae, S. C.; Luijten, E.; Granick, S. Linking Synchronization to Self-Assembly Using Magnetic Janus Colloids. *Nature* **2012**, 491, 578-581.

66.   Perro, A.; Meunier, F.; Schmitt, V.; Ravaine, S. Production of Large Quantities of "Janus" Nanoparticles Using Wax-in-Water Emulsions. *Colloids and Surfaces A: Physicochemical and Engineering Aspects* **2009**, 332, 57-62.

67.   Bradley, M.; Rowe, J. Cluster Formation of Janus Polymer Microgels. *Soft Matter* **2009**, 5, 3114-3119.

68.   Zhang, G.; Wang, D.; Möhwald, H. Decoration of Microspheres with Gold Nanodots - Giving Colloidal Spheres Valences. *Angewandte Chemie - International Edition* **2005**, 44, 7767-7770.

69.   Zhang, G.; Wang, D.; Möhwald, H. Patterning Microsphere Surfaces by Templating Colloidal Crystals. *Nano Letters* **2005**, 5, 143-146.

70.   Pawar, A. B.; Kretzschmar, I. Patchy Particles by Glancing Angle Deposition. *Langmuir* **2007**, 24, 355-358.

71.   Pawar, A. B.; Kretzschmar, I. Multifunctional Patchy Particles by Glancing Angle Deposition. *Langmuir* **2009**, 25, 9057-9063.

72.	Kwak, M. K.; Jeong, H.-E.; Kim, T.-i.; Yoon, H.; Suh, K. Y. Bio-Inspired Slanted Polymer Nanohairs for Anisotropic Wetting and Directional Dry Adhesion. *Soft Matter* **2010**, 6, 1849-1857.

73.	Zhu, J.; Zhang, S.; Zhang, F.; Wooley, K. L.; Pochan, D. J. Hierarchical Assembly of Complex Block Copolymer Nanoparticles into Multicompartment Superstructures through Tunable Interparticle Associations. *Advanced Functional Materials* **2012**. DOI: 10.1002/adfm.201202323.

74.	O'Reilly, R. K. Self-Assembled Nanoparticles. In *Supramolecular Chemistry*; John Wiley & Sons, Ltd: **2012**.

75.	Binder, K.; Müller, M. Monte Carlo Simulation of Block Copolymers. *Current Opinion in Colloid & Interface Science* **2000**, 5, 314-322.

76.	Liu; Abetz, V.; Müller, A. H. E. Janus Cylinders. *Macromolecules* **2003**, 36, 7894-7898.

77.	Xiang, H.; Shin, K.; Kim, T.; Moon, S. I.; McCarthy, T. J.; Russell, T. P. Block Copolymers under Cylindrical Confinement. *Macromolecules* **2004**, 37, 5660-5664.

78.	Wu, Y.; Cheng, G.; Katsov, K.; Sides, S. W.; Wang, J.; Tang, J.; Fredrickson, G. H.; Moskovits, M.; Stucky, G. D. Composite Mesostructures by Nano-Confinement. *Nat Mater* **2004**, 3, 816-822.

79.	Higuchi, T.; Tajima, A.; Motoyoshi, K.; Yabu, H.; Shimomura, M. Frustrated Phases of Block Copolymers in Nanoparticles. *Angewandte Chemie International Edition* **2008**, 47, 8044-8046.

80.	Yu, B.; Li, B.; Jin, Q.; Ding, D.; Shi, A.-C. Self-Assembly of Symmetric Diblock Copolymers Confined in Spherical Nanopores. *Macromolecules* **2007**, 40, 9133-9142.

81.	Li, Z.; Kesselman, E.; Talmon, Y.; Hillmyer, M. A.; Lodge, T. P. Multicompartment Micelles from Abc Miktoarm Stars in Water. *Science* **2004**, 306, 98-101.

82.	Yabu, H.; Higuchi, T.; Shimomura, M. Unique Phase-Separation Structures of Block-Copolymer Nanoparticles. *Advanced Materials* **2005**, 17, 2062-2065.

83.	Fang, B.; Walther, A.; Wolf, A.; Xu, Y.; Yuan, J.; Müller, A. H. E. Undulated Multicompartment Cylinders by the Controlled and Directed Stacking of Polymer Micelles with a Compartmentalized Corona. *Angewandte Chemie International Edition* **2009**, 48, 2877-2880.

84.	Walther, A.; Drechsler, M.; Rosenfeldt, S.; Harnau, L.; Ballauff, M.; Abetz, V.; Müller, A. H. E. Self-Assembly of Janus Cylinders into Hierarchical Superstructures. *Journal of the American Chemical Society* **2009**, 131, 4720-4728.

85.	Walther, A.; Hoffmann, M.; Müller, A. H. E. Emulsion Polymerization Using Janus Particles as Stabilizers. *Angewandte Chemie International Edition* **2008**, 47, 711-714.

86.	Huang, H.; Liu, H. Synthesis of the Raspberry-Like Ps/Pan Particles with Anisotropic Properties Via Seeded Emulsion Polymerization Initiated by Γ-Ray Radiation. *Journal of Polymer Science Part A: Polymer Chemistry* **2010**, 48, 5198-5205.

87.	Kraft, D. J.; Hilhorst, J.; Heinen, M. A. P.; Hoogenraad, M. J.; Luigjes, B.; Kegel, W. K. Patchy Polymer Colloids with Tunable Anisotropy Dimensions. *The Journal of Physical Chemistry B* **2010**, 115, 7175-7181.

88.		Hu, S.-H.; Gao, X. Nanocomposites with Spatially Separated Functionalities for Combined Imaging and Magnetolytic Therapy. *Journal of the American Chemical Society* **2010**, 132, 7234-7237.
89.		Shah, R. K.; Kim, J.-W.; Weitz, D. A. Janus Supraparticles by Induced Phase Separation of Nanoparticles in Droplets. *Advanced Materials* **2009**, 21, 1949-1953.
90.		Dyab, A. K. F.; Ozmen, M.; Ersoz, M.; Paunov, V. N. Fabrication of Novel Anisotropic Magnetic Microparticles. *Journal of Materials Chemistry* **2009**, 19, 3475-3481.
91.		Grzelczak, M.; Vermant, J.; Furst, E. M.; Liz-Marzán, L. M. Directed Self-Assembly of Nanoparticles. *ACS Nano* **2010**, 4, 3591-3605.
92.		Sharma, A.; Walz, J. Y. Direct Measurement of the Depletion Interaction in a Charged Colloidal Dispersion. *Journal of the Chemical Society, Faraday Transactions* **1996**, 92, 4997-5004.
93.		Manoharan, V. N.; Elsesser, M. T.; Pine, D. J. Dense Packing and Symmetry in Small Clusters of Microspheres. *Science* **2003**, 301, 483-487.
94.		Yake, A. M.; Panella, R. A.; Snyder, C. E.; Velegol, D. Fabrication of Colloidal Doublets by a Salting out−Quenching−Fusing Technique. *Langmuir* **2006**, 22, 9135-9141.
95.		Yin, Y.; Lu, Y.; Gates, B.; Xia, Y. Template-Assisted Self-Assembly: A Practical Route to Complex Aggregates of Monodispersed Colloids with Well-Defined Sizes, Shapes, and Structures. *Journal of the American Chemical Society* **2001**, 123, 8718-8729.
96.		Yin, Y.; Xia, Y. Self-Assembly of Spherical Colloids into Helical Chains with Well-Controlled Handedness. *Journal of the American Chemical Society* **2003**, 125, 2048-2049.
97.		Sung, K. E.; Vanapalli, S. A.; Mukhija, D.; McKay, H. A.; Mirecki Millunchick, J.; Burns, M. A.; Solomon, M. J. Programmable Fluidic Production of Microparticles with Configurable Anisotropy. *Journal of the American Chemical Society* **2008**, 130, 1335-1340.
98.		Badaire, S.; Cottin-Bizonne, C.; Woody, J. W.; Yang, A.; Stroock, A. D. Shape Selectivity in the Assembly of Lithographically Designed Colloidal Particles. *Journal of the American Chemical Society* **2006**, 129, 40-41.
99.		Acharya, G.; Shin, C. S.; McDermott, M.; Mishra, H.; Park, H.; Kwon, I. C.; Park, K. The Hydrogel Template Method for Fabrication of Homogeneous Nano/Microparticles. *Journal of Controlled Release* **2010**, 141, 314-319.
100.	Seiffert, S. Functional Microgels Tailored by Droplet-Based Microfluidics. *Macromolecular Rapid Communications* **2011**, 32, 1600-1609.
101.	Zhao, Y.; Gu, H.; Xie, Z.; Shum, H. C.; Wang, B.; Gu, Z. Bioinspired Multifunctional Janus Particles for Droplet Manipulation. *Journal of the American Chemical Society* **2012**, 135, 54-57.
102.	Shum, H. C.; Zhao, Y.-j.; Kim, S.-H.; Weitz, D. A. Multicompartment Polymersomes from Double Emulsions. *Angewandte Chemie International Edition* **2011**, 50, 1648-1651.
103.	Bong, K. W.; Pregibon, D. C.; Doyle, P. S. Lock Release Lithography for 3d and Composite Microparticles. *Lab on a Chip* **2009**, 9, 863-866.
104.	Nie, Z.; Li, W.; Seo, M.; Xu, S.; Kumacheva, E. Janus and Ternary Particles Generated by Microfluidic Synthesis: Design, Synthesis, and Self-Assembly. *Journal of the American Chemical Society* **2006**, 128, 9408-9412.

105.   Shepherd, R. F.; Conrad, J. C.; Rhodes, S. K.; Link, D. R.; Marquez, M.; Weitz, D. A.; Lewis, J. A. Microfluidic Assembly of Homogeneous and Janus Colloid-Filled Hydrogel Granules. *Langmuir* **2006**, 22, 8618-8622.

106.   Seiffert, S.; Thiele, J.; Abate, A. R.; Weitz, D. A. Smart Microgel Capsules from Macromolecular Precursors. *Journal of the American Chemical Society* **2010**, 132, 6606-6609.

107.   Chu, L.-Y.; Utada, A. S.; Shah, R. K.; Kim, J.-W.; Weitz, D. A. Controllable Monodisperse Multiple Emulsions. *Angewandte Chemie International Edition* **2007**, 46, 8970-8974.

108.   Utada, A. S.; Lorenceau, E.; Link, D. R.; Kaplan, P. D.; Stone, H. A.; Weitz, D. A. Monodisperse Double Emulsions Generated from a Microcapillary Device. *Science* **2005**, 308, 537-541.

109.   Kanai, T.; Lee, D.; Shum, H. C.; Shah, R. K.; Weitz, D. A. Gel-Immobilized Colloidal Crystal Shell with Enhanced Thermal Sensitivity at Photonic Wavelengths. *Advanced Materials* **2010**, 22, 4998-5002.

110.   Dendukuri, D.; Pregibon, D. C.; Collins, J.; Hatton, T. A.; Doyle, P. S. Continuous-Flow Lithography for High-Throughput Microparticle Synthesis. *Nat Mater* **2006**, 5, 365-369.

111.   Dendukuri, D.; Doyle, P. S. The Synthesis and Assembly of Polymeric Microparticles Using Microfluidics. *Advanced Materials* **2009**, 21, 4071-4086.

112.   Bong, K. W.; Bong, K. T.; Pregibon, D. C.; Doyle, P. S. Hydrodynamic Focusing Lithography. *Angewandte Chemie International Edition* **2010**, 49, 87-90.

113.   Andrady, A. L. Electrospinning Basics. In *Science and Technology of Polymer Nanofibers*; John Wiley & Sons, Inc.: **2007**; pp 55-80.

114.   Bhardwaj, N.; Kundu, S. C. Electrospinning: A Fascinating Fiber Fabrication Technique. *Biotechnology Advances* **2010**, 28, 325-347.

115.   Greiner, A.; Wendorff, J. H. Electrospinning: A Fascinating Method for the Preparation of Ultrathin Fibers. *Angewandte Chemie International Edition* **2007**, 46, 5670-5703.

116.   Bhaskar, S.; Pollock, K. M.; Yoshida, M.; Lahann, J. Towards Designer Microparticles: Simultaneous Control of Anisotropy, Shape, and Size. *Small* **2010**, 6, 404-411.

117.   Lahann, J. Recent Progress in Nano-Biotechnology: Compartmentalized Micro- and Nanoparticles Via Electrohydrodynamic Co-Jetting. *Small* **2011**, 7, 1149-1156.

118.   Wang, C.; Yan, K.-W.; Lin, Y.-D.; Hsieh, P. C. H. Biodegradable Core/Shell Fibers by Coaxial Electrospinning: Processing, Fiber Characterization, and Its Application in Sustained Drug Release. *Macromolecules* **2010**, 43, 6389-6397.

119.   Liao, I. C.; Chen, S.; Liu, J. B.; Leong, K. W. Sustained Viral Gene Delivery through Core-Shell Fibers. *Journal of Controlled Release* **2009**, 139, 48-55.

120.   McCann, J. T.; Li, D.; Xia, Y. Electrospinning of Nanofibers with Core-Sheath, Hollow, or Porous Structures. *Journal of Materials Chemistry* **2005**, 15, 735-738.

121.   Roh, K.-H.; Martin, D. C.; Lahann, J. Biphasic Janus Particles with Nanoscale Anisotropy. *Nat Mater* **2005**, 4, 759-763.

122.   Roh, K.-H.; Yoshida, M.; Lahann, J. Water-Stable Biphasic Nanocolloids with Potential Use as Anisotropic Imaging Probes. *Langmuir* **2007**, 23, 5683-5688.

123. Bhaskar, S.; Hitt, J.; Chang, S.-W. L.; Lahann, J. Multicompartmental Microcylinders. *Angewandte Chemie International Edition* **2009**, 48, 4589-4593.
124. Mandal, S.; Bhaskar, S.; Lahann, J. Micropatterned Fiber Scaffolds for Spatially Controlled Cell Adhesion. *Macromolecular Rapid Communications* **2009**, 30, 1638-1644.
125. Saha, S.; Copic, D.; Bhaskar, S.; Clay, N.; Donini, A.; Hart, A. J.; Lahann, J. Chemically Controlled Bending of Compositionally Anisotropic Microcylinders. *Angewandte Chemie International Edition* **2012**, 51, 660-665.
126. Lee, K. J.; Yoon, J.; Rahmani, S.; Hwang, S.; Bhaskar, S.; Mitragotri, S.; Lahann, J. Spontaneous Shape Reconfigurations in Multicompartmental Microcylinders. *Proceedings of the National Academy of Sciences* **2012**, 109, 16057-16062.
127. Misra, A. C.; Bhaskar, S.; Clay, N.; Lahann, J. Multicompartmental Particles for Combined Imaging and Sirna Delivery. *Advanced Materials* **2012**, 24, 3850-3856.
128. Huang, Z.-M.; Zhang, Y. Z.; Kotaki, M.; Ramakrishna, S. A Review on Polymer Nanofibers by Electrospinning and Their Applications in Nanocomposites. *Composites Science and Technology* **2003**, 63, 2223-2253.
129. Teo, W. E.; Ramakrishna, S. A Review on Electrospinning Design and Nanofibre Assemblies. *Nanotechnology* **2006**, 17, R89.
130. Schiffman, J. D.; Schauer, C. L. A Review: Electrospinning of Biopolymer Nanofibers and Their Applications. *Polymer Reviews* **2008**, 48, 317-352.
131. Doshi, N.; Zahr, A. S.; Bhaskar, S.; Lahann, J.; Mitragotri, S. Red Blood Cell-Mimicking Synthetic Biomaterial Particles. *Proceedings of the National Academy of Sciences* **2009**, 106, 21495-21499.
132. Lee, K. J.; Hwang, S.; Yoon, J.; Bhaskar, S.; Park, T.-H.; Lahann, J. Compartmentalized Photoreactions within Compositionally Anisotropic Janus Microstructures. *Macromolecular Rapid Communications* **2011**, 32, 431-437.
133. Lim, D. W.; Hwang, S.; Uzun, O.; Stellacci, F.; Lahann, J. Compartmentalization of Gold Nanocrystals in Polymer Microparticles Using Electrohydrodynamic Co-Jetting. *Macromolecular Rapid Communications* **2010**, 31, 176-182.
134. Bhaskar, S.; Lahann, J. Microstructured Materials Based on Multicompartmental Fibers. *Journal of the American Chemical Society* **2009**, 131, 6650-6651.
135. Lv, W.; Lee, K. J.; Li, J.; Park, T.-H.; Hwang, S.; Hart, A. J.; Zhang, F.; Lahann, J. Anisotropic Janus Catalysts for Spatially Controlled Chemical Reactions. *Small* **2012**, 8, 3116-3122.
136. Bhaskar, S.; Roh, K.-H.; Jiang, X.; Baker, G. L.; Lahann, J. Spatioselective Modification of Bicompartmental Polymer Particles and Fibers Via Huisgen 1,3-Dipolar Cycloaddition. *Macromolecular Rapid Communications* **2008**, 29, 1655-1660.
137. Bhaskar, S.; Gibson, C. T.; Yoshida, M.; Nandivada, H.; Deng, X.; Voelcker, N. H.; Lahann, J. Engineering, Characterization and Directional Self-Assembly of Anisotropically Modified Nanocolloids. *Small* **2011**, 7, 812-819.
138. Hwang, S.; Lahann, J. Differentially Degradable Janus Particles for Controlled Release Applications. *Macromolecular Rapid Communications* **2012**, 33, 1178-1183.
139. Huebsch, N.; Mooney, D. J. Inspiration and Application in the Evolution of Biomaterials. *Nature* **2009**, 462, 426-432.
140. Burgert, I.; Fratzl, P. Actuation Systems in Plants as Prototypes for Bioinspired Devices. *Philosophical Transactions of the Royal Society A: Mathematical, Physical and Engineering Sciences* **2009**, 367, 1541-1557.

141.   Dawson, C.; Vincent, J. F. V.; Rocca, A.-M. How Pine Cones Open. *Nature* **1997**, 390, 668-668.

142.   Harrington, M. J.; Razghandi, K.; Ditsch, F.; Guiducci, L.; Rueggeberg, M.; Dunlop, J. W. C.; Fratzl, P.; Neinhuis, C.; Burgert, I. Origami-Like Unfolding of Hydro-Actuated Ice Plant Seed Capsules. *Nat Commun* **2011**, 2, 337.

143.   Forterre, Y.; Skotheim, J. M.; Dumais, J.; Mahadevan, L. How the Venus Flytrap Snaps. *Nature* **2005**, 433, 421-425.

144.   McConney, M. E.; Anderson, K. D.; Brott, L. L.; Naik, R. R.; Tsukruk, V. V. Bioinspired Material Approaches to Sensing. *Advanced Functional Materials* **2009**, 19, 2527-2544.

145.   Yoshida, R. Self-Oscillating Gels Driven by the Belousov–Zhabotinsky Reaction as Novel Smart Materials. *Advanced Materials* **2010**, 22, 3463-3483.

146.   Huck, W. T. S. Responsive Polymers for Nanoscale Actuation. *Materials Today* **2008**, 11, 24-32.

147.   Sidorenko, A.; Krupenkin, T.; Taylor, A.; Fratzl, P.; Aizenberg, J. Reversible Switching of Hydrogel-Actuated Nanostructures into Complex Micropatterns. *Science* **2007**, 315, 487-490.

148.   Ohm, C.; Kapernaum, N.; Nonnenmacher, D.; Giesselmann, F.; Serra, C.; Zentel, R. Microfluidic Synthesis of Highly Shape-Anisotropic Particles from Liquid Crystalline Elastomers with Defined Director Field Configurations. *Journal of the American Chemical Society* **2011**, 133, 5305-5311.

149.   Roh, K.-H.; Martin, D. C.; Lahann, J. Triphasic Nanocolloids. *Journal of the American Chemical Society* **2006**, 128, 6796-6797.

150.   Pregibon, D. C.; Toner, M.; Doyle, P. S. Multifunctional Encoded Particles for High-Throughput Biomolecule Analysis. *Science* **2007**, 315, 1393-1396.

CHAPTER 2

Shape-Shifting of Microcylinders

The material in this chapter has been adapted with minor modifications from the following published article:

2.1. Motivation and Background

The precise engineering of particle properties is important for many biomedical applications including self-assembly, drug delivery, and medical diagnostics.[1-7] Beyond particle chemistry, physical properties such as size[2,8] or shape[9,10] have been identified as key attributes that govern particle fate in a number of biomedical and biotechnological applications. In fact, nature provides a number of anisotropic nano- and microstructures with specific functions.[11] For example, nature's particles, i.e., viruses or cells, can rapidly change major attributes, such as shape, size, or mechanical properties in response to environmental stimuli.[12,13] In an attempt to mimic the complexity of biological particles, a number of increasingly sophisticated, multifunctional particles with anisotropy and

directionality have been devised.[14-18] However, with few exceptions,[9,19] these particles lack the ability to undergo spontaneous reconfiguration in response to environmental stimuli (such as temperature pH, light, salt content, or solvent). So far, the response of polymer structures upon external stimuli includes swelling/shrinking,[20-24] color change/fading,[25-27] and change of state.[28] Thus, in order for a broad spectrum of environmentally-responsive particles, it is essential to select appropriate polymers. Additionally, the combination of properties such as shapes, surface functionalities, along with inner compartmentalization is necessary for the next generation of reconfigurable particle system.

Here, we introduce anisotropic microcylinders that can rapidly reconfigure into multiple compartmental spheres. Notably, these particles can undergo defined shape-shifting of either the entire particles or individual compartments. Stimulus-reconfigurable particles may find applications for targeted drug delivery, re-programmable biohybrid carriers, or microactuators. Furthermore, reconfiguration of particles will bring up new synthetic pathways of anisotropic particles with unique shapes and functions. Shape-shifting of multicompartmental microcylinders was performed by ultrasound-mediated heat treatment. When relatively hydrophobic PLGA microcylinders were treated with ultrasound in water, the particle temperature increased above Tg of polymer, and the cylindrical particles were reconfigured into spheres due to the minimization of surface-to-volume ratio. After a short period, all the cylinders were converted to spheres, and the inner compartments were fully retained in the particles after shape-shifting. Moreover, polymers with different properties in response to temperature were introduced to produce unique shaped particles.

2.2. Experimental Methods

2.2.1. Materials

All polymers including poly(DL-lactide-co-glycolide) (PLGA) (85:15, Mw = 50 – 75,000 g/mol), poly(methyl methacrylate) (PMMA) (Mw = 350,000 g/mol), poly(vinyl cinnamate) (PVCi) (Mw = 200,000 g/mol), polystyrene (PS) (Mw = 280,000 g/mol) were purchased from Sigma-Aldrich, USA. The fluorescence dyes poly[(m-phenylenevinylene)-alt-(2,5-dibutoxy-pphenylenevinylene)] (MEHPV) and poly[tris(2,5-bis(hexyloxy)-1,4-henylenevinylene)-alt-(1,3-phenylenevinylene)] (PTDPV), which were used as CLSM markers with blue and green emission, were purchased from Sigma-Aldrich, USA. The red-emitting dye ADS306PT was purchased from American Dye Source, Canada. The solvents chloroform and N,N'-dimethylformamide (DMF) were purchased from Sigma-Aldrich, USA and used without further purification.

2.2.2. Instrumental Details

Confocal Laser Scanning Microscopy (CLSM): Particles were visualized using an Olympus FluoView 500. Three different lasers, 405 nm laser, 488 nm Argon laser, and 533 nm Helium-Neon green (HeNeG) laser, were used to excite the dyes MEHPV, PTDPV, and ADS306PT, respectively. The barrier filters were set to 430-460 nm for MEHPV, 505-525 nm for PTDPV, and 560-600 nm for ADS306PT.

Scanning electron microscopy (SEM): The samples were coated with gold before analysis and the particle morphology was examined using an AMRAY 1910 Field Emission Scanning Electron Microscope (FEG-SEM) and FEI Nova Nanolabs.

Differential Scanning Calorimetry (DSC) analysis: The glass transition temperatures of PLGA and PMMA were evaluated based on their DSC thermograms. The measurements were carried out using a Perkin-Elmer DSC-7 at a scanning rate of 5 $^{\circ}$C/min. Each polymer was kept in aluminum pans and an empty pan was used as the reference.

2.2.3. Preparation of Microcylinders

Microcylinders are prepared by EHD co-jetting[29] of two or more polymer solutions and subsequent microsectioning.[30] Figure 2-1 illustrates the fabrication process of poly(lactic-co-glycolic acid) (PLGA) microcylinders. Large populations of microcylinders with close-to-identical diameters and well-defined and controllable length were obtained. Moreover, microcylinders with multiple and variable compartments were prepared using a range of different nozzle configurations including side-by-side, pie-shape, or core/shell arrangements. If a PLGA shell stream was employed during EHD co-jetting, simultaneous processing of substantially dissimilar materials was possible and allowed for a broad diversification of the compartment compositions. In addition, EHD co-jetting can provide access to distinct and stable colloidal microcylinders with diameters ranging from hundreds of nanometers to tens of micrometers. Depending on the composition selected for the individual microcompartments, these microcylinders can undergo programmable shape-shifting of individual compartments or entire particles.

Typical procedure for preparing bicompartmental microcylinders is as follows. The experimental setup contained a syringe pump (Fisher Scientific Inc., USA), a power supply (DC voltage source, Gamma High Voltage Research, USA), and a rotary collector

(Synthecon Inc., modified to experimental requirements). The PLGA solutions were delivered at a constant flow rate of 0.05 ml/h via vertically positioned syringes equipped with 26 G needles (Hamilton, USA). A driving voltage of 11 kV resulted in a stable jet and fiber bundles were collected at a tip-to-ground distance of 5 cm. Refer to Table 2-1 for detailed needle arrangements and preparation procedures for different types of multicompartmental Microfibers. Microsectioning of the fiber bundles was done using a cryostat microtome (Microm HM550, Thermo Fisher Scientific Inc., Germany). The samples were embedded into a sectioning medium (Tissue-Tek O.C.T. Compound, Andwin Scientific, USA), cooled to −20 °C, and microsectioned at a desired length.

2.2.4. Shape-Shifting of Microcylinders

The typical shape-shifting procedure of PLGA microcylinders involved dispersion of approximately 10,000 cylinders in 1 mL of medium in Eppendorf tube and treatement with ultrasound (Ultrasonic Processor, Cole-Parmer, USA) at room temperature. The medium used for the ultrasound treatment was either 2 v/v% Tween 20/DI water or a mixture of ethanol and 2 v/v% Tween 20/DI water (1:1, v/v). The detailed experimental conditions for each shape-shifting process of multicompartmental microcylinders are listed in Table 2-2.

2.3. Results and Discussion

For polymer particles, the thermodynamically most favorable state is that of a sphere and most of particle fabrication methods have resulted in spherical polymer

particles so far. Thus, particle engineers have been accustomed to almost exclusively dealing with spherical polymer particles. Recent exceptions include the synthesis of certain inherently non-spherical polymer particles,[31-33] energy-driven conversion of spherical particles into shaped particles via stretching at elevated temperatures,[34] and the electrohydrodynamic co-jetting procedure used herein to create microcylinders.[30] If multicompartmental microcylinders are comprised of polymers below their glass transition temperature, their shapes are arrested in the cylindrical shape and the particles remain stable over extended times (Figure 2-2A). Here PLGA was used, because it is biodegradable, has a glass temperature (Tg) of 47–48 °C, and a relatively low surface tension (The water/air contact angle of a film casted from the PLGA used in this study was 92°). Figure 2-2B shows a population of PLGA-based microcylinders, which was stored below the glass transition temperature of the polymer for three days ($T_g > T_p$ regimen, where T_g = glass transition temperature and T_p = polymer temperature). To induce shape-shifting, one can either increase T_p or lower T_g.[35] Ultrasound treatment for two minutes in water converted the microcylinders completely and homogenously into spheres (Figure 2-2C). The choice of ultrasound as the stimulus for shape reconfiguration has a number of advantages; it can be applied remotely and has already been broadly used in medical and nondestructive imaging.[36] If the microcylinders were treated with ultrasound in an ice bath, the localized heating effect of the ultrasound was suppressed and shape-shifting into spheres was no longer observed (Figure 2-2D). In this case, the particles remained in the $T_g > T_p$ regimen and their initial cylindrical shapes were maintained, albeit there was a rounding of the edges of the microcylinders. Ultrasound-mediated cavitations as well as other mechanical effects were ruled out as the driving

force for shape-shifting, because they should be approximately temperature-independent.[37] For a particle above its glass transition temperature, shape-shifting is favored by higher free surface energy of the particle surface and lower polymer viscosity.[34] Assuming a close-to constant polymer viscosity, the driving force for particle reconfiguration should be dominated by minimization of the free surface energy. The shape-shifting thus depends on the surface tension of the solvent, in which the reconfiguration is carried out. To confirm this hypothesis, we suspended PLGA microcylinders in either apolar heptane ($\varepsilon = 1.9$) or polar water ($\varepsilon = 80$). After treatment with ultrasound for 2 min, particles underwent shape-shifting in water, but not in heptane. This finding confirms that minimization of free surface energy of the polymer particles plays a dominating factor for particle reconfiguration (Figure 2-2E).

Once this shifting mechanism was confirmed and procedures for quantitative shifting were established, we assessed whether shape-shifting can be extended to microcylinders with multiple distinct compartments (Figure 2-3A). Specifically, PLGA microcylinders with an average aspect ratio of 1.48 ± 0.10 and two equally sized compartments were prepared and exposed to ultrasound for 3 min (Figures 2-3B – 2-3D). The average diameter after shape-shifting was 26.85 ± 0.88 μm as compared to an average diameter of 20.06 ± 0.56 μm for the microcylinders prior to shape-shifting. The mean aspect ratio of the microcylinders changed from 1.48 ± 0.10 to 1.05 ± 0.03, which is indicative of nearly perfect spheres. In addition, confocal laser scanning microscopy (CLSM) analysis after shape-shifting confirmed maintenance of well-defined, bicompartmental particle architectures. To further demonstrate the generality of the shape-shifting approach, we prepared bicompartmental microcylinders with a diameter of

16.27 ± 0.67 μm and lengths of 30.19 ± 0.76 μm (Figure 2-3E), and a diameter of 20.69 ±

0.69 μm and lengths of 71 ± 0.89 μm (Figure 2-3G) corresponding to diameters of 23.80

± 1.22 μm (Figure 2-3F) and 46.27 ± 1.36 μm (Figure 2-3H). In both cases, perfect

spheres were obtained via shape-shifting with aspect ratios of 1.05 ± 0.03 and 1.02 ± 0.01,

respectively. Subsequent shape-shifting resulted in microspheres with diameters of 37.17

± 1.22 μm and aspect ratios of 1.02 ± 0.01 (Figure 2-3H). Again, the bicompartmental

architecture of the particles was fully maintained.

Beyond bicompartmental architectures, one may expect a higher propensity for

inhomogeneities during shape-shifting, as the number of compartments increases or the

size of individual compartments decreases. Developing a thorough understanding of these

subtle limitations of the shape-shifting process may become increasingly important, as

recent work suggests that microcylinders with as many as seven compartments can be

experimentally created.[30] We thus prepared two types of tricompartmental microcylinders:

those with sequential (Fig. 2-4A, left) and pie-shaped compartmentalization (Figure 2-4B,

left). As shown in CLSM analysis of the compartmentalized particles confirmed that the

original compartmentalization patterns were fully maintained after shape-shifting

(Figures 2-4A and 2-4B, right). Similarly, heptacompartmental particles can be prepared

by shape-shifting of corresponding microcylinders. Interestingly, the direct synthesis of

heptacompartmental microspheres via electrospraying has so far not been realized, which

elevates the fact that the procedure reported here can be used to create a broad range of

compartmentalized microspheres (Figure 2-4C). In this specific case, the microcylinders

further contained 28 nm magnetite nanocrystals as inorganic payload, which were also

confined into one compartment after shape-shifting (Figure 2-4D).

In principle, one of the major advantages of using compartmentalized microcylinders for shape-shifting is that appropriate selection of the compartment materials may lead to partial shape-shifting – i.e., only certain compartments of the microcylinders are converted into spherical shapes, while the rest is not switched. Such partial shape reconfiguration can be expected to yield colloidal particles with entirely new shapes. The experimental validation required microcylinders with compartments that feature polymers with distinct Tg, plasticizability or rigidity. Here, poly(methyl methacrylate) (PMMA) and PLGA were used for electrohydrodynamic cojetting, because PMMA has a Tg of 115 – 116 °C, which is substantially higher than that of PLGA (47 – 48 °C). Heating the bicompartmental microcylinders to a temperature between the two glass transition temperatures resulted in selective shape-shifting of the PLGA compartment only (Figure 2-5).

Using this approach, a wide range of particles was realized through programmable reconfiguration of microcylinders with previously unseen shapes. Figure 2-6 shows two examples of reconfigured polymer particles. When the weight percentage of PMMA was decreased from 100% (Figure 2-5) to 10% in one compartment (Figure 2-6A), particles underwent increasing bending, which may be attributed to a decreased rigidity of the particles. We further prepared bicompartmental particles with poly(vinyl cinnamate) (PVCi) confined in one compartment. Because PVCi is a photocrosslinkable polymer, exposure to UV light can be used to render the PVCi containing compartments inert to the ultrasound-induced reconfiguration (Figures 2-7D – 2-7F).[38,39] The particle shapes observed here closely resembled the theoretically predicted equilibrium shapes. Specifically, the simulated equilibrium states for bicompartmental PLGA/PLGA (Figure

2-7A – 2-7C) and PVCi/PLGA microcylinders (Figure 2-7D – 2-7F) were in excellent agreement with the experimentally observed particle shapes (See Appendix for the simulational studies in detail). Similarly, tricompartmental PLGA/(PLGA+PVCi)/PLGA cylinders were reconfigured into particles with centrosymmetric polymer backbones (Figure 2-6B). In addition, EHD co-jetting can provide access to distinct and stable colloidal microcylinders with diameters ranging from hundreds of nanometers to hundreds of micrometers (Figure 2-8A). This suggests the potential use of the particles for various applications where colloidal size range is required. Moreover, changes in the aspect ratios of bicompartmental colloidal particles yielded "bull-head" or "ring" particles (Figures 2-8B and 2-8C).

2.4. Summary

In summary, multicompartmental microcylinders with appropriately designed compartments can undergo defined shape-shifting. As multicompartmental microcylinders are exposed to ultrasound as the external stimulus, they reconfigured into near perfect spheres. An interesting aspect of these multicompartmental microcylinders is that compartments can be made of different polymers, which selectively respond to different temperature. The controlled reconfiguration of multicompartmental microcylinders constitutes an important step towards the biomimetic development of adaptive materials with potential applications as sensors, actuators, or switchable drug delivery carriers.

2.5. Figures and Tables
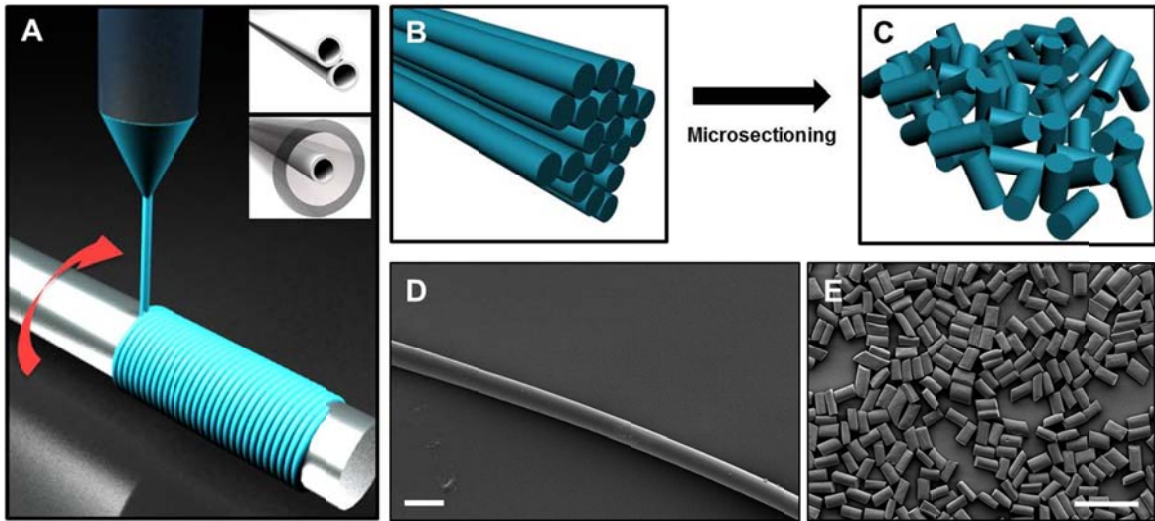
Figure 2-1. EHD co-jetting followed by microsectioning process leads to multicompartmenal microcylinders. (A) Diagram of EHD co-jetting process. Well-aligned PLGA fibers were obtained using a rotating wheel collector. Insets show needle configurations used in this work. (B, D) Scheme and SEM images of microfibers obtained after the jetting. (C, E) Scheme and SEM images of microcylinders that were sectioned from the microfibers at a desired length (30 μm in this case). Scale bars for D and E are 20 μm and 100 μm, respectively.
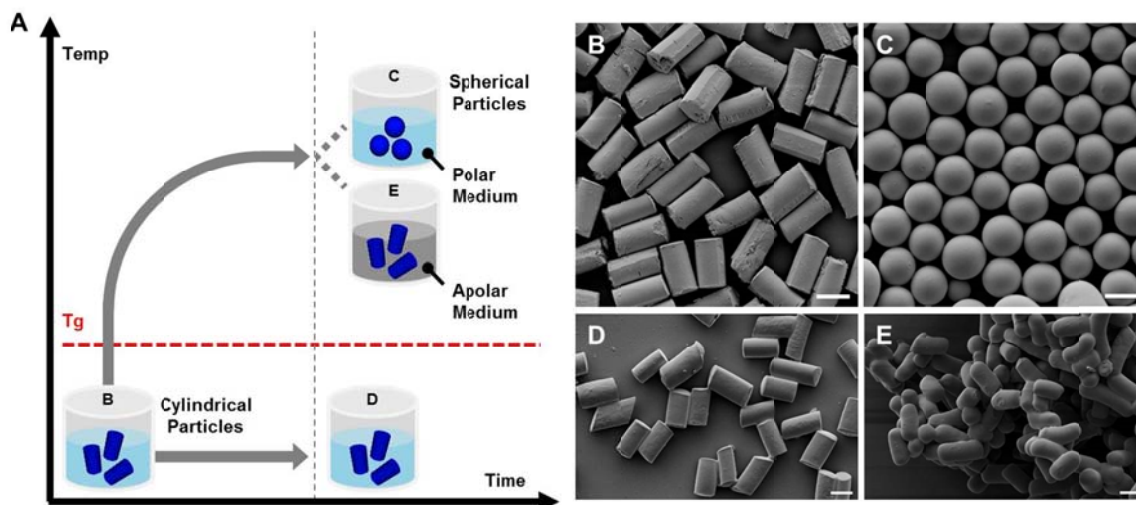
Figure 2-2. Reconfiguration of polymeric microcylinders into microspheres. (A) A graphical representation of temperature versus time relations for the shape-shifting process. (B, C) When polymeric microcylinders are treated with ultrasound, the increase in temperature above the Tg of the polymer causes cylindrical particles to take on a spherical envelope. (D) As control experiments, the microcylinders were treated with ultrasound in an ice bath. The ice bath is used for keeping the temperature below Tg of polymer during sonication. (E) The microcylinders after ultrasound treatment in heptane (bp = 98 °C). Heptane is used as an apolar medium, which does not favor reconfiguration of the microcylinders into spheres. Scale bars are all 20 μm.
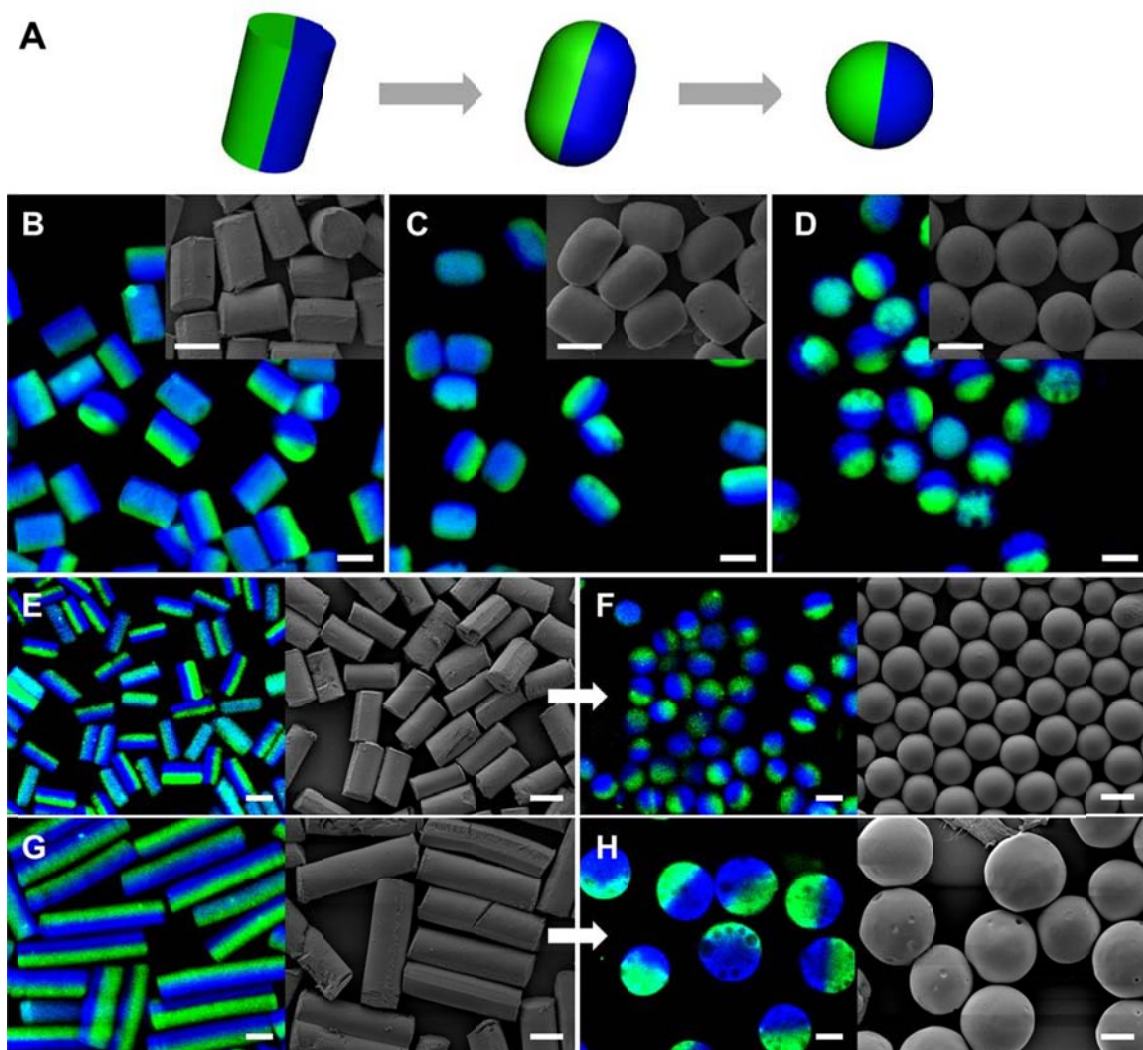
Figure 2-3. Isotropic shape-shifting of microcylinders into microspheres. (A) Scheme of the shape-shifting of bicompartmental particles by ultrasound. (B-D) Corresponding CLSM and SEM (inset) images of bicompartmental microcylinders with 20 μm in diameter and 30 μm in length, before and after shape-shifting (left to right, C indicates an intermediate state). (E-H) Reconfiguration of bicompartmental microcylinders with two different sizes, 15 μm x 30 μm and 20 μm x 70 μm, before (E, G) and after (F, H) shape-shifting. All scale bars are 20 μm.
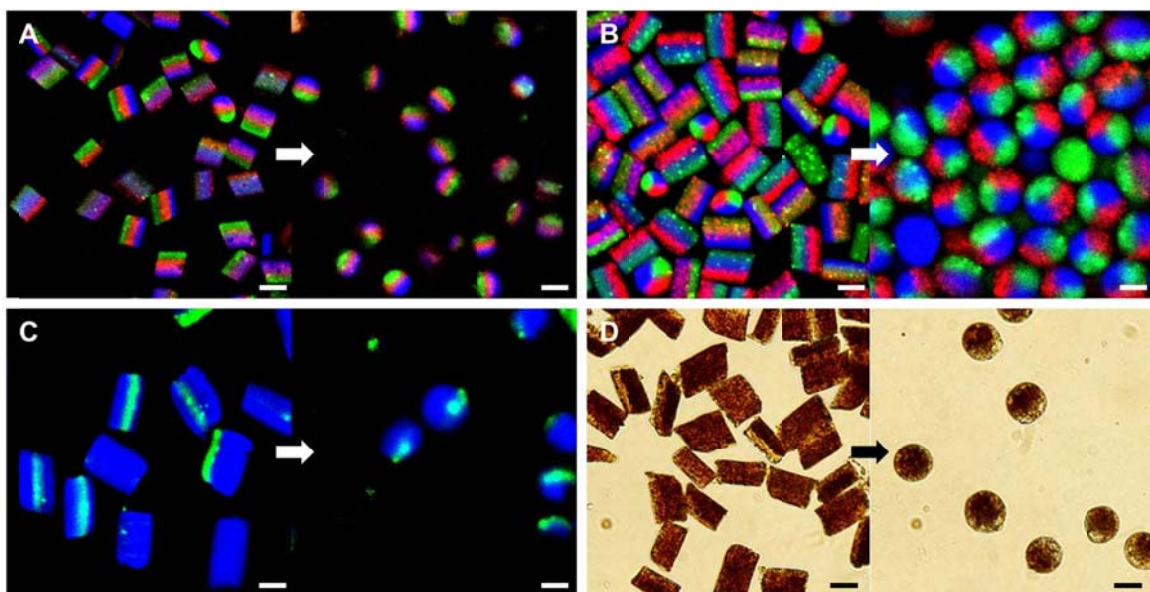
Figure 2-4. More examples of isotropic shape-shifting of microcylinders. (A-D) Reconfiguration of side-by-side tricompartmental, pie-shaped tricompartmental, 7-compartmental, magnetic bicompartmental microcylinders before (left) and after (right) shape-shifting. All scale bars are 20 μm.
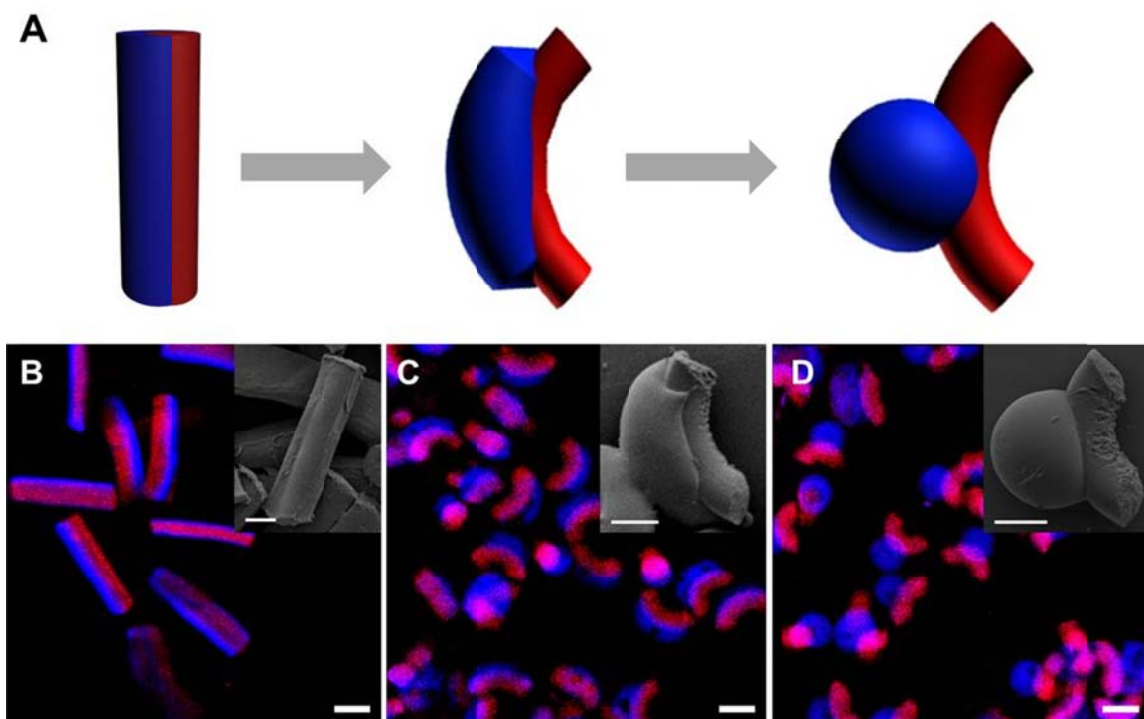
Figure 2-5. Anisotropic shape-shifting of multicompartmental microcylinders. (A) Scheme of the shape-shifting from B to D. (B-D) CLSM and SEM (inset) images of bicompartmental PMMA/PLGA microcylinders before and after (left to right) shape-shifting. The blue and red fluorescent dyes were incorporated in PLGA and PMMA, respectively. Upon ultrasound treatment, only the PLGA compartments were reconfigured into spherical shapes (C indicates an intermediate state). Scale bars in CLSM and SEM images are 20 μm and 10 μm, respectively.
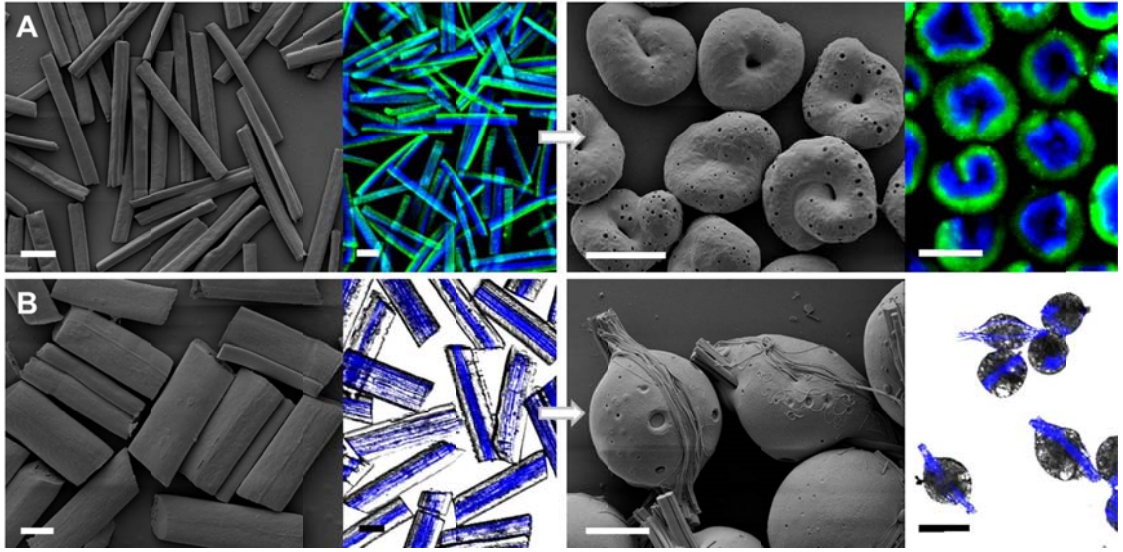
Figure 2-6. Unique shapes of multicompartmental particles with different polymers that were produced from the similar process. (A) SEM (left) and CLSM (right) images of bicompartmenal PLGA/(PLGA+PMMA) microparticles before and after shape-shifting. (B) Tricompartmental PLGA/(PLGA+PVCi)/ PLGA microparticles before and after shape-shifting. Scale bars in A and B are 50 μm and 20 μm, respectively.
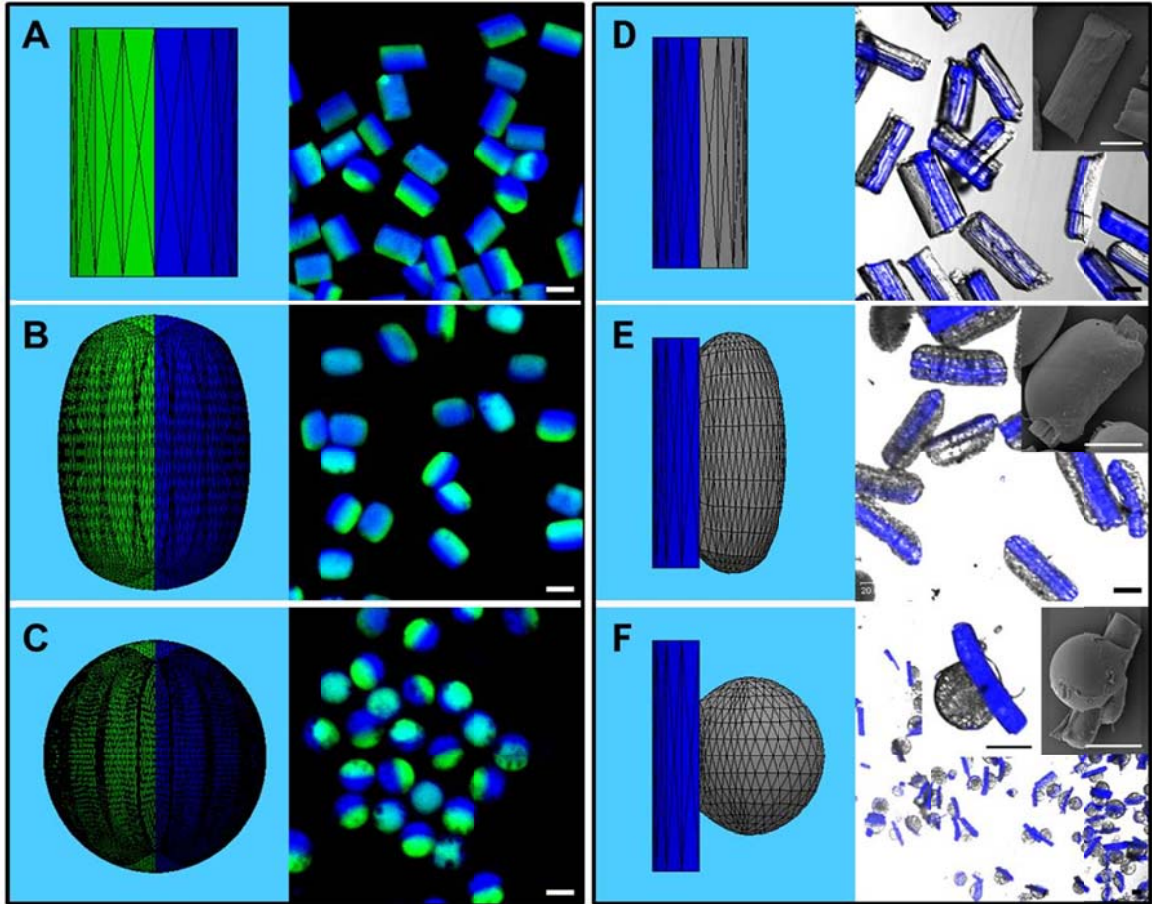
Figure 2-7. Comparison of experimentally obtained shape-shifted particles with expected equilibrium envelopes. (A-C) Bicompartmental PLGA/PLGA microcylinders (top) after evolving into spheres (bottom). (E-F) Bicompartmental PVCi/PLGA microcylinders (top) after evolving into spheres (bottom). In all cases, computational models (left) show good agreements with the CLSM (right) images of each particle. Scale bars are all 20 μm.
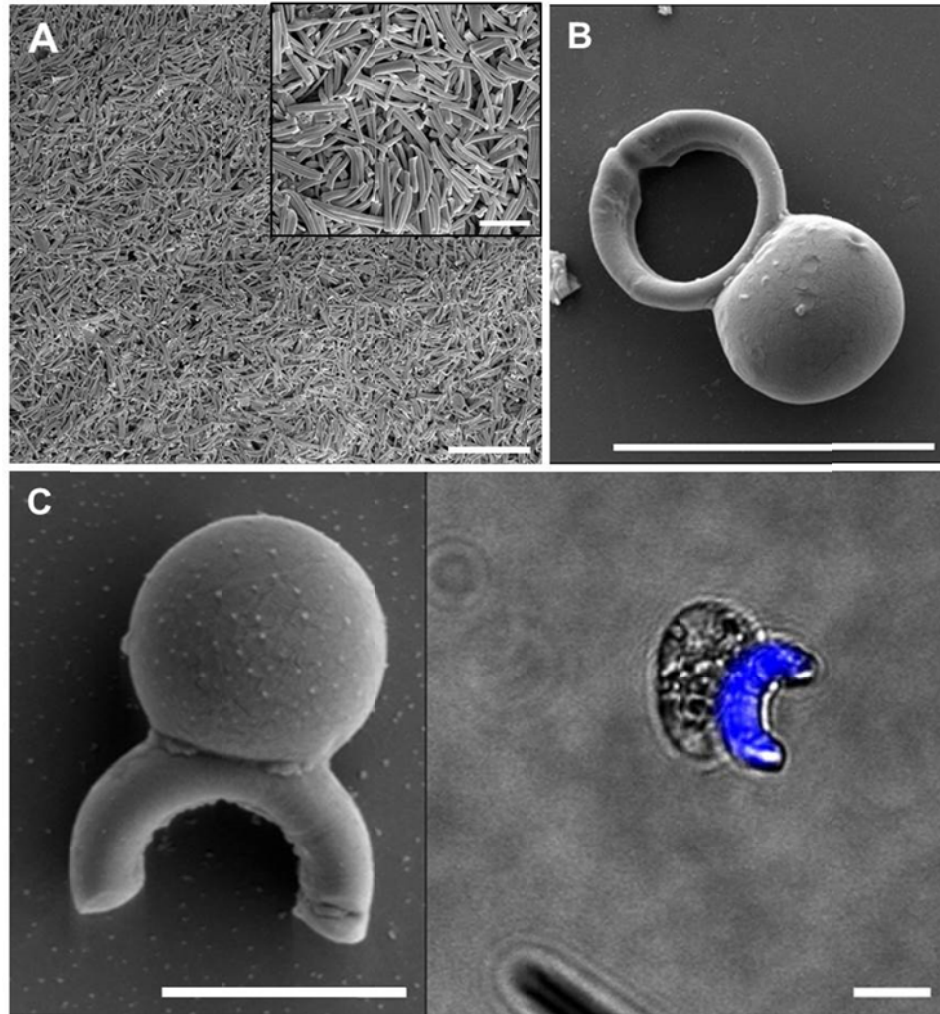
Figure 2-8. (A) SEM images of bicompartmental cylinders showing the possibility of making colloidal size. Scale bars are 20 µm and 5 µm for the inset. (B,C) SEM and CLSM (bottom right) images of bicompartmental PLGA/PS particles after shape-shifting. Scale bars in B and C are 10 µm and 5 µm, respectively.

Microcylinders	Needle Type	Polymer Compositions for Each Compartment
Figures 2-3B – 2-3D		1) 30 % PLGA, blue dye 2) 30 % PLGA, green dye
Figures 2-3E, 2-3F		1) 30 % PLGA, blue dye 2) 30 % PLGA, green dye
Figures 2-3G, 2-3H		1) 30 % PLGA, green dye 2) 30 % PLGA, red dye 3) 30 % PLGA, blue dye
Figures 2-3I, 2-3J		1-6) 30 % PLGA, blue dye 7) 30 % PLGA, green dye
Figures 2-3K, 2-3L		1) 30 % PLGA, green dye 2) 30 % PLGA, red dye 3) 30 % PLGA, blue dye
Figures 2-4B – 2-4D		Shell) 30 % PLGA, blue dye Core) 25 % PMMA, red dye
Figure 2-4E		1) 30 % (PLGA+PMMA, 9:1), blue dye 2) 30 % PLGA, green dye
Figure 2-4F		Shell) 30 % PLGA, no dye Core) 30 % PVCi, no dye
Figure 2-4G		1) 30 % PLGA, no dye 2) 30 % (PLGA + PVCi, 7:3), no dye 3) 30 % PLGA, no dye
Figures 2-6A, 2-6B		Shell) 35 % PLGA, green dye Core) 30 % PS, blue dye

Table 2-1. Summary of the preparation methods for each multicompartmental microcylinder.

Micro-Cylinders	Cylinder Length (μm)	Sonication Medium	Sonication Duration Time (min)
Figure 2-3C	30	2 v/v% Tween 20/DI water	1.5
Figure 2-3D	30	2 v/v% Tween 20/DI water	3
Figure 2-3F	70	2 v/v% Tween 20/DI water	5
Figure 2-3H	30	2 v/v% Tween 20/DI water	3
Figure 2-3J	30	2 v/v% Tween 20/DI water	3
Figure 2-3L	30	2 v/v% Tween 20/DI water	3
Figure 2-4C	50	Ethanol : (2 v/v% Tween 20/DI water), 1:1	1
Figure 2-4D	50	Ethanol : (2 v/v% Tween 20/DI water), 1:1	1.5
Figure 2-4E	200	2 v/v% Tween 20/DI water	2
Figure 2-4F	50	2 v/v% Tween 20/DI water	5
Figure 2-4G	70	2 v/v% Tween 20/DI water	3
Figure 2-6B	10	Ethanol : (2 v/v% Tween 20/DI water), 1:1	1

Table 2-2. Summary of the shape-shifting process for each multicompartmental microcylinder.

2.6. References

1.   Langer, R.; Tirrell, D. A. Designing Materials for Biology and Medicine. *Nature* **2004**, 428, 487-492.
2.   Mitragotri, S.; Lahann, J. Physical Approaches to Biomaterial Design. *Nat Mater* **2009**, 8, 15-23.
3.   Petros, R. A.; DeSimone, J. M. Strategies in the Design of Nanoparticles for Therapeutic Applications. *Nat Rev Drug Discov* **2010**, 9, 615-627.
4.   Kaehr, B.; Shear, J. B. Multiphoton Fabrication of Chemically Responsive Protein Hydrogels for Microactuation. *Proceedings of the National Academy of Sciences* **2008**, 105, 8850-8854.
5.   Yoo, J.-W.; Irvine, D. J.; Discher, D. E.; Mitragotri, S. Bio-Inspired, Bioengineered and Biomimetic Drug Delivery Carriers. *Nat Rev Drug Discov* **2011**, 10, 521-535.
6.   Sacanna, S.; Pine, D. J. Shape-Anisotropic Colloids: Building Blocks for Complex Assemblies. *Current Opinion in Colloid & Interface Science* **2011**, 16, 96-105.
7.   Yoon, J.; Lee, K. J.; Lahann, J. Multifunctional Polymer Particles with Distinct Compartments. *Journal of Materials Chemistry* **2011**, 21, 8502-8510.
8.   Kohane, D. S. Microparticles and Nanoparticles for Drug Delivery. *Biotechnology and Bioengineering* **2007**, 96, 203-209.
9.   Merkel, T. J.; Jones, S. W.; Herlihy, K. P.; Kersey, F. R.; Shields, A. R.; Napier, M.; Luft, J. C.; Wu, H.; Zamboni, W. C.; Wang, A. Z.*; et al.* Using Mechanobiological Mimicry of Red Blood Cells to Extend Circulation Times of Hydrogel Microparticles. *Proceedings of the National Academy of Sciences* **2011**, 108, 586-591.
10.   Decuzzi, P.; Ferrari, M. The Receptor-Mediated Endocytosis of Nonspherical Particles. *Biophysical Journal* **2008**, 94, 3790-3797.
11.   Stevens, M. M.; George, J. H. Exploring and Engineering the Cell Surface Interface. *Science* **2005**, 310, 1135-1138.
12.   Cabeen, M. T.; Jacobs-Wagner, C. Bacterial Cell Shape. *Nat Rev Micro* **2005**, 3, 601-610.
13.   Young, K. D. The Selective Value of Bacterial Shape. *Microbiology and Molecular Biology Reviews* **2006**, 70, 660-703.
14.   Chen, Q.; Bae, S. C.; Granick, S. Directed Self-Assembly of a Colloidal Kagome Lattice. *Nature* **2011**, 469, 381-384.
15.   Yoshida, M.; Lahann, J. Smart Nanomaterials. *ACS Nano* **2008**, 2, 1101-1107.
16.   Stuart, M. A. C.; Huck, W. T. S.; Genzer, J.; Muller, M.; Ober, C.; Stamm, M.; Sukhorukov, G. B.; Szleifer, I.; Tsukruk, V. V.; Urban, M.*; et al.* Emerging Applications of Stimuli-Responsive Polymer Materials. *Nat Mater* **2010**, 9, 101-113.
17.   Lv, S.; Dudek, D. M.; Cao, Y.; Balamurali, M. M.; Gosline, J.; Li, H. Designed Biomaterials to Mimic the Mechanical Properties of Muscles. *Nature* **2010**, 465, 69-73.
18.   Oh, J. K.; Drumright, R.; Siegwart, D. J.; Matyjaszewski, K. The Development of Microgels/Nanogels for Drug Delivery Applications. *Progress in Polymer Science* **2008**, 33, 448-477.
19.   Yoo, J.-W.; Mitragotri, S. Polymer Particles That Switch Shape in Response to a Stimulus. *Proceedings of the National Academy of Sciences* **2010**, 107, 11205-11210.

20.   Schmidt, D. J.; Cebeci, F. C.; Kalcioglu, Z. I.; Wyman, S. G.; Ortiz, C.; Van Vliet, K. J.; Hammond, P. T. Electrochemically Controlled Swelling and Mechanical Properties of a Polymer Nanocomposite. *ACS Nano* **2009**, 3, 2207-2216.

21.   Ancla, C.; Lapeyre, V.; Gosse, I.; Catargi, B.; Ravaine, V. Designed Glucose-Responsive Microgels with Selective Shrinking Behavior. *Langmuir* **2011**, 27, 12693-12701.

22.   Tokarev, I.; Tokareva, I.; Minko, S. Optical Nanosensor Platform Operating in near-Physiological Ph Range Via Polymer-Brush-Mediated Plasmon Coupling. *ACS Applied Materials & Interfaces* **2011**, 3, 143-146.

23.   Fenzl, C.; Wilhelm, S.; Hirsch, T.; Wolfbeis, O. S. Optical Sensing of the Ionic Strength Using Photonic Crystals in a Hydrogel Matrix. *ACS Applied Materials & Interfaces* **2012**, 5, 173-178.

24.   Bartlett, R. L.; Medow, M. R.; Panitch, A.; Seal, B. Hemocompatible Poly(Nipam-Mba-Amps) Colloidal Nanoparticles as Carriers of Anti-Inflammatory Cell Penetrating Peptides. *Biomacromolecules* **2012**, 13, 1204-1211.

25.   Hirata, S.; Tsuji, T.; Kato, Y.; Adachi, C. Reversible Coloration Enhanced by Electrochemical Deposition of an Ultrathin Zinc Layer onto an Anodic Nanoporous Alumina Layer. *Advanced Functional Materials* **2012**, 22, 4195-4201.

26.   Thakur, V. K.; Ding, G.; Ma, J.; Lee, P. S.; Lu, X. Hybrid Materials and Polymer Electrolytes for Electrochromic Device Applications. *Advanced Materials* **2012**, 24, 4071-4096.

27.   Evans, R. C.; Knaapila, M.; Willis-Fox, N.; Kraft, M.; Terry, A.; Burrows, H. D.; Scherf, U. Cationic Polythiophene–Surfactant Self-Assembly Complexes: Phase Transitions, Optical Response, and Sensing. *Langmuir* **2012**, 28, 12348-12356.

28.   Ahn, S.-k.; Kasi, R. M.; Kim, S.-C.; Sharma, N.; Zhou, Y. Stimuli-Responsive Polymer Gels. *Soft Matter* **2008**, 4, 1151-1157.

29.   Bhaskar, S.; Lahann, J. Microstructured Materials Based on Multicompartmental Fibers. *Journal of the American Chemical Society* **2009**, 131, 6650-6651.

30.   Bhaskar, S.; Hitt, J.; Chang, S.-W. L.; Lahann, J. Multicompartmental Microcylinders. *Angewandte Chemie International Edition* **2009**, 48, 4589-4593.

31.   Dendukuri, D.; Tsoi, K.; Hatton, T. A.; Doyle, P. S. Controlled Synthesis of Nonspherical Microparticles Using Microfluidics. *Langmuir* **2005**, 21, 2113-2116.

32.   Shum, H. C.; Zhao, Y.-j.; Kim, S.-H.; Weitz, D. A. Multicompartment Polymersomes from Double Emulsions. *Angewandte Chemie International Edition* **2011**, 50, 1648-1651.

33.   Rolland, J. P.; Maynor, B. W.; Euliss, L. E.; Exner, A. E.; Denison, G. M.; DeSimone, J. M. Direct Fabrication and Harvesting of Monodisperse, Shape-Specific Nanobiomaterials. *Journal of the American Chemical Society* **2005**, 127, 10096-10100.

34.   Champion, J. A.; Katare, Y. K.; Mitragotri, S. Making Polymeric Micro- and Nanoparticles of Complex Shapes. *Proceedings of the National Academy of Sciences* **2007**, 104, 11901-11904.

35.   Sung, K. E.; Vanapalli, S. A.; Mukhija, D.; McKay, H. A.; Mirecki Millunchick, J.; Burns, M. A.; Solomon, M. J. Programmable Fluidic Production of Microparticles with Configurable Anisotropy. *Journal of the American Chemical Society* **2008**, 130, 1335-1340.

36.   Ferrara, K. W.; Borden, M. A.; Zhang, H. Lipid-Shelled Vehicles: Engineering for Ultrasound Molecular Imaging and Drug Delivery. *Accounts of Chemical Research* **2009**, 42, 881-892.

37.   Caruso, M. M.; Davis, D. A.; Shen, Q.; Odom, S. A.; Sottos, N. R.; White, S. R.; Moore, J. S. Mechanically-Induced Chemical Changes in Polymeric Materials. *Chemical Reviews* **2009**, 109, 5755-5798.

38.   Brakke, K. The Surface Evolver. *Exp Math* **1992**, 1, 141-165.

39.   Lee, K. J.; Hwang, S.; Yoon, J.; Bhaskar, S.; Park, T.-H.; Lahann, J. Compartmentalized Photoreactions within Compositionally Anisotropic Janus Microstructures. *Macromolecular Rapid Communications* **2011**, 32, 431-437.

CHAPTER 3

Self-Assembly of Amphiphilic Particles at Liquid-Liquid Interfaces

The material in this chapter has been adapted with minor modifications from the following article:

J. Yoon, S. Bhaskar, A. Kota, A. Tuteja, J. Lahann," Colloidal Surfactants based on Amphiphilic Janus Particles", *In Preparation*

3.1. Motivation and Background

Janus particles, i.e., particles displaying two regions of distinct properties, have been widely studied for the past years because of their wide range of potential applications.[1-14] Such particles are important for colloidal surfactants,[1-4] therapeutic delivery,[5-7] imaging,[8] sensing materials,[9] display device,[10,11] or catalysts.[12-14] In particular, Janus particles having distinctly different polarities may align at the interface between different immiscible media, similar to surfactants. In addition, unlike isotropic particles, Janus particles can provide selective control over the surface chemistry of each half compartment.[15-17] Binks and coworkers investigated the assembly of various particles on liquid-liquid interfaces. Their theoretical studies suggest that "Janus" particles have a higher stability upon adsorption to liquid-liquid interfaces than isotropic particles.[18] This

was attributed to the surfactant-like amphiphilicity of Janus particles creating greater changes in surface tension of liquid than isotropic particles. Furthermore, there have been studies emphasizing the role of different shapes on the self-assembly of amphiphilic Janus particles.[3,19]

Current progress is, however, hampered by the lack of suitable synthesis routes, which allow for precise engineering of critical particle properties, such as the chemical nature and geometric distribution of the surface patches or the variable choice of materials combinations for the individual compartments.[20] Therefore, the area of synthesizing amphiphilic Janus particles with diverse spectrum of shape, size, and functionality could potentially serve as useful tools for developing new types of colloidal systems.

In this work, we report electrohydrodynamic (EHD) co-jetting[21-23] as a facile method to produce amphiphilic Janus particles with precisely tailored interfacial properties. By passing two or more parallel polymer solutions through electrified capillaries, solid particles with multiple compartments can be prepared.[21] This method has been used to create meso- to nanoscale particles and fibers displaying independent control over bulk properties as well as surface functionalities of the particles.[6,24,25]

In this study, we extended the existing experimental approach to prepare Janus particles that are composed of both hydrophilic and hydrophobic interfacial regions. To impart hydrophobicity, a highly fluorinated fluorodecyl-polyhedral oligomeric silsesquioxane (F-POSS) was selectively introduced in one of the compartments. Such molecules are known to form superhydrophobic surfaces when deposited as thin films, owing to their extremely low surface energy.[26,27] To create amphiphilic properties, the

second compartment was comprised of poly(vinyl acetate) (PVAc), which, after partial hydrolysis into a poly(vinyl alcohol), displayed pronounced hydrophilic surface properties. The appropriate balance of hydrophilic and hydrophobic domains resulted in colloidal particles with surfactant-like properties, such as spontaneous self-assembly at liquid-air and liquid-liquid interfaces.

3.2. Experimental Methods

3.2.1. Materials

Poly(methyl methacrylate) (PMMA, Mw = 120 000 g mol-1), poly(vinyl acetate) (PVAc, Mw = 140 000 g mol-1), sodium hydroxide (NaOH), N-(3-Dimethylaminopropyl)-N′-ethylcarbodiimide (EDC) were purchased from Sigma-Aldrich, USA, N-Hydroxysulfosuccinimide (NHS) was purchased from Thermo Scientific, and rhodamine polyethylene glycol acid (RB-PEG-COOH, Mw = 3 000 g mol-1) was purchased from Nanocs, Inc, USA. 1H,1H,2H,2H-Heptadecafluorodecyl polyhedral oligomeric silsequioxane (F-POSS) was synthesized as described elsewhere.[26,28] The fluorescence dyes poly[(m-phenylenevinylene)-alt-(2,5-dibutoxy-p-phenylenevinylene)] (MEHPV) and poly[tris(2,5-bis(hexyloxy)-1,4-henylenevinylene)-alt-(1,3-phenylenevinylene)] (PTDPV), which were used as confocal laser scanning microscopy (CLSM) markers with blue and green emission, were purchased from Sigma-Aldrich, USA. The solvents tetrahydrofuran (THF), N,N'-dimethyl formamide (DMF), heptane, and hexadecane were purchased from Sigma-Aldrich, USA, Asahiklin AK-225 (AK) was purchased from SPI Supplies, USA. All solvents were used without further purification.

3.2.2. Instrumental Details

Confocal laser scanning microscopy (CLSM): The particles were visualized using a CLSM (Olympus, FluoView 500). Three different lasers, 405 nm laser, 488 nm Argon laser, and 533 nm Helium-Neon green (HeNeG) laser, were used to excite the dyes MEHPV, PTDPV, and rhodamine groups of RB-PEG-COOH, respectively. The barrier filters were set to 430-460 nm for MEHPV, 505-525 nm for PTDPV, and 560-600 nm for RB-PEG-COOH.

Scanning electron microscopy (SEM): The samples were coated with gold before analysis and the particle morphology was examined using an AMRAY 1910 Field Emission Scanning Electron Microscope (FEG-SEM).

Zeta Potential: The zeta potential of particles before and after the hydrolysis reaction were determined by using Zetasizer Nano ZS (Malvern Instrument, UK)

Fourier transformed infrared (FT-IR) spectroscopy: The particle suspensions before and after the hydrolysis were deposited on Au-coated Si substrates and dried under vacuum for overnight. The measurements were performed on a Nicolet 6700 spectrometer utilizing the grazing angle accessory (Smart SAGA) at a grazing angle of 85°.

3.2.3. Preparation of PMMA Janus Particles

Two different polymer solutions were prepared in separate vials. 3 w/v % of PMMA was dissolved in a solvent mixture of THF, DMF, and AK (50 : 45 : 5, v/v/v), and 0.3 w/v % (10 % by weight of PMMA) of F-POSS was incorporated in the same solution. Another solution contained both PMMA and PVAc (1 : 2, w/w), with a

concentration of 3 w/v % of total weight of polymers, were dissolved in the same ratios of solvents. The experimental setup contained a syringe pump (Fisher Scientific, Inc., USA), a power supply (DC voltage source, Gamma High Voltage Research, USA), and an aluminum foil as a flat collector. The two polymer solutions were delivered at a constant flow rate of 0.1 ml/h via vertically positioned syringes equipped with 26 G needles (Hamilton Company, USA). When a driving voltage of 6 kV was applied to the polymer solution, stable Taylor cone was formed and particles were collected at a distance of 40 cm. The temperature and humidity were maintained to 25 $^{\circ}$C and 32 %, respectively.

3.2.4. Surface Hydrolysis of Particles

4 mL of 0.01 M NaOH solution was added to 11 mL of the particle suspension (5.0 x 10^6 particles/mL), and the solution was stirred at 40 $^{\circ}$C for 1 hr for the surface hydrolysis of PVAc to PVA. After the reaction, the particles were washed with a centrifugal filter to remove excess NaOH until the pH of solution reached 7.

3.2.5. Rhodamine-labled Particles by EDC/NHS Coupling

Surface hydrolysis of the particles was confirmed by conjugating dye molecules selectively on one side of the particles. The carboxyl groups of RB-PEG-COOH was activated with EDC and sulfo-NHS to form reactive NHS esters, and then covalently attached to the hydroxyl groups on the particle surface. Detailed reaction conditions are as follows. 950 uL of 10 mM RB-PEG-COOH/PBS with 0.01 v/v% Tween 20 was stirred with 40 mM EDC for 10 min, and then 10 mM NHS was incorporated into the solution

for 10 min. Next, 50 uL of the particle suspension (5.0×10^7 particles/mL in 0.01 v/v% Tween 20/PBS) was reacted with the solution for 2 hours. After the reaction, the particles were washed 20 times by centrifugation to remove any unreacted chemicals.

3.2.6. Fractionation of Particles

Once particles were collected from the jetting collector, it was required to fractionate the particles prior to their applications. Centrifugation allowed suspended particles to be separated into fractions of different sizes (Figure 3-3A). The PMMA Janus particles were fractionated by centrifugation (Centrifuge 5810R, Eppendorf) at 2000 RPM for 1 min. The pellet had an average particle size of 2 $\alpha\mu$m, and was resuspended in a different vial (Figure 3-3B). The supernatant had an average particle size of 300 nm, as confirmed by DLS (Zetasizer Nano ZS, Malvern Instruments, UK), and was suspended separately (Figure S1B). The particle concentration of 5.0×10^7 particles/mL was measured by using particle analyzer (qNano, Izon).

3.2.7. Surface Energy Analysis

The substrates for surface energy analysis were prepared by spin-coating silicon wafers (2 cm long x 2 cm wide) with the desired polymer solution at 2000 RPM using a Specialty Coating Systems Spincoater G3P–8.

The contact angle measurements were conducted using a Ramé-Hart 200-F1 goniometer. All the advancing contact angles reported in this work were measured by advancing a small volume of liquid ($\sim$ 2 μL) onto the surface using a 2 mL micrometer syringe (Gilmont). At least three measurements were performed on each substrate.

3.2.8. Self-Assembly of Particles at Oil-Water Interfaces

0.5 mL of particle suspension (5.0×10^7 particles/mL) and 0.5 mL of heptane were mixed by ultrasonication (Qsonica Q700, amplitude 10 %) for 5 sec for vigorous mixing of two liquids. In the case of the particles surrounding oil droplets in water, 5 uL of hexadecane were agitated with 0.5 mL of particle suspension and placed in a glass bottom well plate for 1 day. The particles at the interface of oil and water were imaged through z-stacks from CLSM and then three-dimensional (3D) reconstruction of the particles was made using Imaris software.

3.2.9. Quantitative Analysis of Selective Particle Orientation at the Interface

The orientation of each particle at the interface was analyzed from microscopic images for a total of 4 different samples using Matlab image processing software. 3D reconstructions of the particles taken from the interface were used for the analysis. Edges of blue and green domains were displayed and overlaid to calculate the average number of particles selectively oriented at the interface.

3.3. Results and Discussion

Conceptionally, the herein developed synthetic route towards amphiphilic colloids was inspired by our previously work on the EHD co-jetting of polymer solutions.[21] By processing two or more parallel polymer solutions with distinct chemical composition through electrified capillaries, solid particles with multiple distinct compartments can be prepared.[21] As outlined in Figure 3-1A, we selected conventional poly(methyl

methacrylate) (PMMA) as the base polymer for all amphiphilic polymer particles that were prepared in this work. PMMA is a widely chosen polymer for its good solubility in common solvents and easy processing via electrohydrodynamic jetting.[24,29,30] It is considered as a hydrophilic polymer with the water contact angle of 75°, and has a rigid backbone that provides good structural support without deformation or degradation overtime. While both solutions contained PMMA as the major polymer component, two different functional additives, either F-POSS or PVAc, were incorporated into the respective jetting solutions. The addition of highly fluorinated F-POSS is a probate mean to impart superhydrophobicity to the surfaces of polymer blends, because it has been well-established that the POSS additives tend to migrate to the surface of the blend due to phase separation between two components.[26,31,32] To induce amphiphilicity, the second compartment was comprised of a blend of PVAc and PMMA. While PVAc is sufficiently apolar to be compatible with the polymers and solvents used for preparing the jetting solutions, this polymer can easily be converted into a hydrophilic polymer, i.e., PVA; after particle preparation. Simple base-catalyzed hydrolysis of interfacial acetate groups leads to hydrophilic PVA segments on the particle surface.

To achieve selective encapsulation of F-POSS and PVAc in the respective PMMA compartment, various jetting parameters had to be considered, including polymer concentration, solvent, and flow rate. As we aimed to produce microparticles, the jetting solutions were prepared at relatively low polymer concentrations (3 w/v%). The intrinsic problem of using F-POSS as an additive is its limited solubility in common organic solvents. In fact, such fluorinated compounds tend to dissolve only in fluorinated solvents, and their low dielectric constants make them difficult to be processed by EHD co-

jetting.[27] Thus, once PMMA was selected as the base polymer, it was important to identify an appropriate solvent system. While the majority of solvents used here are comprised of THF and DMF, which were chosen to provide uniform particle shapes, a minimum amount of fluorinated solvent (AK-225, 5 vol% of total solvents) had to be added to dissolve the F-POSS. Hence, the hydrofluorocarbon (AK-225) was mixed with organic solvents (THF : DMF : AK-225 = 50 : 45 : 5) and two different jetting solutions - one containing PMMA/POSS and the second containing PMMA/PVAc - were separately transferred through adjacent capillaries at a constant flow rate of 0.1 ml/h. When a voltage of 6 kV was applied, the droplet which was formed at the end tip of capillaries started to eject to create highly uniform bicompartmental particles.

After synthesis, the Janus character of the particles was confirmed via direct visualization. Either blue or green fluorescent dyes were added to the two different jetting solutions. These dyes enabled subsequent differentiation between the compartments of the as-jetted particles by CLSM. CLSM images demonstrate the successful preparation of bicompartmental particles as indicated by the confinement of blue (PMMA/PVAc) and green (PMMA/F-POSS) fluorescent dyes within distinct compartments of the same particles (Figure 2B).

For these Janus particles to exhibit amphiphilic properties, the compartmentalization of the additives is a necessary, but not sufficient requisite. Moreover, the surface-active additives will have to be present at the surface of the representative hemisphere. In the case of the highly fluorinated F-POSS, previous work already showed that F-POSS migrates onto the surface of particles.[26] Here, we confirmed a similar behavior in the blend of PMMA and F-POSS in model studies with thin

polymer films. For this purpose, the same polymer blend used for electrohydrodynamic co-jetting was spin-casted. The surface topography was directly observed through atomic force microscopy (AFM) to identify POSS domains. Additionally, contact angle measurements of the film were performed to confirm the presence of the POSS molecules on the surface.[26]

Secondly, to unambiguously confirm the presence of polar hydroxyl groups in the PVA/PVAc compartment, control particles were prepared by EHD co-jetting. The acetate groups were partially hydrolyzed to yield partially protected poly(vinyl alcohol) (PVA) (Figure 3A). While increasing the hydroxyl groups on the hemisphere surface promotes hydrophilicity, it is important to perform the hydrolysis reaction under mild conditions. This is to prevent full deprotection of PVAc, which will render this polymer water-soluble and could result in dissolution of the polymers leaving behind the more hydrophobic PMMA. As shown in Figure 3B, particle morphologies were still maintained after hydrolysis indicating that the hydrolysis of PVAc was restricted to the surface, and did not occur throughout the entire bulk.

Next, the shape of the bicompartmental PMMA particles was characterized by SEM (Figure 3-2A). The SEM images confirm that EHD co-jetting of bicompartmental PMMA solutions resulted in uniform spherical particles, albeit with a bimodal size distribution. The narrow distribution and uniform shapes of particles are important factors in stabilizing immiscible liquids as they lead to very efficient packing of particles at the interface.[33,34] We estimated that the tolerable polydispersity in subsequent self-assembly experiments is in the range of 20 % to 30 %. Thus, we decided to refine the initial particle population by centrifugal separation (Figure 3-3A). Centrifugation at 2,000 rpm for 1min

resulted in two sets of particle samples having average particle diameters of 0.30 ± 0.04 μm (Figure 3-3B) and 2.19 ± 0.47 μm, respectively (Figure 3-3C). The particle sizes of 300 nm can be expected to be preferential for a range of different applications because smaller particles are more efficient in preparing well-packed layer at the interface[33]. However, we continued the study with the particles with 2 μm fraction, and this was due to the resolution limit of confocal microscopy. The micrometer-sized particles had to be used to ensure proper visualization of the orientation of individual particles at the interface.

The presence of hydroxyl groups on the particle surface was further demonstrated by zeta potential measurements and FT-IR spectroscopy. Figure 3C shows FT-IR spectra of particles before and after surface hydrolysis of PVAc. The increase in the intensity of characteristic peaks of OH groups near 3300 cm^{-1} indicates partial hydrolysis of acetate groups to hydroxyl groups. Additionally, zeta potential values of the particles support the results obtained in the FT-IR analysis. The zeta potential of the particles before the hydrolysis of PVAc was + 0.05 mV demonstrating there are acrylate and acetyl groups with neutral surface charge. After conversion of PVAc to PVA, the zeta potential values decreased to - 18.3 mV. The negative surface charge was attributed to the dissociation of a proton from newly created hydroxyl groups on the surface. Thus, as the particles become hydrolyzed, the hydroxyl contents increase, and that makes the surface more negatively charged. Finally, the distribution of hydroxyl groups on the particle surfaces was unambiguously demonstrated by conjugation of a carboxylic acid-terminated fluorescent probe to free interfacial hydroxyl groups. For this purpose, rhodamine-PEG-carboxlic acid was activated using 1-ethyl-3-(3-dimethylaminopropyl) carbodiimide

hydrochloride (EDC) and N-hydroxysulfo-succinimide sodium salt (NHS, Figure 4A). After the reaction, the resulting rhodamine-conjugated particles were characterized by CLSM (Figure 4B and 4C). Red fluorescence was restricted to the PMMA/PVA compartment, which was encoded with a blue dye. No overlay of red fluorescence with the green fluorescence of the PMMA/POSS compartment was observed indicating successful confinement of the hydroxyl groups to one hemisphere only.

In order to quantify the degree of hydrophilicity and hydrophobicity of our Janus particles, we estimated the surface energy using the Owens-Wendt approach.[35] According to this approach, the solid surface energy is the sum of contributions from two types of intermolecular forces at the surface:

$$\gamma_{sv} = \gamma_{sv}^d + \gamma_{sv}^p \tag{1}$$

Here γ_{sv}^d is the component that accounts for the dispersive forces, while γ_{sv}^p is the component that accounts for the polar forces. Further, this approach postulates that:

$$\gamma_{sl} = \gamma_{sv} + \gamma_{lv} - 2\sqrt{\gamma_{sv}^d \gamma_{lv}^d} - 2\sqrt{\gamma_{sv}^p \gamma_{lv}^p} \tag{2}$$

Here, γ_{lv}^d and γ_{lv}^p are the dispersive and polar components of the liquid surface tension, respectively. Combining Eqs. 1 and 2 with the Young's equation[36] and recognizing that the polar component of liquid surface tension is zero ($\gamma_{lv}^p = 0$) for non-polar liquids such as oils, the dispersive component of solid surface energy is given as:

$$\gamma_{sv}^d = \gamma_{lv}\left(\frac{1+\cos\theta}{2}\right)^2 \tag{3}$$

In Eq. 3, γ_{lv} is the surface tension of a non-polar liquid and θ is the equilibrium

contact angle of the same non-polar liquid on the solid surface. We used hexadecane (γ_{lv}

= 27.5 mN/m) as the non-polar liquid to estimate γ_{sv}^{d}. After determining the dispersive

component γ_{sv}^{d}, combining Eqs. 1 and 2 with the Young's equation for a polar liquid (γ_{lv}^{p}

$\neq$ 0), the polar component of the solid surface energy is given as:

$$\gamma_{sv}^{p} = \frac{1}{\gamma_{lv}^{p}} \left[\frac{\gamma_{lv}(1+\cos\theta)}{2} - \sqrt{\gamma_{sv}^{d}\gamma_{lv}^{d}} \right]^{2}$$

(4)

In Eq. 4, γ_{lv} is the surface tension of a polar liquid and θ is the equilibrium

contact angle for the same polar liquid on the solid surface. We used water (γ_{lv}^{d} = 21.1

mN/m and γ_{lv}^{p} = 51.0 mN/m) as the polar liquid to estimate γ_{sv}^{p}.

Table 3-1 summarizes the solid surface energy values estimated by the Owens-

Wendt approach. These values were estimated by measuring the advancing contact angles

(θ_{adv}) for hexadecane and water on substrates spin-coated with blends of PMMA +

fluorodecyl POSS and PMMA + PVAc (both before and after hydrolysis). The PMMA +

fluorodecyl POSS blend possesses a low solid surface energy with a predominant

dispersive component. This renders the surface of PMMA + fluorodecyl POSS blend

hydrophobic. In comparison, PMMA + PVAc blend before hydrolysis possesses a higher

surface energy with a higher polar component. Consequently, the surface of PMMA +

PVAc blend before hydrolysis is relatively more hydrophilic compared to the surface of

PMMA + F-POSS blend. Upon hydrolysis, the polar component of surface energy for

PMMA + PVAc blend increases further, thereby increasing its hydrophilicity.

Although it is difficult to measure contact angles of a particle at a liquid-liquid interface, the water contact angle measurements of the polymer films can be a reliable evidence to demonstrate wetting behaviors of each polymer compositions. The approach introduced here not only reveals the amphiphilic character of the particles, but also signifies the ways to characterize the detachment energy of the particles at the liquid-liquid interface, which can be useful in monitoring the stability of colloidal surfactants.

Finally, we experimentally confirmed the surfactant-like behavior of these amphiphilic Janus particles placed on mixtures of two immiscible liquids. Initially, the Janus particles were immersed into a mixture of heptane and water. From our initial experiments, we concluded that the particles were amphiphilic, i.e., they possess both hydrophobic and hydrophilic surface regions. For self-assembly, the particle geometry, e.g., shape, size, and size distribution, are important factors that can influence the degree of self-organization at liquid-liquid interfaces. Thus, the shape of the bicompartmental PMMA particles was analyzed by SEM (Figure 2A). The SEM images confirm that EHD co-jetting of bicompartmental PMMA solutions resulted in uniform spherical particles, albeit with a bimodal size distribution. A narrow size distribution and uniform shapes of particles are believed to lead to more efficient organization of the surfactant-like particles at the interface.[33,34] Thus, we further refined the initial particle population by centrifugal separation. Centrifugation at 2,000 rpm for 1 min resulted in two sets of particle samples having average particle diameters of 0.30 ± 0.04 μm and 2.19 ± 0.47 μm, respectively (Figure S1). The particle sizes of 300 nm can be expected to be preferential for a range of different applications, because smaller particles tend to be more efficient in preparing well-packed layer at the interface[33]. However, we still conducted the self-assembly study

with particles with an average diameter of 2 μm to ensure proper visualization of the compartments of individual particles at the interface by CLSM. This is a prerequisite for confirming the orientation of the Janus particles at the liquid-liquid interface.

After initial agitation, the aqueous suspension of particles spontaneously self-assembled at the interface between the oil and water phases (Figure 5A, right). In order to confirm their equilibrium orientation, the bicompartmental particles were then imaged by CLSM. As expected, the selected size range of the microparticles allowed for direct imaging of the orientation of the assembled particles. The compartments presenting polar hydroxyl groups were facing the aqueous phase, while the F-POSS-containing PMMA compartments pointed towards the heptane phase (Figure 5B and see Supporting Information Movie S1). Much like surfactants, the amphiphilic Janus particles were minimizing interfacial energy by self-organizing into two-dimensional colloidal sheets. The quantitative analysis of these images confirmed that more than 94 % of the particles were selectively oriented at the interface (Figure S2). These results correlate well with the case, where the amphiphilic particles were incubated with hexadecane-in-water mixtures. Again, the stabilization of hexadecane droplets in water was promoted by the bicompartmental microparticles, as observed by CLSM imaging (Figure 5C). Due to their surfactant-like properties, the hydrophilic and hydrophobic compartments were fully exposed to either aqueous or oil phases, respectively. For reference, isotropic particles that were composed of PMMA only preferred to locate in the water phase (Figure 5A, left).

3.4. Summary

Diverse synthetic routes to fabricate amphiphilic Janus particles are beneficial for the rapid advancement in colloidal surfactants. Here, we have introduced an efficient approach to fabricate well-defined amphiphilic Janus particles by using our EHD co-jetting method. This approach allows for fully decoupling the choice of materials used in two compartments of the same particle. Selective encapsulation of F-POSS in a first compartment significantly lowered the surface energy of one hemisphere. Encapsulation and subsequent hydrolysis of PVAc in the second compartment increased the hydrophilicity of the second hemisphere, while maintaining their uniform size and shape. Moreover, successful integration of asymmetrical (i.e., polar and apolar) functionalities in each compartment was demonstrated by self-assembly of the obtained particles at liquid-liquid interfaces. We believe this straightforward approach may have significant influences on further theoretical studies as well as a number of different applications.
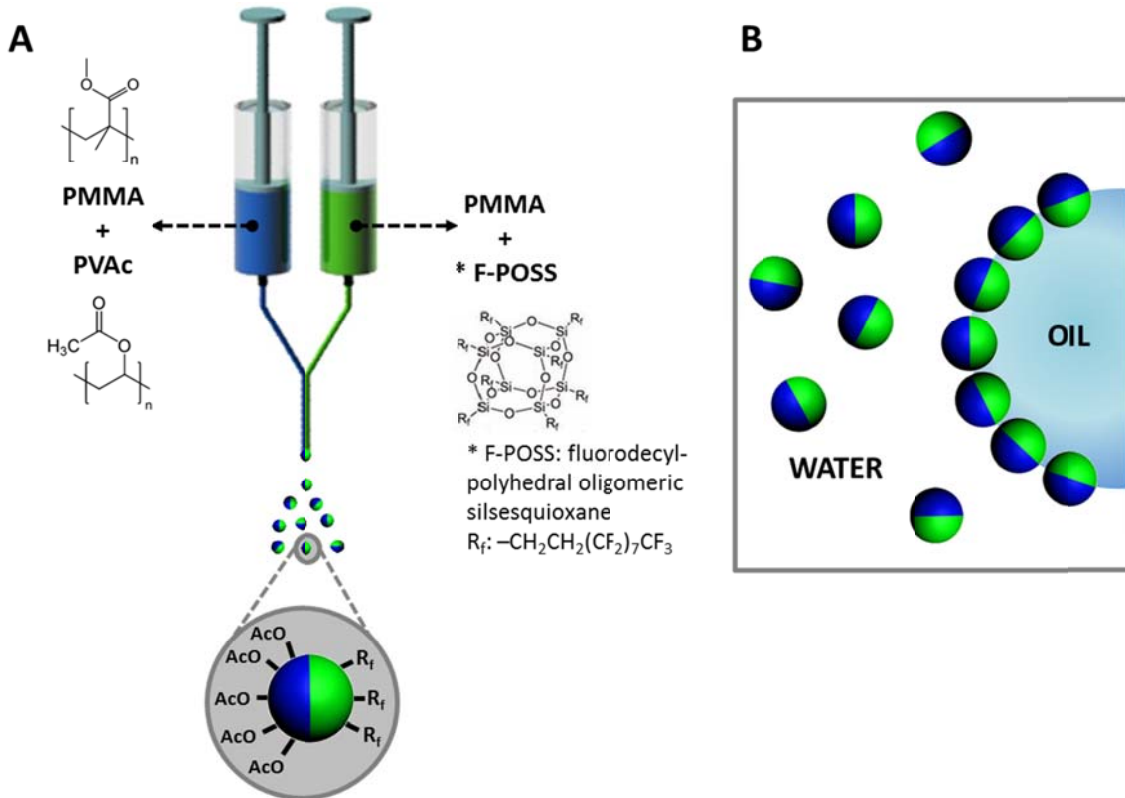
Figure 3-1. Preparation of amphiphilic Janus particles. (A) Fabrication scheme of bicompartmental PMMA particles having PVAc and F-POSS in each compartment via EHD co-jetting. (B) Diagram showing possible self-assembly of resulting particles at a liquid-liquid interface.
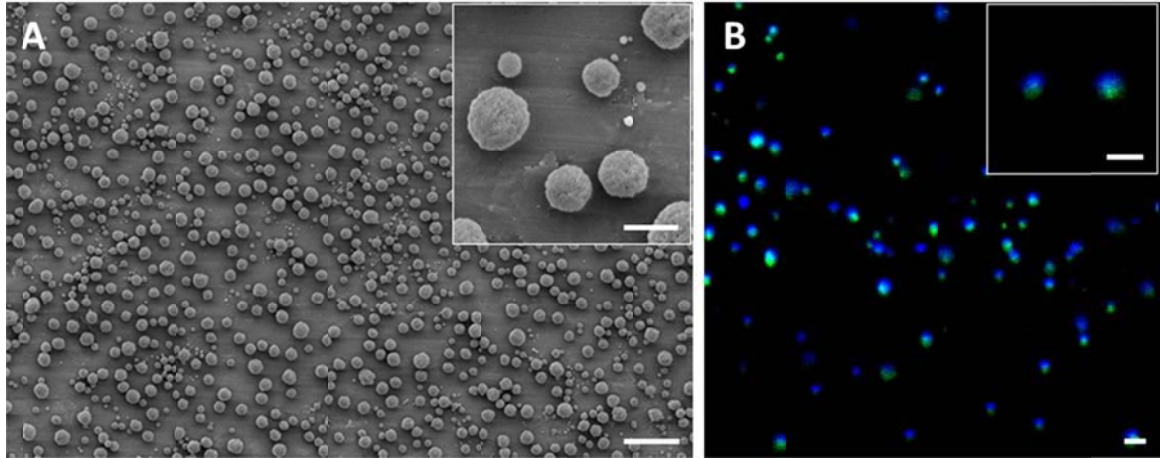
Figure 3-2. Bicompartmental PMMA particles directly after preparation through EHD co-jetting. Two additives, PVAc or F-POSS, were confined in two different hemispheres. (A) SEM images showing well-defined spherical shapes of the obtained particles. Scale bars are 10 μm and 2 μm for the inset. (B) CLSM images of the corresponding particles. Each compartment was labeled with blue (PMMA/PVAc) and green (PMMA/F-POSS) fluorescent dyes for the visualization. Scale bars are all 2 μm.
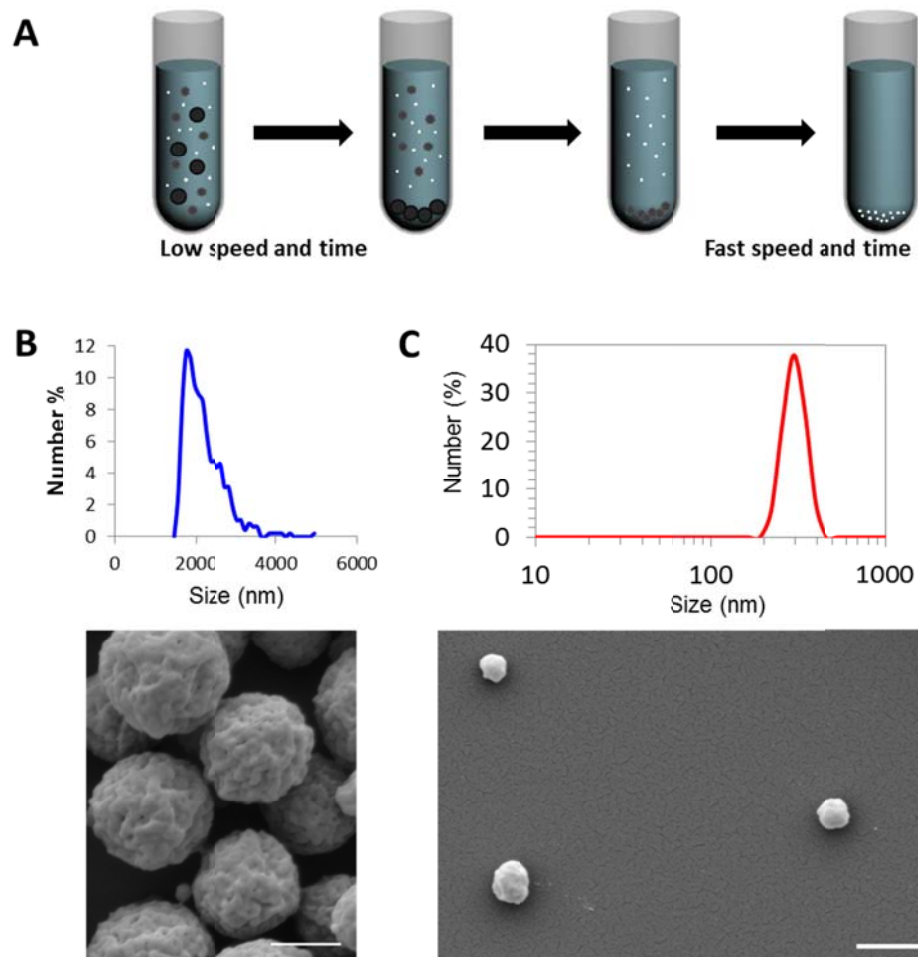
Figure 3-3. Fractionation of particles by using centrifugation. (A) Scheme showing basic principles of centrifugal separation. (B, C) Size distribution analysis and SEM images of the fractionated particles with average diameters of 2 μm (B, as confirmed by tunable resistive pulse sensing (qNano)) and 300 nm (C, as confirmed by DLS). All scale bars are 1 μm.
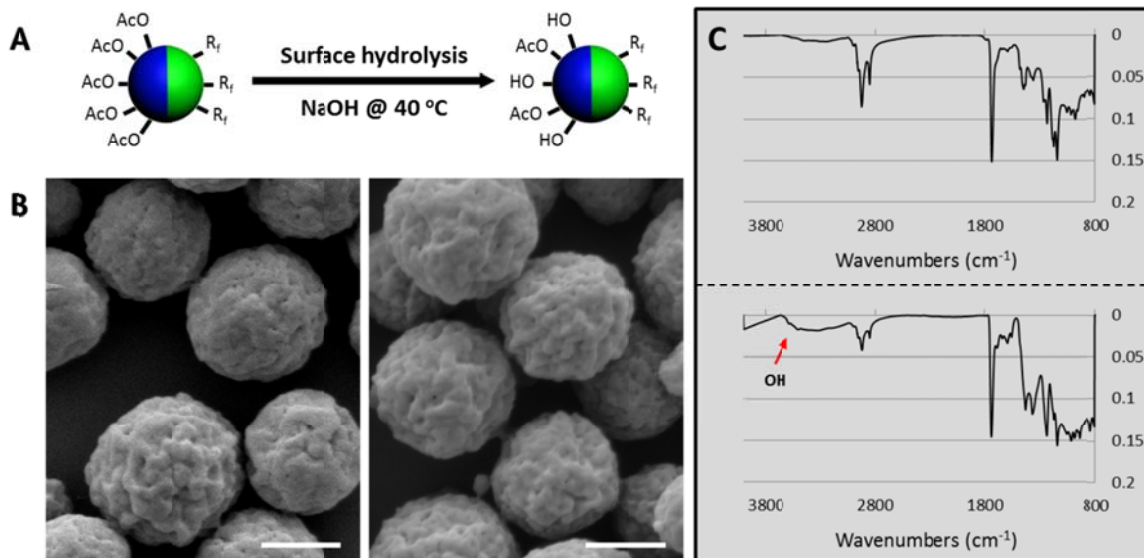
Figure 3-4. Surface modification of bicompartmental PMMA particles. (A) Surface hydrolysis of PVAc to PVA under basic condition. Selective hydrolysis of the PVAc (blue) compartment renders this hemispheric surface hydrophilic. (B) SEM images of the particles before (left) and after (right) hydrolysis show no changes in particle morphology, which indicates that the reaction was restricted to the particle surfaces. Scale bars are all 1 μm. (C) FT-IR spectra of the corresponding particles before (top) and after (bottom) hydrolysis.
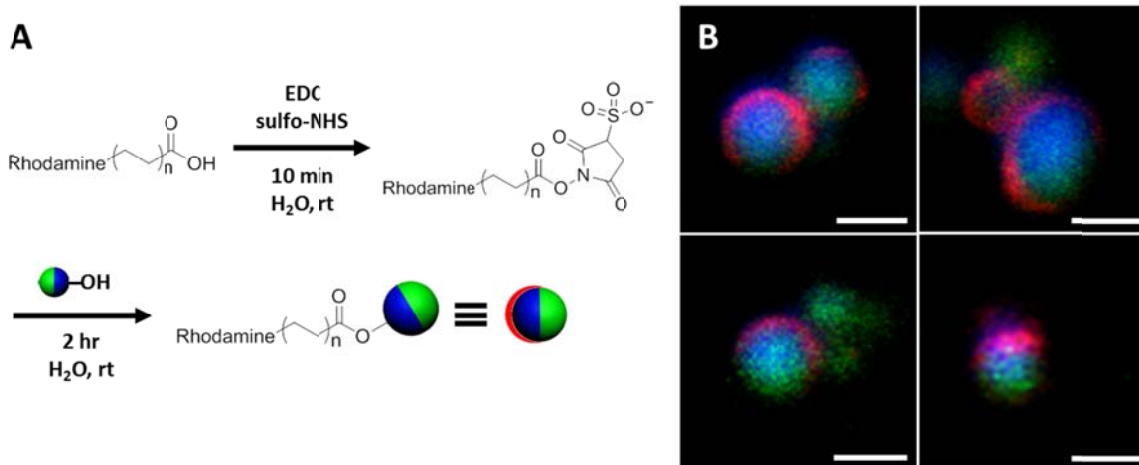
Figure 3-5. The presence of hydroxyl groups on the particle surface was confirmed by EDC/NHS coupling. (A) Reaction scheme. (B) CLSM images of selective conjugation of Rhodamine on the particles. All scale bars are 1μm.
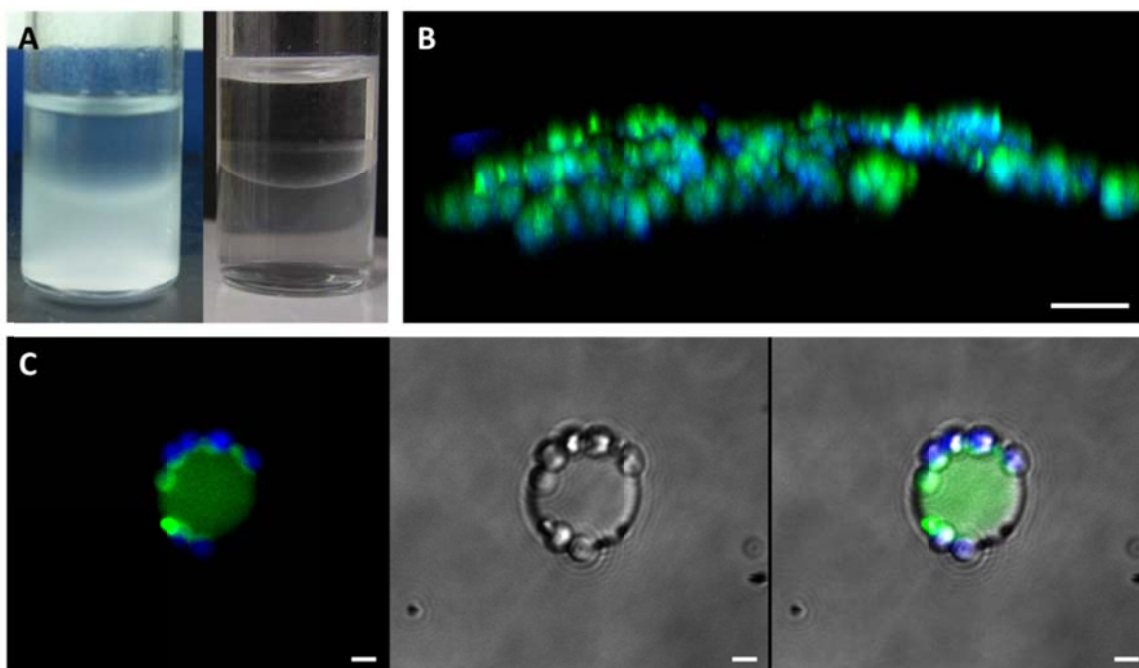
Figure 3-6. Self-assembly of particles at a liquid-liquid interface. (A) Comparison of monophasic PMMA (left) and amphiphilic PMMA (right) particles, placed at the heptane-water interface. The images clearly show that the amphiphilic particles were self-assembled at the interface. (B) CLSM image of the orientation of these amphiphilic PMMA particles at the interface. 3D reconstruction of self-assembled particle layer shows apolar compartment (green) directing oil phase, while polar compartment (blue) facing water. (C) Adsorption of the same particles self-assembled around hexadecane droplet in water. The fluorescence image (left) and differential interference contrast (DIC) micrograph (middle) are overlaid (right).
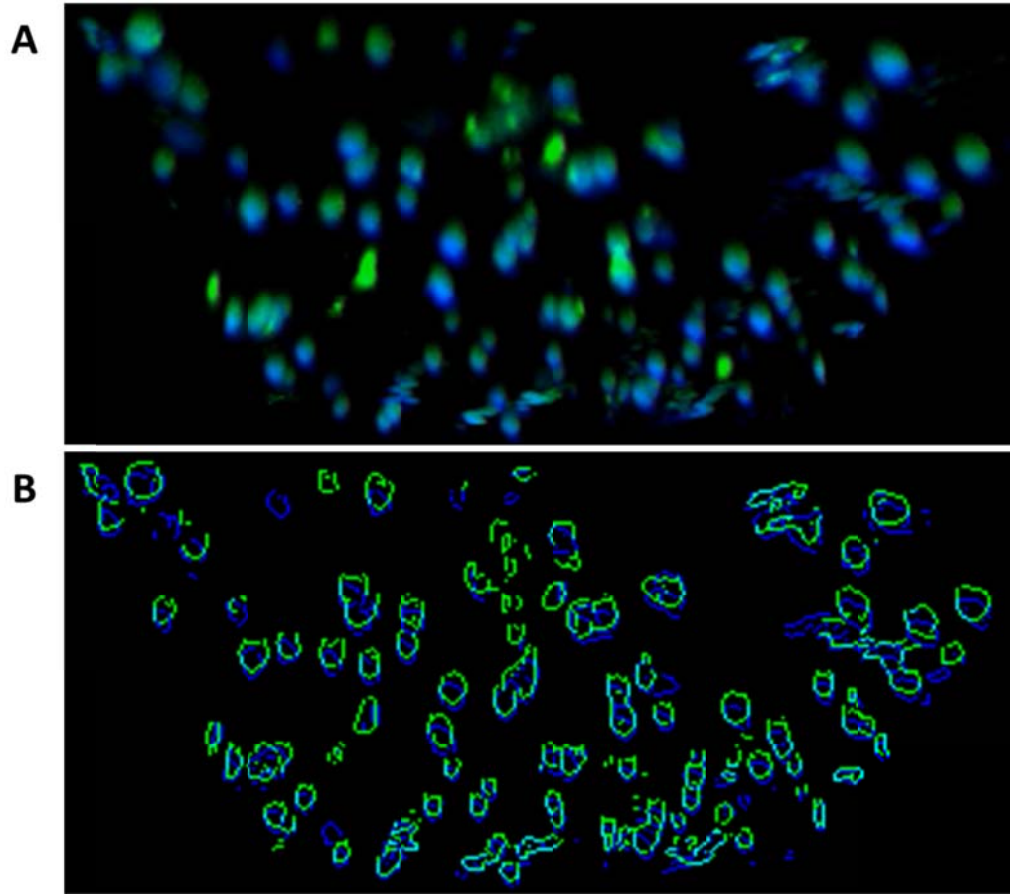
Figure 3-7. 3D reconstruction of Janus particles self-assembled at the liquid-liquid interface. (A) Experimentally obtained CLSM images. (B) The corresponding particles after Matlab image processing.

	θ_{adv} (water)	θ_{adv} (hexadecane)	γ_{sv}^{d} (mN/m)	γ_{sv}^{p} (mN/m)	γ_{sv} (mN/m)
PMMA + F-POSS	120° ± 2°	76° ± 2°	10.6	0.2	10.8
PMMA + PVAc Before Hydrolysis	83° ± 4°	19° ± 2°	26.1	5.8	31.9
PMMA + PVAc After Hydrolysis	73° ± 4°	17° ± 2°	26.3	10.2	36.5

Table 3-1. The estimated dispersive component, polar component and the total surface energy for blends of PMMA + F-POSS and PMMA + PVAc (both before and after hydrolysis).

3.6.   References

1.   Teo, B. M.; Suh, S. K.; Hatton, T. A.; Ashokkumar, M.; Grieser, F. Sonochemical Synthesis of Magnetic Janus Nanoparticles. *Langmuir* **2010**, 27, 30-33.
2.   Park, B. J.; Brugarolas, T.; Lee, D. Janus Particles at an Oil-Water Interface. In *Soft Matter*; The Royal Society of Chemistry: 2011; pp 6413-6417.
3.   Kim, S.-H.; Abbaspourrad, A.; Weitz, D. A. Amphiphilic Crescent-Moon-Shaped Microparticles Formed by Selective Adsorption of Colloids. *Journal of the American Chemical Society* **2011**, 133, 5516-5524.
4.   Ding, S.; Zhang, C.; Wei, W.; Qu, X.; Liu, J.; Yang, Z. Amphiphilic Patchy Composite Colloids. *Macromolecular Rapid Communications* **2009**, 30, 475-480.
5.   Moon, J. J.; Huang, B.; Irvine, D. J. Engineering Nano- and Microparticles to Tune Immunity. *Advanced Materials* **2012**, 24, 3724-3746.
6.   Misra, A. C.; Bhaskar, S.; Clay, N.; Lahann, J. Multicompartmental Particles for Combined Imaging and Sirna Delivery. *Advanced Materials* **2012**, 24, 3850-3856.
7.   An, H. Z.; Helgeson, M. E.; Doyle, P. S. Nanoemulsion Composite Microgels for Orthogonal Encapsulation and Release. *Advanced Materials* **2012**, 24, 3838-3844.
8.   Sotiriou, G. A.; Franco, D.; Poulikakos, D.; Ferrari, A. Optically Stable Biocompatible Flame-Made Sio2-Coated Y2o3:Tb3+ Nanophosphors for Cell Imaging. *ACS Nano* **2012**, 6, 3888-3897.
9.   Pregibon, D. C.; Toner, M.; Doyle, P. S. Multifunctional Encoded Particles for High-Throughput Biomolecule Analysis. *Science* **2007**, 315, 1393-1396.
10.   Nisisako, T.; Torii, T.; Takahashi, T.; Takizawa, Y. Synthesis of Monodisperse Bicolored Janus Particles with Electrical Anisotropy Using a Microfluidic Co-Flow System. *Advanced Materials* **2006**, 18, 1152-1156.
11.   Kim, S.-H.; Sim, J. Y.; Lim, J.-M.; Yang, S.-M. Magnetoresponsive Microparticles with Nanoscopic Surface Structures for Remote-Controlled Locomotion. *Angewandte Chemie International Edition* **2010**, 49, 3786-3790.
12.   Takahara, Y. K.; Ikeda, S.; Ishino, S.; Tachi, K.; Ikeue, K.; Sakata, T.; Hasegawa, T.; Mori, H.; Matsumura, M.; Ohtani, B. Asymmetrically Modified Silica Particles: A Simple Particulate Surfactant for Stabilization of Oil Droplets in Water. *Journal of the American Chemical Society* **2005**, 127, 6271-6275.
13.   Lv, W.; Lee, K. J.; Li, J.; Park, T.-H.; Hwang, S.; Hart, A. J.; Zhang, F.; Lahann, J. Anisotropic Janus Catalysts for Spatially Controlled Chemical Reactions. *Small* **2012**, 8, 3116-3122.
14.   Faria, J.; Ruiz, M. P.; Resasco, D. E. Phase-Selective Catalysis in Emulsions Stabilized by Janus Silica-Nanoparticles. *Advanced Synthesis & Catalysis* **2010**, 352, 2359-2364.
15.   Wang, Y.; Fan, D.; He, J.; Yang, Y. Silica Nanoparticle Covered with Mixed Polymer Brushes as Janus Particles at Water/Oil Interface. *Colloid Polym Sci* **2011**, 289, 1885-1894.
16.   Tanaka, T.; Okayama, M.; Minami, H.; Okubo, M. Dual Stimuli-Responsive "Mushroom-Like" Janus Polymer Particles as Particulate Surfactants†. *Langmuir* **2010**, 26, 11732-11736.

17.   Meng, X.; Guan, Y.; Zhang, Z.; Qiu, D. Fabrication of a Composite Colloidal Particle with Unusual Janus Structure as a High-Performance Solid Emulsifier. *Langmuir* **2012**, 28, 12472-12478.

18.   Binks, B. P.; Fletcher, P. D. I. Particles Adsorbed at the Oil-Water Interface: A Theoretical Comparison between Spheres of Uniform Wettability and "Janus" Particles. *Langmuir* **2001**, 17, 4708-4710.

19.   Ruhland, T. M.; Groschel, A. H.; Walther, A.; Müller, A. H. E. Janus Cylinders at Liquid-Liquid Interfaces. *Langmuir* **2011**, 27, 9807-9814.

20.   Jiang, S.; Granick, S. Janus Balance and Emulsions Stabilized by Janus Particles. In *Janus Particle Synthesis, Self-Assembly and Applications*; Jiang, S., Granick, S., Eds.; RSC: 2012; pp 244-256.

21.   Roh, K.-H.; Martin, D. C.; Lahann, J. Biphasic Janus Particles with Nanoscale Anisotropy. *Nat Mater* **2005**, 4, 759-763.

22.   Roh, K.-H.; Martin, D. C.; Lahann, J. Triphasic Nanocolloids. *Journal of the American Chemical Society* **2006**, 128, 6796-6797.

23.   Bhaskar, S.; Gibson, C. T.; Yoshida, M.; Nandivada, H.; Deng, X.; Voelcker, N. H.; Lahann, J. Engineering, Characterization and Directional Self-Assembly of Anisotropically Modified Nanocolloids. *Small* **2011**, 7, 812-819.

24.   Lee, K. J.; Yoon, J.; Rahmani, S.; Hwang, S.; Bhaskar, S.; Mitragotri, S.; Lahann, J. Spontaneous Shape Reconfigurations in Multicompartmental Microcylinders. *Proceedings of the National Academy of Sciences* **2012**, 109, 16057-16062.

25.   Saha, S.; Copic, D.; Bhaskar, S.; Clay, N.; Donini, A.; Hart, A. J.; Lahann, J. Chemically Controlled Bending of Compositionally Anisotropic Microcylinders. *Angewandte Chemie International Edition* **2012**, 51, 660-665.

26.   Tuteja, A.; Choi, W.; Ma, M.; Mabry, J. M.; Mazzella, S. A.; Rutledge, G. C.; McKinley, G. H.; Cohen, R. E. Designing Superoleophobic Surfaces. *Science* **2007**, 318, 1618-1622.

27.   Nuraje, N.; Khan, W. S.; Lei, Y.; Ceylan, M.; Asmatulu, R. Superhydrophobic Electrospun Nanofibers. *Journal of Materials Chemistry A* **2013**, 1, 1929-1946.

28.   Mabry, J. M.; Vij, A.; Iacono, S. T.; Viers, B. D. Fluorinated Polyhedral Oligomeric Silsesquioxanes (F-Poss). *Angewandte Chemie International Edition* **2008**, 47, 4137-4140.

29.   Lahann, J. Recent Progress in Nano-Biotechnology: Compartmentalized Micro- and Nanoparticles Via Electrohydrodynamic Co-Jetting. *Small* **2011**, 7, 1149-1156.

30.   Lee, K. J.; Hwang, S.; Yoon, J.; Bhaskar, S.; Park, T.-H.; Lahann, J. Compartmentalized Photoreactions within Compositionally Anisotropic Janus Microstructures. *Macromolecular Rapid Communications* **2011**, 32, 431-437.

31.   Hosaka, N.; Otsuka, H.; Hino, M.; Takahara, A. Control of Dispersion State of Silsesquioxane Nanofillers for Stabilization of Polystyrene Thin Films. *Langmuir* **2008**, 24, 5766-5772.

32.   Wu, J.; Mather, P. T. Poss Polymers: Physical Properties and Biomaterials Applications. *Polymer Reviews* **2009**, 49, 25-63.

33.   Aveyard, R.; Binks, B. P.; Clint, J. H. Emulsions Stabilised Solely by Colloidal Particles. *Advances in Colloid and Interface Science* **2003**, 100-102, 503-546.

34.   Hunter, T. N.; Pugh, R. J.; Franks, G. V.; Jameson, G. J. The Role of Particles in Stabilising Foams and Emulsions. *Advances in Colloid and Interface Science* **2008**, 137, 57-81.

35.   Owens, D. K.; Wendt, R. C. Estimation of the Surface Free Energy of Polymers. *Journal of Applied Polymer Science* **1969**, 13, 1741-1747.

36.   Young, T. An Essay on the Cohesion of Fluids. *Philosophical Transactions of the Royal Society of London* **1805**, 95, 65-87.

CHAPTER 4

Cell-Based Biohybrid Actuators

4.1. Motivation and Background

The field of tissue engineering has advanced considerably to the point where it is possible to precisely control cell culture environment.[1-4] Various nano- and microfabrication techniques now provide scaffolds with diverse scope of size, shape, or topology.[3,5-7] Three dimensional structures are being studied instead of two dimensional films, and the effect of pore architectures on regulating cells are also being investigated.[8,9] Moreover, microstructures with controllable functionalities are of interests as they are capable of directing cell behaviors such as cell adhesion, migration and proliferation.[10,11] In fact, broad ranges of investigations have reported on cell culturing matrix with specific functions such as bio-active,[7,12] non-fouling,[13-15] or stimuli-responsive[11,16] properties.

Among these, one of the interesting developments in recent years is the fabrication of biohybrid microstructures actuated by motion of living cells.[17] The integration of real muscular cells into synthetic structures is essential for many studies related to repairing damaged muscles. Different from conventional artificial actuators, such as shape memory alloys[18] or conducting polymers,[19,20] biohybrid actuators are self-actuated and require no

external energy sources. For example, if one could integrate self-beating of heart muscles into complex polymer structures, they could generate spontaneous motion with the presence of natural energy source such as glucose.[21] Toward realizing polymer actuator by cell movement, it is necessary to guide cells to be highly synchronized. Several attempts have been made to investigate the effect of topology on cell alignment.[22-24] Cardiomyocytes were seeded on both grooved and flat surfaces, and it was shown that the cells that were cultured on the grooved pattern were proven to be more effective in aligning and orienting themselves, whereas the flat surface had the cells randomly adhered without providing any regulations.[23,24] Topology is not only useful for recruiting cells, but also effective tools for quantitative measurement of contractile force of the attached cells. Morishima et al. developed hydrogel pillars on a surface for a cardiomyocyte seeding, and calculated the displacement of the pillars that are attached to the cells.[25] In addition to these studies, several reports have been focus on engineering three dimensional microstructures as cardiac cell culture model. Micropatterned PDMS cantilevers were investigated to precisely measure the contractile force of cardiomyocytes.[26-28] Feinberg et al. produced PDMS thin films containing cardiomyocytes in an arranged pattern, and demonstrated diverse movements through applied electric field.[29] Using similar concept, the same group further developed a microstructure that resembles the movement of jellyfish.[30] Moreover, synthetic micropumps[31,32] as artificial hearts were demonstrated, and more recently, carbon nanotubes were incorporated to enhance mechanical properties of a hydrogel muscular patch.[33] While such examples to date present meaningful improvements on the

performance and usability of bio-integrated structures, there is still a need for more compact and miniaturized actuating devices that can scale down to tens of micron size.

In this chapter, we design to build novel biohybrid microcylinders that have capability of actuating in response to self-beating of heart cells. The microcylinders were created through electrohydrodynamic (EHD) co-jetting, which provides easy processing of materials with desired functions.[34] So far, the use of conventional electrospinning method for building scaffolds has been focused on resembling native extracellular matrix.[35-37] Due to its easy tailoring of porosity and pore size, electrospun fibers were randomly deposited as non-woven structures. Furthermore, with the help of rotary colleting technique, highly aligned nanofibers were utilized for directional cell growth.[38,39] Both cases, however, are lacking to regulate cells within a single fiber. In fact, we have previously reported bicompartmental PLGA microfibers through EHD co-jetting that are capable of guiding cell adhesion on individual fibers.[7] Through surface modification of cell adhesive peptide, we were able to demonstrate selective cell attachment on a single microfiber.[7] To assess the potential of our previous work, we aim to guide cardiomyocytes on a single microcylinder and study their cell-induced actuation behavior.

4.2. Experimental Methods

4.2.1. Materials

Poly(DL-lactide-co-glycolide) (PLGA, 85:15, Mw = 50 – 75 000 g/mol), poly(DL-lactide-co-caprolactone) (PLCL, lactide 86 mol%), Tween 20, poly[(m-phenylenevinylene)-alt-(2,5-dibutoxy-p-phenylenevinylene)] (MEHPV), which was used as confocal laser scanning microscopy (CLSM) markers for blue emission, were purchased from Sigma-Aldrich, USA. Cyclooctyne-functionalized poly(lactic acid) (COT-PLA) was prepared as described elsewhere. Human plasma fibronectin (FN) and albumin from bovine serum (BSA, Alexa Fluor-647 Conjugate) were purchased from Life Technologies, USA. Iron oxide nanocrystals (15 nm in diameter) suspended in chloroform was purchased from Ocean Nanotech, USA, and 8-arm PEG-azide (Mw = 40 000 g/mol) was purchased from Creative PEGWorks, USA. NIH 3T3 fibroblasts and primary rat cardiac myocytes were purchased from ATCC and Lonza, USA, respectively. The solvents chloroform, N,N'-dimethyl formamide (DMF), and cyclohexane were purchased from Sigma-Aldrich, USA, and were used without further purification.

4.2.2. Instrumental Details

Confocal laser scanning microscopy (CLSM): The particles were visualized using a CLSM (Olympus, FluoView 500). 405 nm laser and 633 nm Helium-Neon Red (HeNeR) laser were used to excite MEHPV and Alexa Fluor 647 (labeling dyes for BSA), respectively. The barrier filters were set to 430-460 nm for MEHPV and > 660 nm for Alexa Fluor 647.

Confocal Raman: Microfibers were dried under vacuum for overnight to remove any remaining solvents. The measurements were performed on WITec alpha300R utilizing 532 nm laser. Spectra were acquired using an integration time of 0.5 sec per pixel with image scan area of 100 pixels x 100 pixels.

Tensile Testing: The mechanical properties of the microfibers were determined by using NanoIndenter II (MTS/Nanoinstruments Inc., Oak Ridge, TN). Each end point of microfiber was held to a piece of paper with epoxy glue for easy handling, and was gripped to a sample holder for stretching. Stress-strain curves were obtained by testing a single fiber with a diameter of 20 μm and a length ranges from 2 mm to 5 mm depending on the sample size. Tensile tests were performed at a rate of 0.08 mm/s. The number of tested samples was 10 for each set.

4.2.3. Fabrication of Bicompartmental Microfibers

Typical procedure for bicompartmental microfibers is as follows. Two different polymer solutions were prepared in separate vials. 30 w/v% of PLGA was dissolved in a solvent mixture of chloroform and DMF (95 : 5, v/v). Another solution contained 30 w/v% of PLGA and COT-PLA with a concentration of 9 w/v % (30 % by weight of PLGA), which were dissolved in the same ratios of solvents. More detailed information for the preparation of microfibers created in this work is stated in Table 4-1. Experimental setup includes a syringe pump (Fisher Scientific, Inc., USA), a power supply (DC voltage source, Gamma High Voltage Research, USA), and a rotary collector. Each set of two polymer solutions was delivered at a constant flow rate of 0.05 ml/h via vertically positioned syringes equipped with 26 G needles (Hamilton Company, USA). When a

driving voltage of 11~12 kV was applied to the polymer solution, stable Taylor Cone was formed and fibers were collected at a distance of 7 cm.

4.2.4. Fabrication of Bicompartmental Microcylinders

Bicompartmental microcylinders were prepared as previously reported method.[34] Briefly, the obtained microfibers (Refer to Table 4-1) were placed in a cryostat mold with a freezing medium, and sectioned at a desired thickness using a cryostat microtome (Microm HM550, Thermo Fisher Scientific Inc., Germany). Once all the sections were collected, the microcylinders were washed extensively with 0.01 v/v% Tween 20/DI water to remove any residual freezing medium.

4.2.5. Selective Surface Modification via Copper-Free Click Chemistry

COT-functionalized bicompartmental microfibers were collected on a glass substrate, and fixed using double-sided tapes. The glass substrates for holding the microfibers were PEGylated via atom transfer radical polymerization (ATRP) of oligo(ethyleneglyocol) methacrylate (OEGMA) (Figure 4-8). It is important to note that in all cases PEGMA-coated substrate were placed with fiber samples because they were proven to create non-fouling surfaces that can repel both protein adsorption and cell adhesion [ref]. The microfibers taped on the PEGMA-coated substrate were then incubated with 45 mg of 8-arm PEG azide in 1 mL of deionized (DI) water, and the reaction was carried out in a 12-well plate by gentle agitation for 24 h at room temperature. After the reaction, the unreacted PEG azide was washed with 0.01 v/v% Tween 20/DI water.

In the case of microcylinders, approximately 50,000 cylinders were incubated with 45 mg of 8-arm PEG azide in an Eppendorf tube containing 1 mL of 0.01 v/v% Tween 20/DI water, and were kept rotating for 24 h at room temperature.

4.2.6. Bovine Serum Albumin (BSA) Incubation

After the click reaction, the microfibers taped on the PEGMA substrate were placed in a 12-well plate and incubated with 100 µg of BSA in phosphate buffered saline (PBS) for 3 h at room temperature. The unreacted BSA molecules were removed by repeated washing with 0.01 v/v% Tween 20/PBS.

In the case of microcylinders, 50,000 cylinders were rotated with 200 µg of BSA in an Eppendorf tube containing 1mL of 0.01 v/v% Tween 20/PBS for 3h at room temperature.

4.2.7. Incubation of NIH3T3 Fibroblasts on Microfibers

Prior to cell seeding, microfibers with PEGMA-coated substrate were first incubated with 50 µg of FN in 1 mL of PBS, and gently agitated in a 12-well plate for 1 h at room temperature. After the FN incubation, the microfibers were washed 3 times with PBS with an interval of 5 min in each wash. Next, NIH 3T3 fibroblasts were cultured with a concentration of 3.8×10^5 cells/ml/well for 6 h in serum-free media. Passages 3-6 were used for all experiments. After 4.5 hours, the cylinders with cells were stained with 10 µM of CellTracker Green CMFDA for 30 minutes, and then fixed in 4% formaldehyde for 15 minutes at room temperature.

4.2.8. Incubation of NIH3T3 Fibroblasts on Microcylinders

100 μg of FN was incubated with 50,000 microcylinders in an Eppendorf tube containing 0.01 v/v% PBS at a total volume of 1 mL, and rotated for 1h at room temperature. Next, NIH 3T3 fibroblasts were cultured with a concentration of 3.8×10^5 cells/ml for 5 h in a 5% CO_2 incubator at 37^oC, after which they were transferred to a stationary PEGMA-coated glass surface on a 12-well plate and incubated in media under the same conditions as rotation. A strong magnet was introduced for the facile separation of the microcylinders from dead cells that were floating in the media. After 4.5 hours, the cylinders with cells were stained with 10 μM of CellTracker Green CMFDA for 30 minutes, and then fixed in 4% formaldehyde for 15 minutes at room temperature.

4.2.9. Incubation of Cardiomyocytes

The PEGMA-coated surfaces and microcylinders were sterilized under UV lamp for overnight at room temperature prior to use. The microcylinders (50,000 cylinders/ml) were first incubated with FN in DI water with a concentration of 100 μg/ml in an Eppendorf tube. This was rotated for 1hr at room temperature. After washing the cylinders three times with DPBS at five minute increments, neonatal rat cardiomyocytes (8×10^5 cells/ml) were thawed and carefully resuspended drop-by-drop (to avoid osmotic shock) in Rat Cardiac Myocyte Cell Medium supplemented with 5-Bromo-2'deoxyuridine in order to prevent fibroblast proliferation. 80% of the media was replaced after 4 h to remove dead cells, and thereafter if necessary 50% of the media was replaced every 72 h. The solution was kept rotating for another 4 h, and transferred into a 24-well plate along with the PEGMA-coated surface. The samples placed in the well

plate were then kept in the incubator until the day 3. 24 h before imaging via CLSM, 1 µmol/l of aldosterone dissolved in ethanol was added to the media in order to enhance cardiomyocyte beating.

4.3. Results and Discussion

The schematic diagram of the preparation of microcylinders is shown in Figure 4-1. First, bicompartmental microfibers with 20 µm in diameter were produced via EHD co-jetting. While PLGA was chosen as a base material for both compartments, cyclooctyne-functionalized poly(lactic acid) (COT-PLA) was selectively introduced in one of the compartments. COT moieties are one of the reactive groups for click chemistry that are known for its copper-free reaction condition and thus non-toxic residues. To design microcylinders that can actuate with cell movement, it was important to arrange cells along the long axis of microcylinders. In this manner, the incorporation of COT groups in the microfibers was necessary for tailoring surfaces to selectively possess cell-repellent behavior. Besides COT-PLA groups, another compartment further contained 15 nm magnetite nanocrystals. The addition of magnetite helped the microcylinders to be easily separated from dead cells when replacing cell media. Hence, the two solutions, PLGA/magnetite and COT-PLA/PLGA, were prepared to form well-defined bicompartmental microfibers through EHD co-jetting, and the obtained microfibers were further processed to create uniform microcylinders as previously reported.[34]

In order to confirm the selective localization of COT groups on the obtained microfibers, the microfibers were characterized by confocal-Raman microscopy (Figure

91

4-2). As seen from the confocal image and the corresponding spectra acquired from image scan, it was unambiguous that only one of the compartments had a peak near 2200 cm^{-1} which is the evidence of triple carbon bonds from the COT groups. Once the COT groups on the half surface were analyzed by confocal-Raman spectra, we then continued to immobilize non-fouling PEG via click chemistry.

As an initial step, microfibers were used instead of microcylinders to test their applicability as novel cell culture scaffolds. This was because microfibers were attached to a flat substrate making them easy to handle during protein and cell assays. In order to impose directional protein adsorption and cell growth on the microfibers, azide-functionalized PEG molecules were selectively introduced to the COT-PLA/PLGA compartment. As an indirect method to prove successful binding of PEG on the surface, fluorescence-labeled bovine serum albumin (BSA, Alexa Fluor-647) was incubated with the microfibers for 3 hours in PBS (Figure 4-3A). As PEG molecules are protein and cell repellents, BSA was shown to adsorb only to the one compartment (Figure 4-3C). This result was compared with the full coverage of BSA on the microfibers where there was no PEG on all surfaces (Figure 4-3B). Likewise, the microcylinders modified with PEG were also proven to be capable of selectively repelling protein adsorption (Figure 4-3D). To demonstrate the feasibility of these microfibers and microcylinders for cell culture environment, NIH 3T3 fibroblasts were first tested as an initial cell line. As seen in Figure 4-4A, two different sets of microfibers, PLGA/PLGA and PLGA/PEG (after surface immobilization of PEG on COT-PLA), were utilized for the selective recruitment of the cells. In turn, with the help of selective coating of cell-adhesive FN, the fibroblasts were adhered and spread only to the compartment where there was no PEG (Figure 4-4C).

In contrast, PLGA/PLGA microfibers showed no selectivity on either the FN adsorption or the cell attachment (Figure 4-4B). Next, we continued to examine the microcylinders. Figure 4-4D demonstrates successfully aligned and proliferated NIH 3T3 fibroblasts after 8 hours of incubation.

Before carrying out to cultivate cardiomyocytes, the mechanical properties of the microcylinders were examined. PLGA is a biodegradable polymer which can be a good candidate for tissue engineering application purpose,[40] but its high stiffness and low strain were considered to be a potential problem for actuation.[41] Poly(ε–caprolactone) (PCL) is also a biodegradable polyester, but unlike PLGA, PCL shows a negative Tg and it is in rubbery state at room temperature.[40] It has very low Young's modulus and high elongation at break.[41] However, because of its low melting point, using pure PCL also can be handicap in some applications. To enhance the applicability of PCL, one well-known way is to copolymerize PCL with PLA or PLGA.[42,43] In fact, PCL copolymerized with PLA was reported to have much more higher strain value than pure PLA.[42] Thus, we designed to create microfibers composed of poly(lactide-co-caprolactone) (PLCL).

In order to compare mechanical properties of PLGA and PLCL microfibers, tensile tests of each single fiber were performed. Based on the stress-strain curves presented in Figure 4-5, it was demonstrated that the PLGA microfibers have very low strain (0.1 ± 0.06) and higher Young's modulus (1585 ± 551 MPa) than PLGA/PLCL (strain: 7.4 ± 1.3, Young's modulus: 476 ± 31 MPa) microfibers. Moreover, when fracture strains for each microfiber with the sample size of 10 were compared, PLGA/PLCL microfibers tend to have more than 70 times higher strain value than that of

PLGA microfibers. With this in mind, PLGA/PLCL microcylinders were prepared and employed to culture heart cells.

Finally, to explore microcylinders as a biohybrid actuator, we switched the cell line from the NIH 3T3 fibroblasts to cardiomyocytes, and seeded cells on the PLGA/PLCL microcylinders with enhanced flexibility. Figure 4-6 shows the selective cultivation of cardiomyocytes on PLGA/PLCL microcylinders treated with PEG. FN was expected to coat on the half surfaces, which will then promote the cell spreading only on the same compartment. The concept of having PEG selectively on the one compartment was very important for the realization of the bending behavior of the microcylinders. This is because if the cells are randomly arranged and not aligned in a certain direction, it is difficult for them to have highly synchronized contraction.

Upon establishing the selective binding of cardiomyocytes, we further investigated the bending behavior of the obtained microcylinders for potential actuating applications. The autonomous beating of the cells was observed after two days and the actuating behavior of microcylinders were taken on the third day of the experiment. Consequently, such microcylinders with exceptional arrangement of cardiomyocytes successfully generated bending motion which was driven by synchronous beating of the heart cells. Moreover, the actuation behavior of the microcylinders was estimated by analyzing CLSM images captured from the video. The bottom end point of the microcylinder was fixed while the displacement of the top end point was measured directly from the video frame (Figure 4-7). From the data shown, the displacement was measured from 9.75 μm to 18 μm, indicating the bending motion of the microcylinder generated by the cell motion.

From our study, we can conclude that having anisotropic feature with non-fouling PEG on the specific compartment significantly influences the cells to attach with a direction along the long axis of the microcylinders, which in turn, allows the microcylinders to deform their shapes in a controlled direction.

4.4. Summary

In summary, a new approach to fabricate biohybrid microcylinders is introduced. Although further studies are needed to study the bending behaviors of the heart cells on these particles, the development of a single microcylinder that can be used for the integration of the motion of living cells may open new steps toward miniaturized biorobots or biomachines.

4.5. Figures and Tables
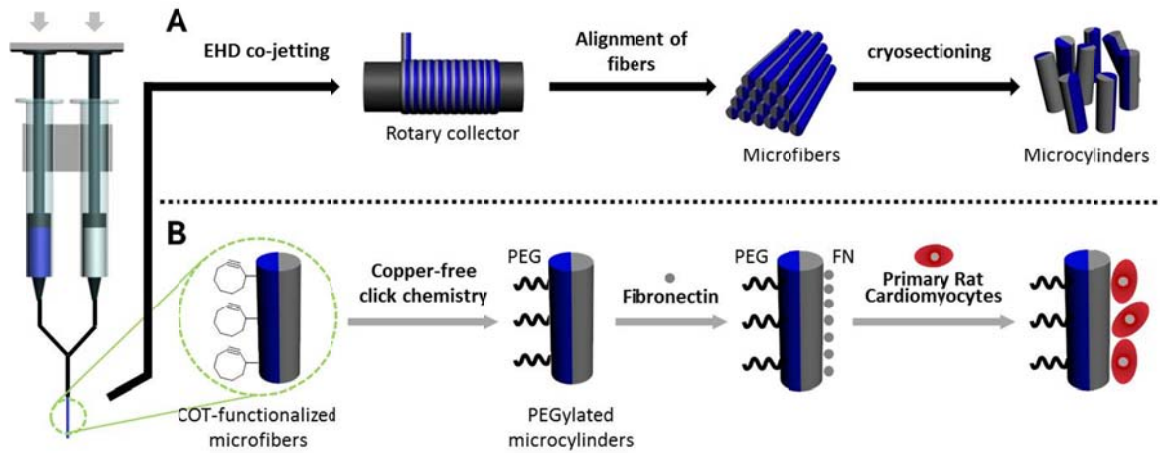
Figure 4-1. Fabrication scheme of bicompartmental microcylinders for bioactuators. (A) The first step involves collecting fibers as aligned bundles followed by cryosectioning at a desired length to prepare microcylinders. (B) The second step is to utilize the obtained microcylinders for selective surface modification with non-fouling PEG molecules. The immobilization of PEG on the half surface of microcylinders results in selective protein adsorption as well as cell attachment.
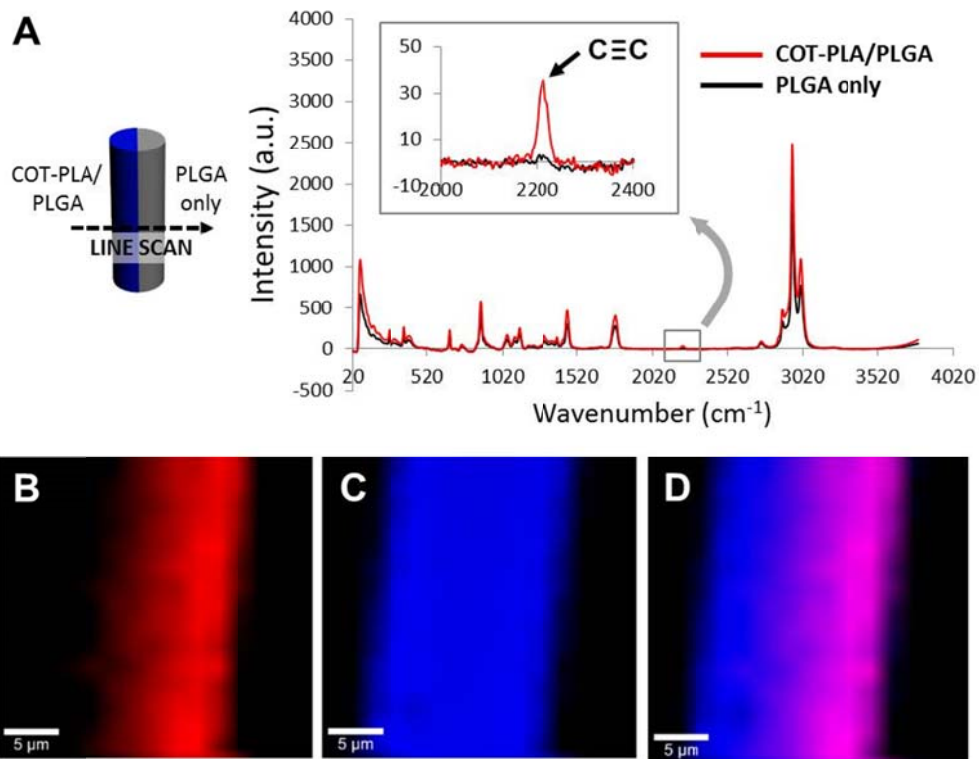
Figure 4-2. Confocal-Raman analysis of COT-functionalized bicompartmental microcylinders. (A) Two different Raman spectra obtained from the cross-sectional image scan of the microcylinders. Characteristic peak near 2200 cm^{-1} shows triple bond of carbon, which indicates the presence of the COT groups in the half compartment. (B-D) Confocal-Raman images of the microcylinders. The red and black spectra in A correspond to B and C, respectively. The overlaid image, as shown in D, demonstrates the localization of the COT groups in one compartment only.
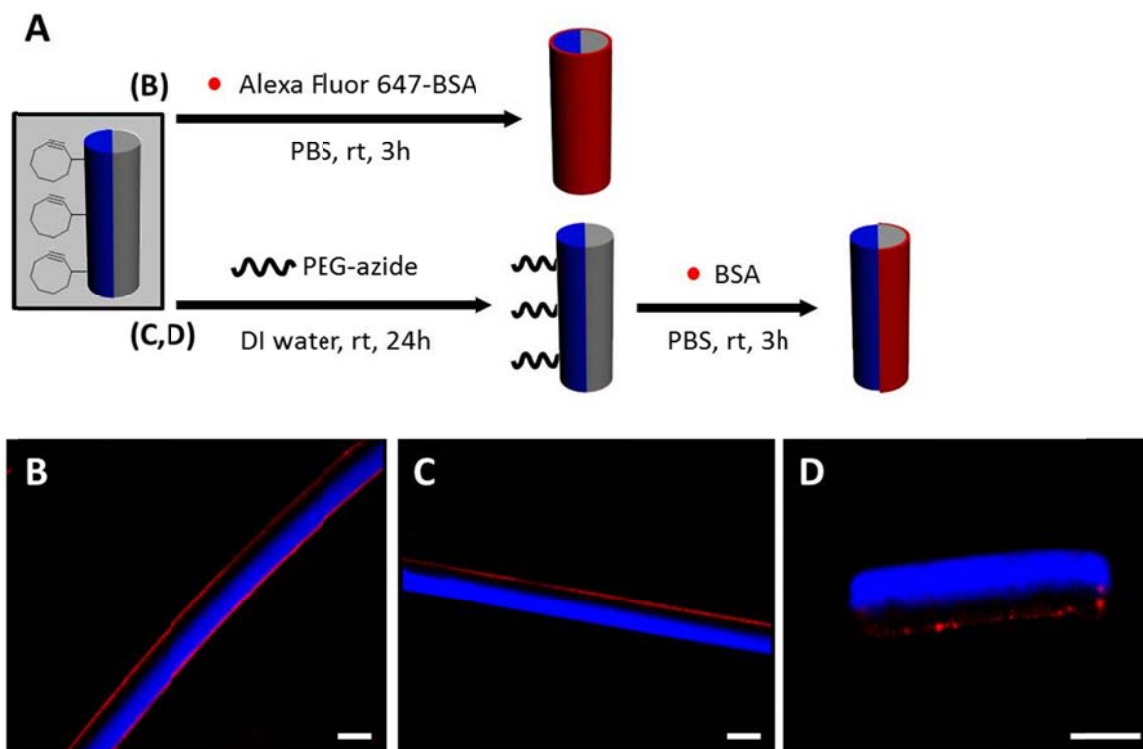
Figure 4-3. Selective adsorption of Alexa Fluor 647-BSA on bicompartmental microfibers and microcylinders. (A) Two different sets of experimental schemes. (B) CLSM images of the microfibers before the surface modification with PEG. The adsorption of BSA was observed everywhere. (C) CLSM images of the microfibers after the selective surface modification with PEG. BSA was adsorbed only on the un-reacted surfaces. (D) Once the hypothesis was established, the selective adsorption of BSA was carried out with the PEGylated microcylinders. CLSM images of the microcylinders after the selective surface modification with PEG. This result matched with C, where the protein adsorption was prevented in the presence of the PEG chains. All scale bars are 20μm.
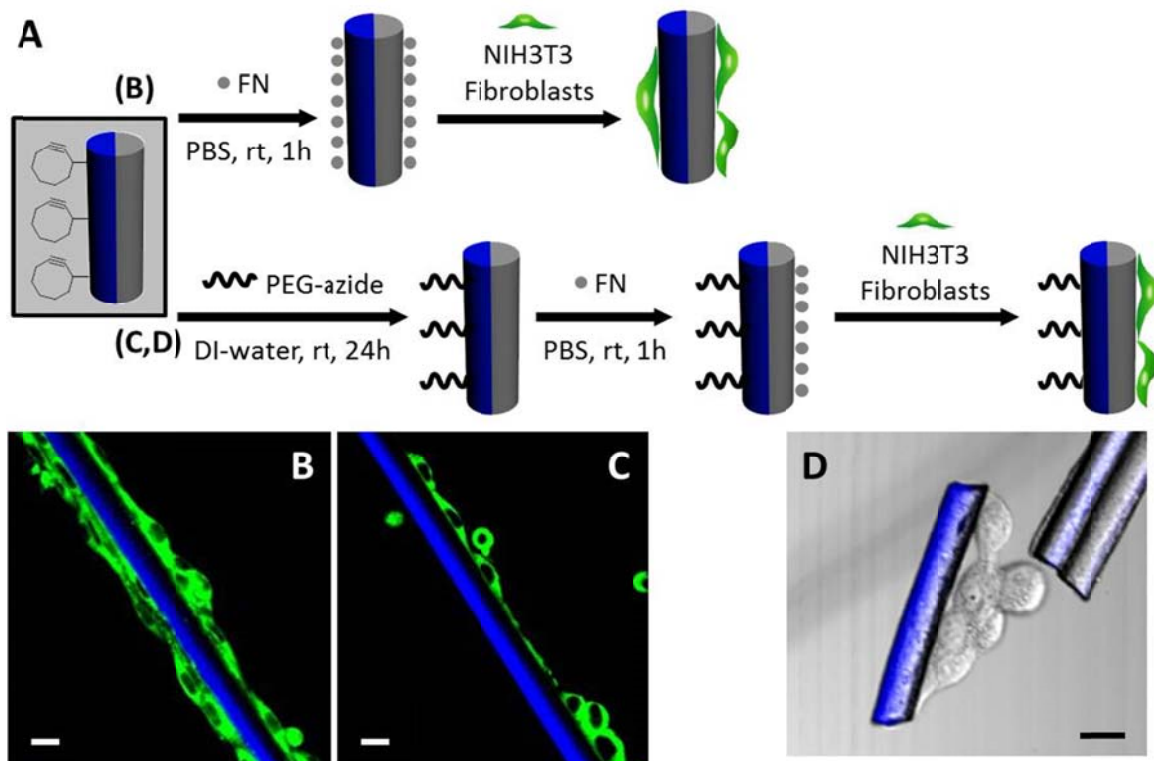
Figure 4-4. Selective recruitment of NIH 3T3 fibroblasts on bicompartmental microfibers and microcylinders. (A) Two different sets of experimental schemes, with and without surface modification with PEG. (B, C) CLSM images of bicompartmental microfibers correspond to each step. B indicated the microfibers before the surface modification with PEG (blue compartment), where the fibroblasts were introduced on both compartments. In contrast, when the microfibers were modified with PEG, the cell attachment was observed on non-PEGylated compartment only. (D) CLSM images of bicompartmental microcylinders after surface modification with PEG (blue). The selective attachment of fibroblasts shows the presence of non-fouling PEG molecules in one half compartment. All scale bars are 20 μm.
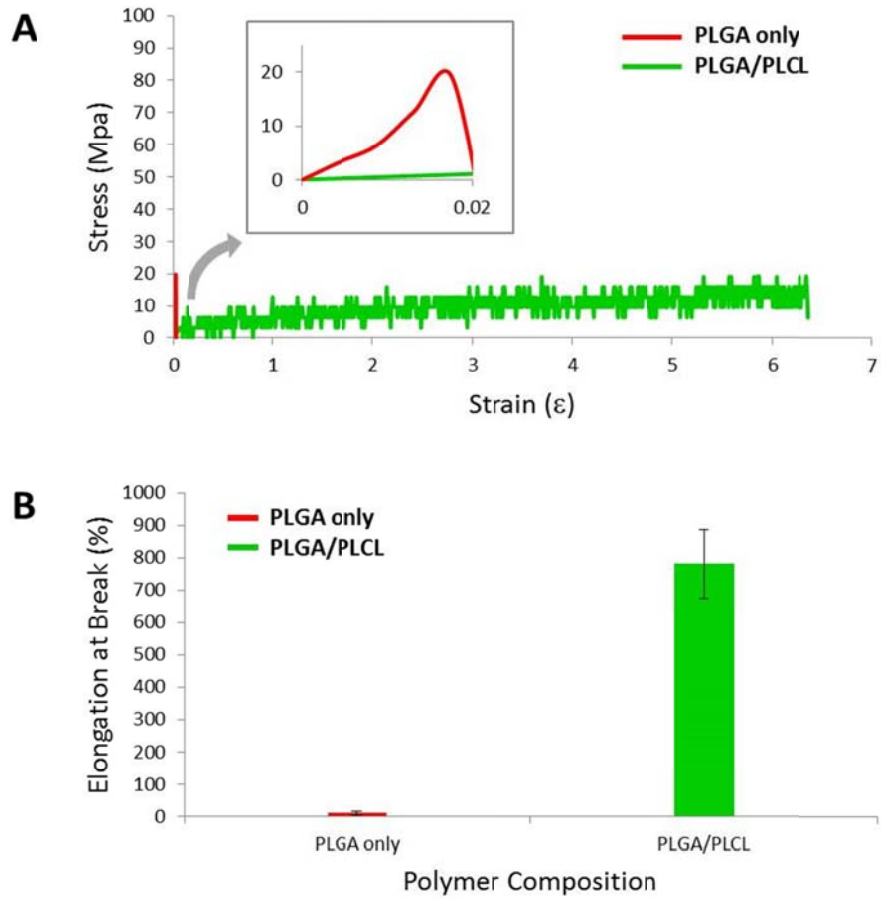
Figure 4-5. Mechanical properties comparing two types of bicompartmental microfibers: PLGA only and PLGA/PLCL. (A) Stress-strain curves. (B) Elongation at break vs. polymer composition.
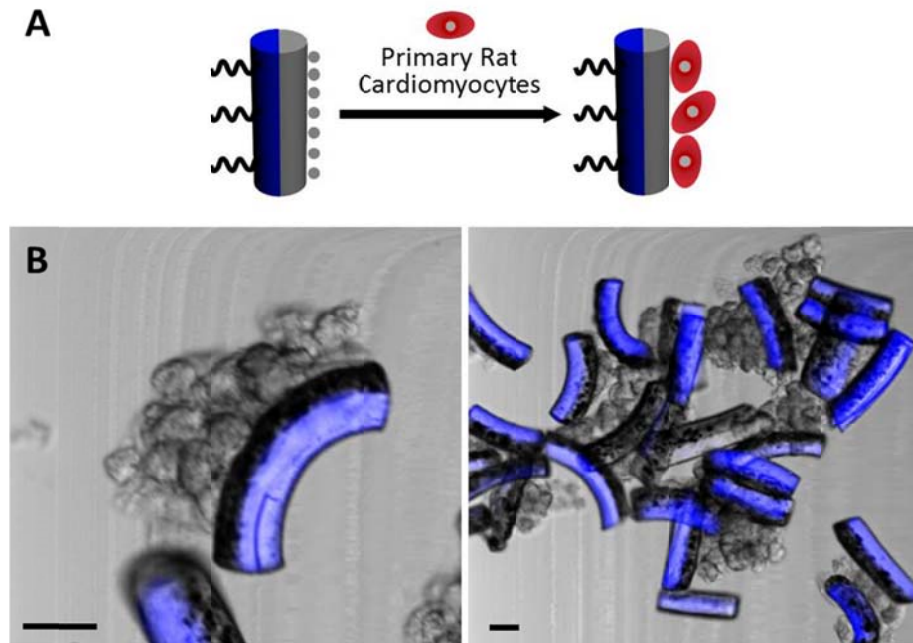
Figure 4-6. Selective attachment of cardiomyocytes on bicompartmental PLGA/PLCL microcylinders. (A) Experimental scheme showing surface modification of one half compartments with PEG, and cardiomyocytes seeding of another half compartments. (B) The microcylinders showing selective recruitment of cardiomyocytes on the non-PEGylated compartment only. All scale bars are 20 µm.
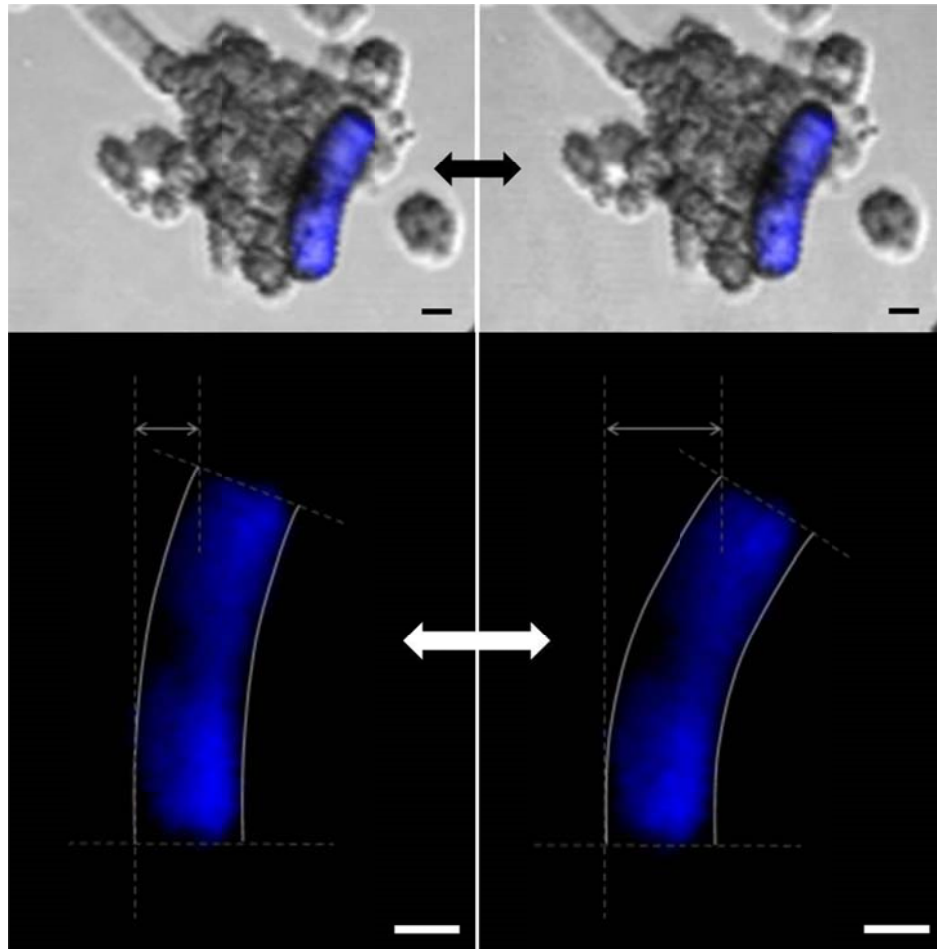
Figure 4-7. The bending behavior of PLGA/PLCL microcylinders driven by the beating of cardiomyocytes. Two CLSM images were captured from the video frame (top) and analyzed to calculate the displacement of the top end point of the microcylinder (bottom). The displacement was measured from 9.75 μm to 18 μm indicating the deformation of microcylinders was occurred upon the cell movement. All scale bars are 10 μm.
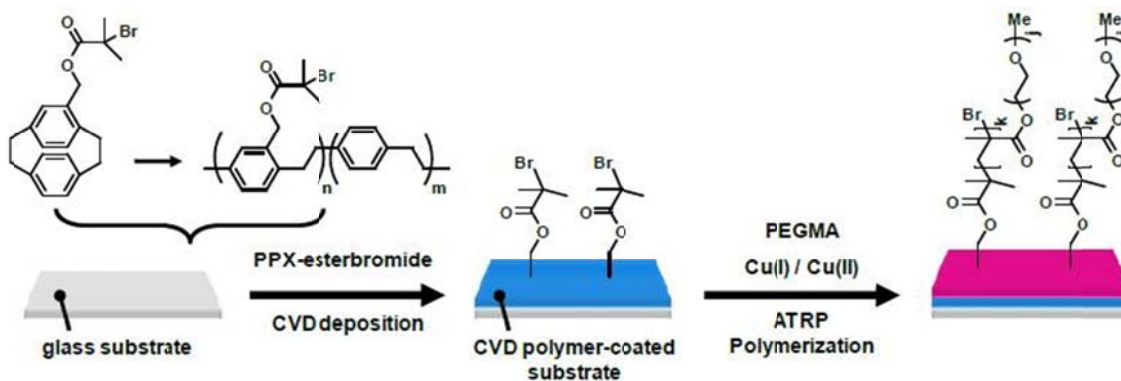
Figure 4-8. Steps required for PEGylation of a glass substrate prior to protein and cell incubation. A glass coverslip was first coated with reactive bromide via chemical vapor deposition (CVD), followed by polymerization through surface-initiated ATRP of PEGMA. These steps were necessary in order to prevent proteins and cells preferentially attaching to the surface while incubating with microfibers or microcylinders.

Microfibers and Microcylinders	Polymer Compositions for Each Compartment	Solvents
Figures 4-4B, 4-4C, 4-5B, 4-5C	1) 30 w/v% PLGA (no dye) 2) 30 w/v% PLGA + 9 w/v% COT-PLA, blue dye	chloroform : DMF, 95 : 5 (v/v)
Figures 4-4D, 4-5D	1) 30 w/v% PLGA + 0.9 w/v% magnetite (no dye) 2) 30 w/v% PLGA + 9 w/v% COT-PLA, blue dye	chloroform : DMF, 95 : 5 (v/v)
Figure 4-7B	1) 25 w/v% PLCL + 0.75 w/v% magnetite (no dye) 2) 30 w/v% PLGA + 9 w/v% COT-PLA, blue dye	chloroform : cyclohexane : DMF, 45 : 50 : 5 (v/v/v)

Table 4-1. Lists of polymer composition of the two jetting solutions for preparing bicompartmental microfiber used in each figure.

4.6.   References

1.   Pilarek, M.; Neubauer, P.; Marx, U. Biological Cardio-Micro-Pumps for Microbioreactors and Analytical Micro-Systems. *Sensors and Actuators B: Chemical* **2011**, 156, 517-526.
2.   Boyang, Z.; Yun, X.; Anne, H.; Nimalan, T.; Milica, R. Micro- and Nanotechnology in Cardiovascular Tissue Engineering. *Nanotechnology* **2011**, 22, 494003.
3.   Stevens, M. M.; George, J. H. Exploring and Engineering the Cell Surface Interface. *Science* **2005**, 310, 1135-1138.
4.   Ravichandran, R.; Sundarrajan, S.; Venugopal, J. R.; Mukherjee, S.; Ramakrishna, S. Advances in Polymeric Systems for Tissue Engineering and Biomedical Applications. *Macromolecular Bioscience* **2012**, 12, 286-311.
5.   Ross, A. M.; Jiang, Z.; Bastmeyer, M.; Lahann, J. Physical Aspects of Cell Culture Substrates: Topography, Roughness, and Elasticity. *Small* **2012**, 8, 336-355.
6.   Kim, H.; Kang, D.-H.; Kim, M.; Jiao, A.; Kim, D.-H.; Suh, K.-Y. Patterning Methods for Polymers in Cell and Tissue Engineering. *Ann Biomed Eng* **2012**, 40, 1339-1355.
7.   Mandal, S.; Bhaskar, S.; Lahann, J. Micropatterned Fiber Scaffolds for Spatially Controlled Cell Adhesion. *Macromolecular Rapid Communications* **2009**, 30, 1638-1644.
8.   Klein, F.; Striebel, T.; Fischer, J.; Jiang, Z.; Franz, C. M.; von Freymann, G.; Wegener, M.; Bastmeyer, M. Elastic Fully Three-Dimensional Microstructure Scaffolds for Cell Force Measurements. *Advanced Materials* **2010**, 22, 868-871.
9.   Berry, S. M.; Warren, S. P.; Hilgart, D. A.; Schworer, A. T.; Pabba, S.; Gobin, A. S.; Cohn, R. W.; Keynton, R. S. Endothelial Cell Scaffolds Generated by 3d Direct Writing of Biodegradable Polymer Microfibers. *Biomaterials* **2011**, 32, 1872-1879.
10.   Yoshida, M.; Roh, K.-H.; Mandal, S.; Bhaskar, S.; Lim, D.; Nandivada, H.; Deng, X.; Lahann, J. Structurally Controlled Bio-Hybrid Materials Based on Unidirectional Association of Anisotropic Microparticles with Human Endothelial Cells. *Advanced Materials* **2009**, 21, 4920-4925.
11.   Kim, J.; Hayward, R. C. Mimicking Dynamic in Vivo Environments with Stimuli-Responsive Materials for Cell Culture. *Trends in Biotechnology* **2012**, 30, 426-439.
12.   Deng, X.; Eyster, T. W.; Elkasabi, Y.; Lahann, J. Bio-Orthogonal Polymer Coatings for Co-Presentation of Biomolecules. *Macromolecular Rapid Communications* **2012**, 33, 640-645.
13.   Lee, J. Y.; Shah, S. S.; Yan, J.; Howland, M. C.; Parikh, A. N.; Pan, T.; Revzin, A. Integrating Sensing Hydrogel Microstructures into Micropatterned Hepatocellular Cocultures. *Langmuir* **2009**, 25, 3880-3886.
14.   Hahn, M. S.; Taite, L. J.; Moon, J. J.; Rowland, M. C.; Ruffino, K. A.; West, J. L. Photolithographic Patterning of Polyethylene Glycol Hydrogels. *Biomaterials* **2006**, 27, 2519-2524.
15.   Suh, K. Y.; Seong, J.; Khademhosseini, A.; Laibinis, P. E.; Langer, R. A Simple Soft Lithographic Route to Fabrication of Poly(Ethylene Glycol) Microstructures for Protein and Cell Patterning. *Biomaterials* **2004**, 25, 557-563.

16.   Pedron, S.; van Lierop, S.; Horstman, P.; Penterman, R.; Broer, D. J.; Peeters, E. Stimuli Responsive Delivery Vehicles for Cardiac Microtissue Transplantation. *Advanced Functional Materials* **2011**, 21, 1624-1630.

17.   Zammaretti, P.; Jaconi, M. Cardiac Tissue Engineering: Regeneration of the Wounded Heart. *Current Opinion in Biotechnology* **2004**, 15, 430-434.

18.   Nespoli, A.; Besseghini, S.; Pittaccio, S.; Villa, E.; Viscuso, S. The High Potential of Shape Memory Alloys in Developing Miniature Mechanical Devices: A Review on Shape Memory Alloy Mini-Actuators. *Sensors and Actuators A: Physical* **2010**, 158, 149-160.

19.   Bar-Cohen, Y. Electroactive Polymers (Eap) as Actuators for Potential Future Planetary Mechanisms. In *Evolvable Hardware, 2004. Proceedings. 2004 NASA/DoD Conference on*; 2004; pp 309-317.

20.   Otero, T. F.; Sanchez, J. J.; Martinez, J. G. Biomimetic Dual Sensing-Actuators Based on Conducting Polymers. Galvanostatic Theoretical Model for Actuators Sensing Temperature. *The Journal of Physical Chemistry B* **2012**, 116, 5279-5290.

21.   Akiyama, Y.; Iwabuchi, K.; Furukawa, Y.; Morishima, K. Long-Term and Room Temperature Operable Bioactuator Powered by Insect Dorsal Vessel Tissue. *Lab on a Chip* **2009**, 9, 140-144.

22.   Nikkhah, M.; Edalat, F.; Manoucheri, S.; Khademhosseini, A. Engineering Microscale Topographies to Control the Cell–Substrate Interface. *Biomaterials* **2012**, 33, 5230-5246.

23.   Au, H. T. H.; Cheng, I.; Chowdhury, M. F.; Radisic, M. Interactive Effects of Surface Topography and Pulsatile Electrical Field Stimulation on Orientation and Elongation of Fibroblasts and Cardiomyocytes. *Biomaterials* **2007**, 28, 4277-4293.

24.   Bursac, N.; Parker, K. K.; Iravanian, S.; Tung, L. Cardiomyocyte Cultures with Controlled Macroscopic Anisotropy: A Model for Functional Electrophysiological Studies of Cardiac Muscle. *Circulation Research* **2002**, 91, e45-e54.

25.   Morishima, K.; Tanaka, Y.; Ebara, M.; Shimizu, T.; Kikuchi, A.; Yamato, M.; Okano, T.; Kitamori, T. Demonstration of a Bio-Microactuator Powered by Cultured Cardiomyocytes Coupled to Hydrogel Micropillars. *Sensors and Actuators B: Chemical* **2006**, 119, 345-350.

26.   Park, J.; Ryu, J.; Choi, S. K.; Seo, E.; Cha, J. M.; Ryu, S.; Kim, J.; Kim, B.; Lee, S. H. Real-Time Measurement of the Contractile Forces of Self-Organized Cardiomyocytes on Hybrid Biopolymer Microcantilevers. *Analytical Chemistry* **2005**, 77, 6571-6580.

27.   Kim, J.; Park, J.; Yang, S.; Baek, J.; Kim, B.; Lee, S. H.; Yoon, E.-S.; Chun, K.; Park, S. Establishment of a Fabrication Method for a Long-Term Actuated Hybrid Cell Robot. *Lab on a Chip* **2007**, 7, 1504-1508.

28.   Kim, J.; Park, J.; Na, K.; Yang, S.; Baek, J.; Yoon, E.; Choi, S.; Lee, S.; Chun, K.; Park, J.*; et al.* Quantitative Evaluation of Cardiomyocyte Contractility in a 3d Microenvironment. *Journal of Biomechanics* **2008**, 41, 2396-2401.

29.   Feinberg, A. W.; Feigel, A.; Shevkoplyas, S. S.; Sheehy, S.; Whitesides, G. M.; Parker, K. K. Muscular Thin Films for Building Actuators and Powering Devices. *Science* **2007**, 317, 1366-1370.

30.   Nawroth, J. C.; Lee, H.; Feinberg, A. W.; Ripplinger, C. M.; McCain, M. L.; Grosberg, A.; Dabiri, J. O.; Parker, K. K. A Tissue-Engineered Jellyfish with Biomimetic Propulsion. *Nat Biotech* **2012**, 30, 792-797.

31.   Tanaka, Y.; Sato, K.; Shimizu, T.; Yamato, M.; Okano, T.; Kitamori, T. A Micro-Spherical Heart Pump Powered by Cultured Cardiomyocytes. *Lab on a Chip* **2007**, 7, 207-212.

32.   Park, J.; Kim, I. C.; Baek, J.; Cha, M.; Kim, J.; Park, S.; Lee, J.; Kim, B. Micro Pumping with Cardiomyocyte-Polymer Hybrid. *Lab on a Chip* **2007**, 7, 1367-1370.

33.   Shin, S. R.; Jung, S. M.; Zalabany, M.; Kim, K.; Zorlutuna, P.; Kim, S. b.; Nikkhah, M.; Khabiry, M.; Azize, M.; Kong, J.*; et al.* Carbon-Nanotube-Embedded Hydrogel Sheets for Engineering Cardiac Constructs and Bioactuators. *ACS Nano* **2013**.

34.   Bhaskar, S.; Hitt, J.; Chang, S.-W. L.; Lahann, J. Multicompartmental Microcylinders. *Angewandte Chemie International Edition* **2009**, 48, 4589-4593.

35.   Luo, C. J.; Stoyanov, S. D.; Stride, E.; Pelan, E.; Edirisinghe, M. Electrospinning Versus Fibre Production Methods: From Specifics to Technological Convergence. *Chemical Society Reviews* **2012**, 41, 4708-4735.

36.   Zong, X.; Bien, H.; Chung, C.-Y.; Yin, L.; Fang, D.; Hsiao, B. S.; Chu, B.; Entcheva, E. Electrospun Fine-Textured Scaffolds for Heart Tissue Constructs. *Biomaterials* **2005**, 26, 5330-5338.

37.   Shin, M.; Ishii, O.; Sueda, T.; Vacanti, J. P. Contractile Cardiac Grafts Using a Novel Nanofibrous Mesh. *Biomaterials* **2004**, 25, 3717-3723.

38.   Xie, J.; MacEwan, M. R.; Schwartz, A. G.; Xia, Y. Electrospun Nanofibers for Neural Tissue Engineering. *Nanoscale* **2010**, 2, 35-44.

39.   Kai, D.; Prabhakaran, M. P.; Jin, G.; Ramakrishna, S. Guided Orientation of Cardiomyocytes on Electrospun Aligned Nanofibers for Cardiac Tissue Engineering. *Journal of Biomedical Materials Research Part B: Applied Biomaterials* **2011**, 98B, 379-386.

40.   Seal, B. L.; Otero, T. C.; Panitch, A. Polymeric Biomaterials for Tissue and Organ Regeneration. *Materials Science and Engineering: R: Reports* **2001**, 34, 147-230.

41.   Serrano, M. C.; Chung, E. J.; Ameer, G. A. Advances and Applications of Biodegradable Elastomers in Regenerative Medicine. *Advanced Functional Materials* **2010**, 20, 192-208.

42.   Wang, L.; Zhang, Z.; Chen, H.; Zhang, S.; Xiong, C. Preparation and Characterization of Biodegradable Thermoplastic Elastomers (Plca/Plga Blends). *J Polym Res* **2010**, 17, 77-82.

43.   Chen, Q.; Liang, S.; Thouas, G. A. Elastomeric Biomaterials for Tissue Engineering. *Progress in Polymer Science* **2013**, 38, 584-671.

CHAPTER 5

Magnetic Particle-Based Optical Displays

5.1. Motivation and Background

With the increase in the demand for thin, flexible, and paper-like displays, there have been various attempts to investigate a wide variety of new display technologies.[1,2] One of them is particle-based display.[2] The particle-based displays utilize particles that can be manipulated by either electric[3-7] or magnetic[8-11] external field. Typically, these particles are sealed between transparent substrates, and display different colors through translational or rotational motion.[2] Among particle-based displays, here we aim to fabricate magnetophoretic display. Scientists have combined their effort to develop magnetic particles with diverse fabrication methods including microfluidics,[12] direct deposition,[13] and phase separation.[14-16] In most cases, the important parameter to achieve highly controllable system was to produce particles with narrow size distribution and highly uniform shapes. Particles with well-defined magnetic regions are necessary for the reliable display, because the location and the concentration of magnetic materials within each particle highly affect the responsiveness of the particles under magnetic gradient.

Here, we design to prepare novel magnetic particles with unique cylindrical shape via electrohydrodynamic (EHD) co-jetting.[17,18] The beauty of using EHD co-jetting lies in its facile control of anisotropy. In other words, the incorporation of magnetite

nanocrystals in pre-defined compartments can control particle anisotropy, and thus, help particles to possess unique and highly synchronized translational and rotational motion. In addition, we aim to create optical color-switching by adding two different optical colorants, black and yellow, in each jetting solution. Other parameters such as particle suspension media, display device, magnetophoretic force were also considered throughout the experiments.

5.2. Experimental Methods

5.2.1. Materials

Poly(lactide-co-glycolide) (PLGA) with a lactide:glycolide ratio of 85:15 (Mw 50,000 – 75,000 g/mol), chloroform, N,N'-dimethylformamide (DMF), ethylene glycol, and Tween 20 and Tween 80 were obtained from Sigma-Aldrich, USA. Color pigments, carbon black and yellow dye (high strength opaque yellow 14) were purchased from General Carbon Company and GFS Chemicals, respectively. Magnetite (Fe_3O_4 nanocrystals in chloroform, 28nm) was obtained from Ocean NanoTech LLC. All reagents were used as received without further purification. Block magnets (4" x 1" x 1" and 2" x 1" x 1" thick, NdFeB) were products of K&J Magnetics, Inc.

5.2.2. Preparation of Bicolor-Coded Magnetic Microcylinders

Bicolor-coded magnetic microcylinders were prepared by modifying the precedent methods.[17] Two jetting solutions were first prepared by dissolving 35 w/v% of PLGA in a solvent mixture of chloroform and DMF (95 : 5, v/v) in each vial. While the

base polymer was PLGA in both compartments, yellow colorant and magnetite/carbon black were included in each solution to produce bicolor-coded magnetic microfibers. The polymer solutions were then separately pumped through a side-by-side dual capillary system (Nordson EFD, 23G) at a flow rate of 0.05 mL/h with a driving voltage of 10 kV. A flat piece of aluminum foil was used as a counter electrode. The distance between the capillary tip and the substrate was maintained in the range of 10 - 15 cm. The resulting fibers were collected and dried under vacuum for overnight to remove any residual solvents.

In order to make microcylinders, the obtained microfibers were solidified in a medium (Tissue-Tek O.C.T. Compound, Andwin Scientific, USA), mounted onto a cryostat chuck at -20 °C, and sectioned by a cryostat microtome (HM550 OMC, Microme) with a given length of 450 μm. The processed particles were then suspended in an aqueous solution containing 2 v/v% Tween 20 prior to use.

5.2.3. Preparation of Display Device

A given feature was drawn both on the double-sided tape and silicone (1/16" and 0.02" thick, McMaster Carr) using SolidWorks DWGeditor software. The tape and silicone were cut by printing the drawings in a vector mode via Epilog Zing 16 Laser. After a piece of double-sided tape was laminated onto a glass slide (bottom of the device, 25 x 75 x 1mm), the silicone (treated with a high frequency generator, Electro-Technic Products, Inc., Model BD-20) was attached on top of the double-sided tape. Likewise, another double-sided tape and silicone were added until reaching a height of 4 mm. The processed particles were suspended in a mixture of ethylene glycol and Tween 80 (2:1,

v/v), and loaded into the given geometries of each device until the particles fully cover the surface. Another glass slide with the double-sided tape was sealed to the top of the device. Finally, the inside of the feature was filled with the medium by injecting through the wall of device using a syringe and a needle.

5.3.   Results and Discussion

Our design of magnetic particles is shown in Figure 5-1A. First, black and yellow bicolor-coded microfibers were fabricated by EHD co-jetting. Magnetite, Fe_3O_4, was selected for the magnetic material and their surface was modified with oleic acid to enhance the solubility in organic solvent which was necessary for the jetting. The previously reported electrospun fiber sizes range from tens of nanometers to tens of micrometers.[19] However, in order to visually distinguish color changes by naked eyes, it was necessary to fabricate fibers with the resolution above 100 μm (ca. 50 μm for each compartment). Hence, we modified the typical procedure for preparing microfibers to increase their diameters suitable in this range. By increasing the concentration of polymer solutions as well as the size of capillaries, and by lowering the electrostatic charge, we successfully produced fibers with 250 μm in diameter (Figure 5-1B). After obtaining the fibers directly through EHD co-jetting process, these microfibers were again sectioned at a length of 500 μm to have highly monodisperse microcylinders with aspect ratio of 2 (Figure 5-1C).

Figure 5-2 depicts our device design. The device consists of silicone rubber with different patterns (i.e., 18 x 18mm square, 8 x 8 mm square of four, and the letters M and

UM), glass slides that were used for covering the silicone rubber from top and bottom, and the particles with appropriate media to keep the good particle dispersion.

Finally, in Figure 5-3A are displayed the rotational and translational motions of magnetic microcylinders that were demonstrated by manipulating magnetic field. S1 indicates a randomly positioned microcylinder where there is no magnet present. By approaching the magnet onto the top of the device (S1 → S2) while keeping the magnetic field parallel to the x direction, the microcylinder aligns to the x direction due to applied magnetic field (S2). Moreover, due to the potential energy difference between the magnetic and non-magnetic compartment of the microcylinder, the microcylinder rotates toward magnetic denser field lines (S2 → S3), resulting in optical black color as seen from the top view. This is more closely shown with zoomed-in images of the microcylinders placed in the square well of the device (Figure 5-3B). As the magnet approaches to the top of the device, randomly distributed microcylinders orient themselves toward magnetic denser field to display black color. In contrast, when the magnet is placed near the bottom of the device, the microcylinders rotate and translate almost perfectly so that the magnetic compartments (black) are facing the bottom, and thus, display yellow color. More examples of magnetic switching of these bicolor-coded microparticles are shown in Figure 5-4. The particle solutions were placed in several different geometries to demonstrate the applicability of these microparticles.

5.4. Summary

In summary, a novel type of bicolor-coded magnetic microparticles was fabricated for magnetophoretic display. The study performed in this chapter explored the efficacy of EHD co-jetting in the areas of particle-based displays. Furthermore, the microparticles utilized in this work have unique features of non-spherical shapes and visible colors, which can also suggest promising studies toward novel display system.

5.5. Figures and Tables
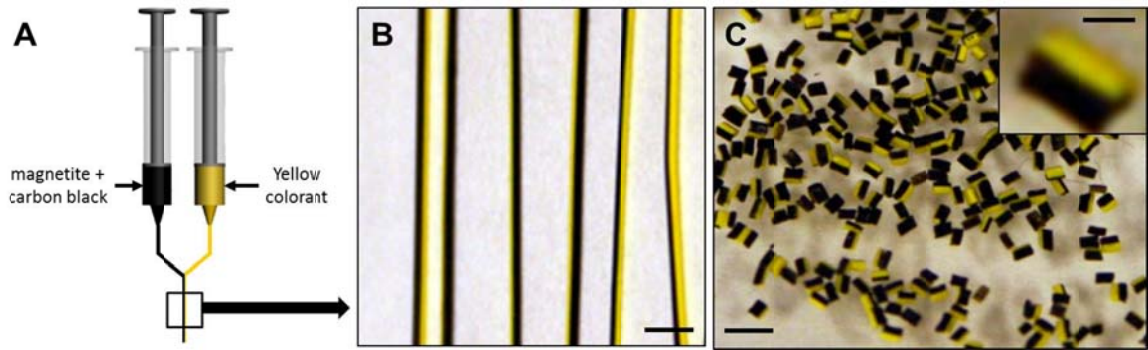
Figure 5-1. Fabrication of bicolor-coded magnetic microfibers. (A) EHD co-jetting setup of bicompartmental PLGA microfibers having yellow colorant and magnetite nanocrystals/carbon black in each compartment. (B, C) Photographs of the corresponding microfibers and microcylinders, respectively.
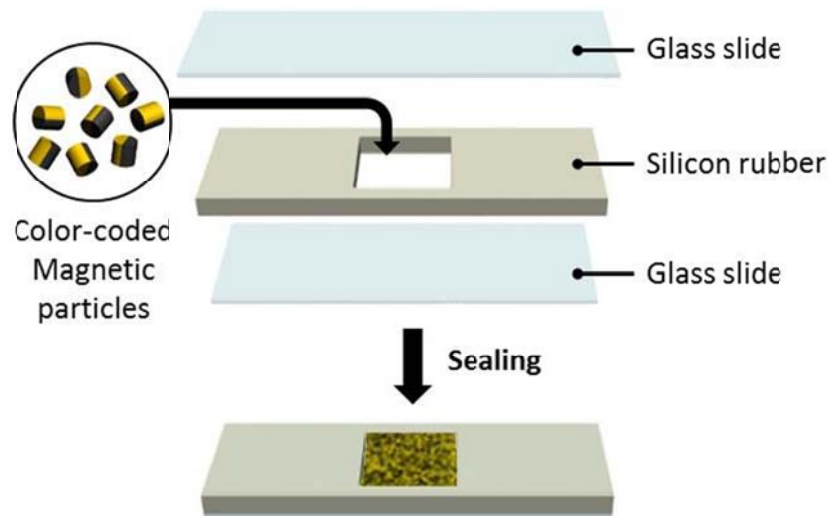
Figure 5-2. Preparation of Display Device. A specifically designed laser-cut silicone rubber (18 x 18 x 4 mm in this case) was sealed with microscope glass slides (25 x 75 x 1 mm) from both top and bottom, and filled with a viscous medium (ethylene glycol/Tween 80 = 2/1, v/v).
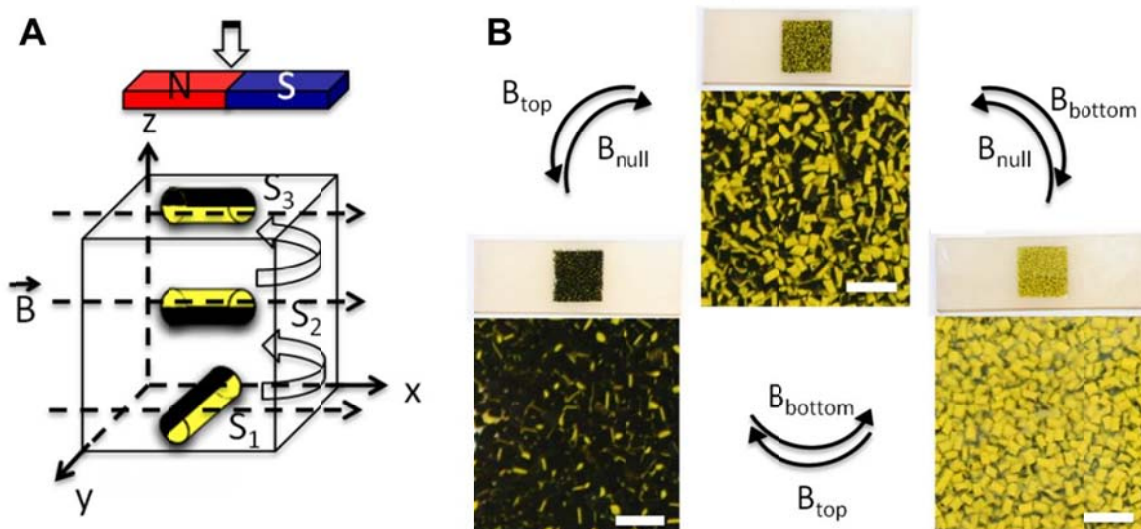
Figure 5-3. Rotational motion of bicompartmental magnetic microcylinders under the application of external magnetic field. (A) Scheme for the movement of the microcylinders with a magnet along the z direction. The direction of magnetic field is in x axis in all cases. S_1 indicates a random position of the particle in the absence of the magnet, S_2 denotes that the long axis of the microcylinder is followed by the magnetic field orientation, and S_3 signifies that the magnetic compartment eventually face toward the magnet due to magnetophoresis. (B) Photographs of color switching of the microcylinders in a device upon approaching a magnet. When there is no magnet present, the particles are randomly located (middle), whereas when the magnet is located either on top (left) or bottom (right) of the device, the microcylinders rotate toward magnetite-rich compartment.
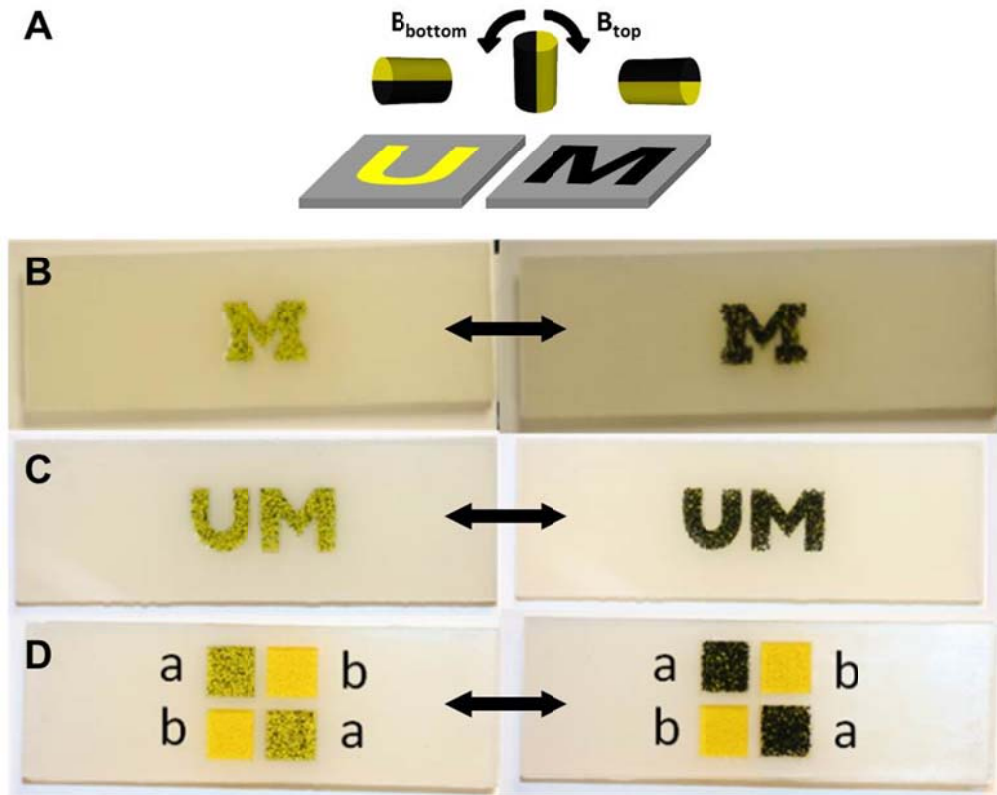
Figure 5-4. Various designs for device. (A) Scheme for color switching of the microcylinders with external magnetic field. (B-C) The letter designs where dimension of each letter, M and UM, is 10 (length) x 2 (thickness of channel) x 4 mm. Depending on the location of magnet, the reversible color changes occur between yellow (magnet on the bottom of the device) and black (magnet on the top of the device). (D) The checkerboard design (each well, 8 x 8 x 4 mm) has both yellow/black bicolored magnetic microcylinders (a) and yellow only microcylinders without magnetite (b) diagonally placed in each well as indicated. 50 – 300 mT magnetic fields are applied.

5.6. References

1.   Sheridon, N. Gyricon Materials for Flexible Displays. In *Flexible Flat Panel Displays*; John Wiley & Sons, Ltd: **2005**; pp 393-407.
2.   Chen, Y.; Au, J.; Kazlas, P.; Ritenour, A.; Gates, H.; McCreary, M. Electronic Paper: Flexible Active-Matrix Electronic Ink Display. *Nature* **2003**, 423, 136-136.
3.   Peng, B.; Meng, X.; Tang, F.; Ren, X.; Chen, D.; Ren, J. General Synthesis and Optical Properties of Monodisperse Multifunctional Metal-Ion-Doped Tio2 Hollow Particles. *The Journal of Physical Chemistry C* **2009**, 113, 20240-20245.
4.   Nisisako, T.; Torii, T.; Takahashi, T.; Takizawa, Y. Synthesis of Monodisperse Bicolored Janus Particles with Electrical Anisotropy Using a Microfluidic Co-Flow System. *Advanced Materials* **2006**, 18, 1152-1156.
5.   Nisisako, T.; Torii, T. Microfluidic Large-Scale Integration on a Chip for Mass Production of Monodisperse Droplets and Particles. *Lab on a Chip* **2008**, 8, 287-293.
6.   Kim, K. S.; Lee, J. Y.; Park, B. J.; Sung, J. H.; Chin, I.; Choi, H. J.; Lee, J. H. Synthesis and Characteristics of Microcapsules Containing Electrophoretic Particle Suspensions. *Colloid Polym Sci* **2006**, 284, 813-816.
7.   Werts, M. P. L.; Badila, M.; Brochon, C.; Hébraud, A.; Hadziioannou, G. Titanium Dioxide−Polymer Core–Shell Particles Dispersions as Electronic Inks for Electrophoretic Displays. *Chemistry of Materials* **2008**, 20, 1292-1298.
8.   Chen, C.-H.; Abate, A. R.; Lee, D.; Terentjev, E. M.; Weitz, D. A. Microfluidic Assembly of Magnetic Hydrogel Particles with Uniformly Anisotropic Structure. *Advanced Materials* **2009**, 21, 3201-3204.
9.   Yuet, K. P.; Hwang, D. K.; Haghgooie, R.; Doyle, P. S. Multifunctional Superparamagnetic Janus Particles. *Langmuir* **2009**, 26, 4281-4287.
10.   Yin, S.-N.; Wang, C.-F.; Yu, Z.-Y.; Wang, J.; Liu, S.-S.; Chen, S. Versatile Bifunctional Magnetic-Fluorescent Responsive Janus Supraballs Towards the Flexible Bead Display. *Advanced Materials* **2011**, 23, 2915-2919.
11.   Kim, S.-H.; Sim, J. Y.; Lim, J.-M.; Yang, S.-M. Magnetoresponsive Microparticles with Nanoscopic Surface Structures for Remote-Controlled Locomotion. *Angewandte Chemie International Edition* **2010**, 49, 3786-3790.
12.   Dendukuri, D.; Doyle, P. S. The Synthesis and Assembly of Polymeric Microparticles Using Microfluidics. *Advanced Materials* **2009**, 21, 4071-4086.
13.   Yan, J.; Bloom, M.; Bae, S. C.; Luijten, E.; Granick, S. Linking Synchronization to Self-Assembly Using Magnetic Janus Colloids. *Nature* **2012**, 491, 578-581.
14.   Dyab, A. K. F.; Ozmen, M.; Ersoz, M.; Paunov, V. N. Fabrication of Novel Anisotropic Magnetic Microparticles. *Journal of Materials Chemistry* **2009**, 19, 3475-3481.
15.   Hu, S.-H.; Gao, X. Nanocomposites with Spatially Separated Functionalities for Combined Imaging and Magnetolytic Therapy. *Journal of the American Chemical Society* **2010**, 132, 7234-7237.
16.   Teo, B. M.; Suh, S. K.; Hatton, T. A.; Ashokkumar, M.; Grieser, F. Sonochemical Synthesis of Magnetic Janus Nanoparticles. *Langmuir* **2010**, 27, 30-33.
17.   Bhaskar, S.; Hitt, J.; Chang, S.-W. L.; Lahann, J. Multicompartmental Microcylinders. *Angewandte Chemie International Edition* **2009**, 48, 4589-4593.
18.   Bhaskar, S.; Lahann, J. Microstructured Materials Based on Multicompartmental Fibers. *Journal of the American Chemical Society* **2009**, 131, 6650-6651.

19.   Bhardwaj, N.; Kundu, S. C. Electrospinning: A Fascinating Fiber Fabrication Technique. *Biotechnology Advances* **2010**, 28, 325-347.

CHAPTER 6

Current State and Future Directions

Although a wide range of anisotropic (e.g., non-spherical shapes, multiple surface functions, inner geometries) particles have been fabricated and we have successfully demonstrated a number of exciting applications so far, practical uses of these particles remain challenging. For instance, sufficiently reliable and reproducible data comes from the uniformity of particles. Therefore, it is not only important to fabricate nano- and microparticles with unique features, but it is also critical to develop defined synthetic methods with limited batch to batch variation that can lead to programmable and readily designable particles with reproducibility. Moreover, synthetic routes carrying substantial promise for larger scale production are required to further extend the potential of this emerging field at the crossroad of materials science and biotechnology.

6.1. Jetting Parameters

As EHD co-jetting deals with multiple polymer solutions to form particles or fibers,[1-3] it is often required to understand the relationship between jetting parameters (e.g., polymer, solvent, surface tension, conductivity, dielectric constant, flow rate, voltage, distance, collector, temperature, humidity) in order to produce a stable jet stream.

6.1.1. Dielectric Constant

Among various jetting parameters, the dielectric constant is one of the important variables to consider for a successful jetting system. The dielectric constant indicates the amount of charge stored in a material by an applied voltage, and is related to the polarity of a material. The dielectric constant is varied by the choice of polymer, solvent, and additives such as salts or surfactants. In fact, it has been demonstrated that adding an ionic surfactant during electrified jetting can result in the reduction of fiber diameters or particle sizes.[4,5] This occurs because as charged ions are incorporated into the jetting solution, the droplet accumulates more charges causing the surface to extend more with significantly reduced diameters.[4-6] Figure 6-1 demonstrates the effect of hexadecyltrimethylammonium bromide (CTAB), a cationic surfactant, on the size of particles. PLGA particles were prepared with and without CTAB and it was clearly shown that the particles with higher CTAB content had much smaller diameters (particle sizes reduced from 10-20 μm to ~200 nm).

We often encounter an unstable Taylor cone when two (or more) different polymers are co-jetted. This can also be explained by the imbalance of the dielectric constants of the polymer solutions in each compartment. As the dielectric constant is mainly determined by the type of polymer and solvent used, it is important to match the two values in a similar range so that the two solutions eject at the same voltage. Figure 6-2 displays bicompartmental PLGA, PLGA/PLCL, and PLCL fibers prepared through EHD co-jetting. The typical solvents used for PLGA fibers are chloroform (ε = 4.81 @ 20°C) and DMF (ε = 37 @ 25°C) (95:5, v/v), and the voltage is 10~11 kV (Figure 6-2A). When PLCL was jetted with the same solvent system, however, it required much lower

voltage (~ 5kV) to eject the solution. In these conditions, it is difficult to co-jet PLGA and PLCL using dual capillaries, because the two solutions will react at the different voltages, which will results in jet splitting. Thus, in order to jet PLCL at the higher voltage, one possible way is to add a solvent that has lower dielectric constant. Introducing cyclohexane (ε = 2.02 @ 20°C), for instance, lowers its overall dielectric constant, and enables PLCL to be jetted in a similar voltage range as PLGA (Figure 6-2C). Once we were able to optimize PLCL jetting simply by changing the solvents used, we then tried to jet bicompartmental PLGA/PLCL fibers and were successful in co-jetting the two polymers (Figure 6-2B). Although there are other parameters which considerably influence the jetting process, the dielectric constant can be easily augmented and corrected with solvent selection, and will certainly be a useful tool for selecting polymers and solvents for future EHD co-jetting.

6.1.2. Humidity

Besides solution parameters (e.g., polymer concentration, molecular weight, solvent, surface tension, and conductivity) and processing parameters (e.g., voltage, flow rate, ground collector, and distance), ambient parameters such as temperature and humidity also play a critical role in EHD co-jetting. For example, jetting at high temperatures may result in highly porous particles and fibers due to the fast evaporation of solvents.[7]

Apart from the temperature effect, jetting may be significantly affected by humidity. Our previous studies have proven that when the humidity was too low (<< 20%), the particle morphology became non-uniform. Examples of a change in particle

morphologies under different humidity conditions are presented in Figure 6-3. PMMA particles that were jetted at a humidity of 35 - 40 % resulted in a uniform, spherical shape, whereas particles jetted under much lower humidity (10 - 15 %) created non-uniform shapes. The particles shown are preliminary data from the work described in Chapter 3, prepared with the same experimental procedure. Of course an ideal solution would be a temperature- and humidity-controlled lab, which can automatically report and adjust ambient conditions to the desired settings. Alternatively, we have fabricated a humidity-controlled jetting chamber that can easily manipulate humidity. The photograph in Figure 6-4 depicts the new jetting chamber that has a simple humidifier next to a jetting set-up, and is sealed tightly with a wall unit. Thus, the chamber introduced here may offer a versatile method to optimize environmental variables for the current jetting system.

6.2. Control of Monodispersity

6.2.1. Fractionation

One of the limitations of EHD co-jetting is the broad distribution of size and shape of directly jetted particles. Once particles are collected from the jetting collector, the samples require separation based on size prior to their applications. As the uniformity of anisotropic particles significantly determines the applicability, many research groups are striving to produce particles with well-defined size and shape. Although in-depth investigations of the jetting parameters may help regulate the obtained particles and fibers, it is crucial to establish new ways to fractionate the obtained particles.

So far, the fractionation methods employed in our group include membrane filtration and centrifugal separation. Membrane filtration utilizes a porous barrier to separate particles based on their size. When particles with a mixture of sizes are flown through the porous membrane, particles that are smaller than the pores pass through the membrane while the larger ones remain on top. Since there are no harsh processing steps involved, this method is useful when handling delicate materials. However, the separation of non-spherical materials such as cylinders or rods can be problematic when using this method.

Alternatively, centrifugation allows suspended particles to be separated into fractions of different sizes. Through a sequential increase of gravitational force or centrifugation time, larger particles sediment faster than smaller particles, and thus a particle suspension can be separated into pellets and supernatant. By a series of pelleting steps, the supernatant can be further centrifuged to separate smaller particles (Figure 6-5). There may be more accurate and precise ways to fractionate particles. For example, we can pass particles through microchannels that can sort the particles with respect to size and shape. If the particles are comprised of electric or magnetic materials, the fractionation may be improved by the addition of external fields.

6.2.2. Sectioning

One of the synthetic methods to build highly monodisperse particles developed in our group is the use of a cryostat microtome to produce microcylinders.[3] Thanks to the consistent diameters of fibers produced through EHD co-jetting, well-defined microcylinders were created with the aid of the sectioning process. Its advantage lies in

the ability to freely control the length of the processed microcylinders, and hence the aspect ratio can be easily manipulated by changing the section thickness. To date, we have reported multicompartmental microcylinders with diverse length scales by using this method.[3,8,9] However, one of the limitations of using the cryostat microtome is that the typical section thickness ranges from 5 μm to 250 μm. This is a potential issue if one needs to process nanoscale particles.

Other options may involve ultramicrotome, which is widely used to prepare samples for transmission electron microscopy (TEM). It allows highly thin sections from tens to hundreds of nanometers, and is capable of sectioning hard materials as it uses either a diamond- or a glass-cutter. The Whitesides group has reported a method called 'nanoskiving' to control nanostructures by using ultramicrotome technique.[10,11] However, the main hurdle for this technique is that the sample needs to be fixed in a rigid embedment (e.g., epoxy resin), which is hard to remove afterwards. Soft materials such as polymers may be severely damaged or otherwise altered by the harsh etching processes required to remove such embedments. Therefore, such sectioning technique by ultramicrotome may be limited in scope.

6.3. Toward Smart Systems

With the novel fabrication methods discussed in the previous chapters, it is now possible to introduce different types of polymers into pre-defined multicompartmental particles. What we need is the development of a more diverse particle system (e.g., stimuli-responsive, bio-active) for potential applications.

6.3.1. Particles with Higher Anisotropy

The anisotropic character of the obtained particles fabricated through EHD co-jetting generally relies on the needle configuration used. The choice of the position of capillaries allows for tailoring both inner geometries and surface area. So far, we have explored side-by-side and pie-shape configurations with up to 7 different compartments. As a next step, the incorporation of a higher number of polymer solutions in a more controlled manner may be considered. For instance, the combination of microfluidic devices with our current jetting system may provide another way of generating complex anisotropic particles.

Furthermore, the impact of topology on particles or fibers may be investigated as it has the potential to mimic structures in nature.[12] The effect of topography on surfaces has been largely studied, but there have not been many reports on three dimensional particles. The selective removal of the PEO compartments in PLGA/PEO tetracompartmental fibers could be a possible example (Figure 6-6). Moreover, adding a specific pattern (e.g., micropillars) onto the obtained particles may also be helpful in producing topology.

6.3.2. Stimuli-Responsive Particles

In chapter 2, we have explored temperature-driven shape-shifting. Recently, we also have found that the same particles can undergo shape-shifting in a boiling aqueous solution. As shown in Figure 6-7, PLGA microcylinders change their shape into spheres by simply stirring them in boiling 1 v/v% Tween 20/DI water solution. This study was further expanded to perform shape-shifting in different pH buffer solutions or aqueous

surfactant solutions. The result showed particles having a variety of pore sizes and structures, with the buckyball-like (Figures 6-7A – 6-7C) and sponge-like (Figures 6-7D – 6-7F) being the most intriguing.

Likewise, we can also tailor particles to respond to other types of stimuli such as solvent or light by incorporation of the corresponding responsive materials. Additionally, the reversibly reconfigurable particles may have the ability to self-repair.[3] Individual control over surface or bulk properties of each compartment allows particles to have different chemical and physical properties which can be used for future reconfigurable system.

6.3.3. Bio-Responsive Particles

Particles that can either promote or inhibit the attachment of biomolecules are of significant as they can selectively guide cell behavior.[13-15] So far, we have introduced various surface modification methods (e.g., click chemistry, aldehyde-hydrazide, EDC coupling, hydrolysis) to enhance the binding affinities of cells.[16,17]

One potential example includes anisotropic particles or fibers containing reactive sites (e.g., bromide end groups) for atom transfer radical polymerization (ATRP). As seen from Figure 6-8, alkyne-functionalized PLGA microfibers underwent a click reaction with a linker that has an ATRP initiator to serially grow oligo(ethyleneglycol) methacrylate (OEGMA) brushes. While this work has already demonstrated its potential in controlling the bending of microstructures,[9] we can also utilize the selectively grown PEGMA brushes as a protein or cell repellent. With the proper selection of a polymer matrix (or a linker) and brush length, the applications are unlimited.

Additionally, microstructures that have binding affinity for carbohydrates are also widely studied.[18] The interactions between carbohydrates and biologically active systems play an important role in understanding cell surface interactions, and can be utilized for various applications such as biosensors, scaffolds, or drug delivery carriers. This can be investigated by incorporating lectin-carbohydrate interactions. Lectins are well-known carbohydrate recognizing proteins, which show reversible and site-specific binding behavior. In a previous study, we have successfully immobilized 2α-mannobiose on a microcontact printed surface and confirmed the presence of mannobiose by coupling with concanavalin A (Con A, mannose-specific lectin).[18] Similarly, we can expand this work to microcylinders. Bicompartmental PLGA microcylinders with hydrazide groups and alkyne groups in separate compartments were proven to selectively immobilize two different carbohydrates on half surfaces (Figure 6-9). The oxidation of mannobiose results in free aldehyde groups, which can further react with the hydrazide groups, and azide-functionalized galactose was simply bound to the alkyne groups by click chemistry. Furthermore, the two carbohydrates on the microcylinders, mannobiose and galactose, were confirmed by binding with site-specific lectins, Con A and peanut agglutinin (PNA), respectively. While the current results are an initial step and were more focused on the synthesis of functional polymers, further investigations will certainly foster a new particle system with rapid and highly sensitive detection of carbohydrate-based molecules.

6.3.4. Tailoring Mechanical Property

When particle or fibers are made of two or more blended polymers, phase segregated domains may be found in the same particle, and this can cause unequal

properties that are difficult to manipulate. EHD co-jetting, which is different from blending of different polymer solutions, can produce fibers (or particles) that are composed of multiple polymers with variant mechanical properties separately placed in each compartment. In this way, the mechanical properties (e.g., elastic modulus or stress/strain at break) of resulting fibers can be simply tuned by adjusting the number of inner compartments with either brittle or elastic materials. Figure 6-10 shows tetracompartmental PLGA/PLCL microfibers comprised of different ratios between compartments composed of either PLGA or PLCL. Through tensile testing of single fibers with a diameter of 20 μm, it was unambiguously proved that the elasticity of microfibers at rupture was simply enhanced by the addition of PLCL compartments. Moreover, when microfibers with anisotropic mechanical property were stretched, unique helical structures were obtained suggesting a novel type of reconfigurable system.

6.4. Future Outlook

So far, novel methods to engineer soft adaptive structures to respond to environmental stimuli have been introduced. As a next step, we need to exploit these multifunctional stimuli-responsive particles in more practical and realistic approach. For example, when mimicking microstructures in nature, the particles should have biological and physiological responses that are similar to the nature's particles. The interactions between the particles and immune system are also considered as an important factor in engineering soft tissues or drug delivery platforms. The physiochemical properties of the particles can be further investigated by studying various parameters such as particle size,

surface charge, biocompatibility, degradation rate, or hydrophobicity/hydrophilicity. In addition, the establishment of standardized characterization method (e.g., cell-based assays) may be helpful in analyzing the obtained particle systems. Consequently, particles that are capable of mimicking cellular microenvironment will enable the full usage of their adaptive properties in biosensors, drug delivery, artificial muscles, or soft electronics.

Moreover, the development of computational models of the shape-shifted particles (discussed in Chapter 2) may help predict their self-assembled structures. Not only can we create particles with anisotropic shapes and functionalities, our particles are now capable of reconfiguring themselves upon external stimuli. The self-assembled structures of these reconfigurable particles are unique because they have different interacting sites from conventional spherical particles, and their packing behavior may be manipulated by environmental perturbation. Thus, if we could demonstrate the relationship between the building blocks (reconfigurable particles) and their assembled structures through both theoretical and experimental aspects, we may further have control over the macroscopic properties of the system.
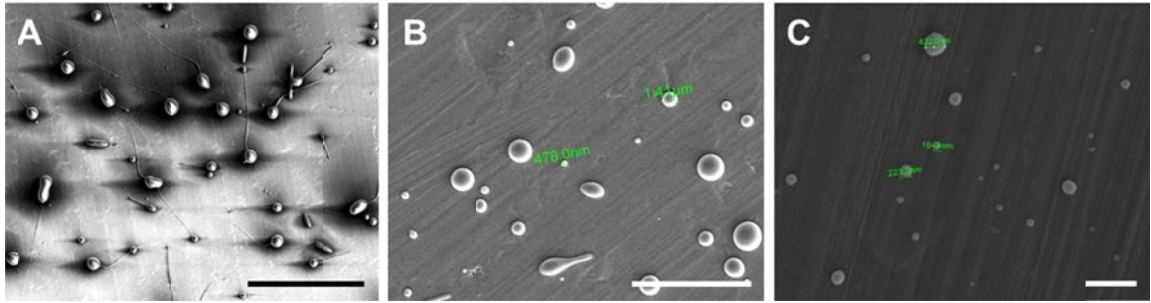
6.5. Figures and Tables

Figure 6-1. The effect of hexadecyltrimethylammonium bromide (CTAB) on the size reduction of bicompartmental PLGA particles (10 w/v% PLGA (50:50, 5-15 kDa), Chloroform : DMF = 95 :5 (v/v)) (A) No CTAB. (B) 0.1 w/v% CTAB. (C) 1 w/v% CTAB. Scale bars are 100 μm, 20 μm, and 1 μm, respectively.
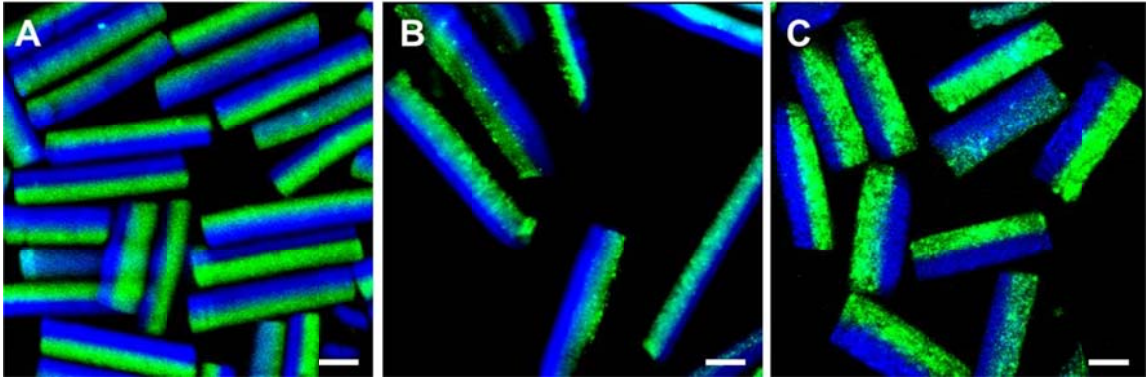
Figure 6-2. CLSM images of the incorporation of two entirely different polymers in one jetting system, and represent preliminary data from the work described in Chapter 4. (A) PLGA (30 w/v%, chloroform : DMF (95:5, v/v) in both compartments. (B) PLGA (blue, 30 w/v%, chloroform : DMF (95:5, v/v)) and PLCL (green, 25 w/v%, chloroform : cyclohexane : DMF, 45:50:5, v/v/v) on each compartment. (C) PLCL (25 w/v%, chloroform : cyclohexane : DMF (45:50:5, v/v/v)) on both compartments. Scale bars are all 20 μm.
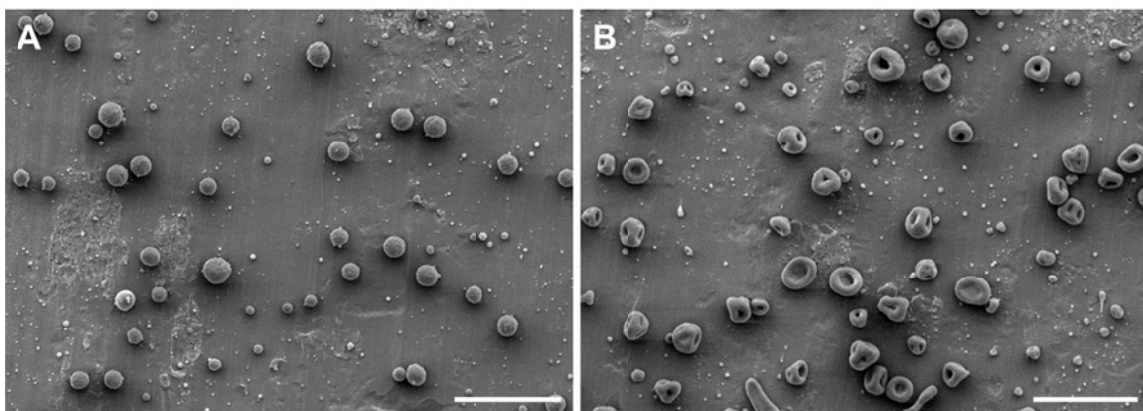
Figure 6-3. The effect of humidity on particle morphology. The particles shown are preliminary data from the work described in Chapter 3. All particles are jetted under the same condition (3 w/v% PMMA in the solvent mixture of THF, DMF, and AK-225 (50:45:5, v/v/v)) other than humidity. (A) 35 – 40 % humidity. (B) 10 – 15 % humidity. All scale bars are 10 μm.
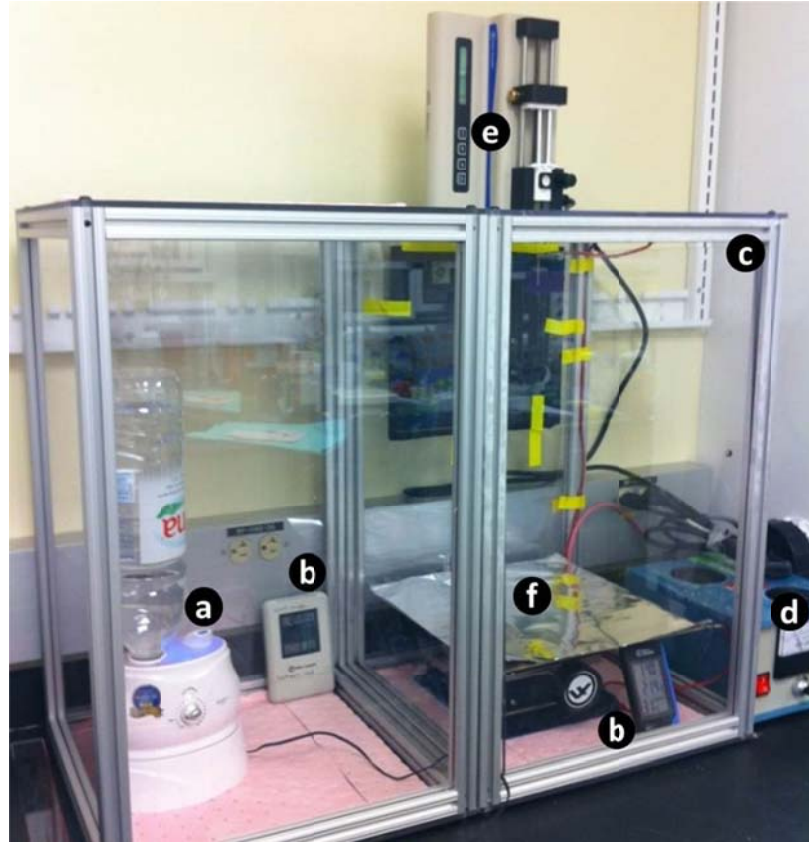
Figure 6-4. Photograph of a humidity-controlled jetting chamber that is comprised of a humidifier (a), humidity/temperature reader (b), wall units for sealing (c), voltage (d), pump (e), and ground collector (f).
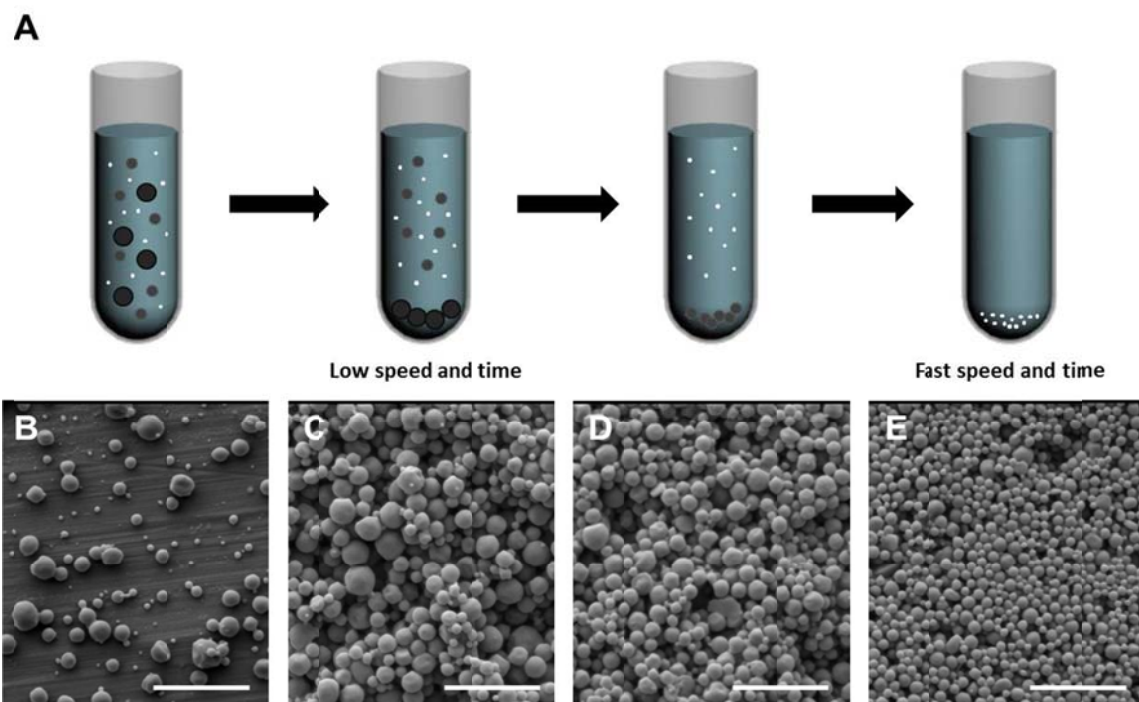
Figure 6-5. Centrifugal separation of particles from a mixture of different sizes. (A) Scheme showing basic principles of centrifugal separation, (B) As-jetted particles, (C-E) The particles obtained after centrifugation with 2000 rpm for 5min, 4000 rpm for 5min, and 4000 rpm for 15 min, respectively. All scale bars are 5 μm.
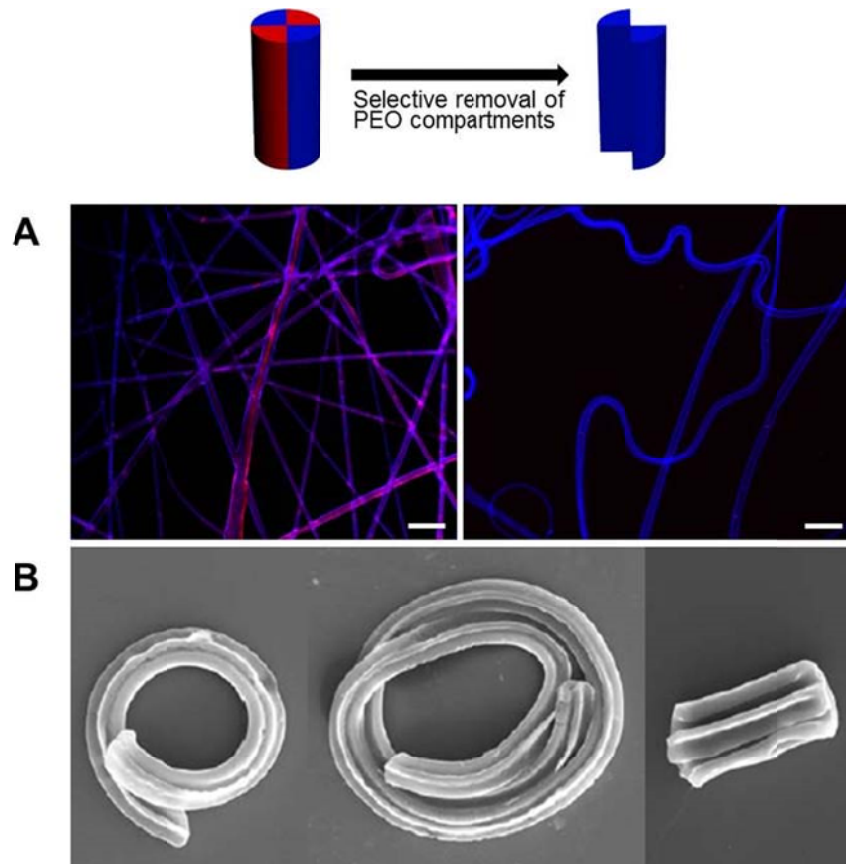
Figure 6-6. Tetracompartmental PLGA/PEO microfibers after the selective removal of PEO compartments. (A) CLSM images of the microfibers before (left) and after (right) dissolving the PEO (red) in an aqueous solution. (B) SEM images of a unique texture created on the microfibers after the removal of PEO.
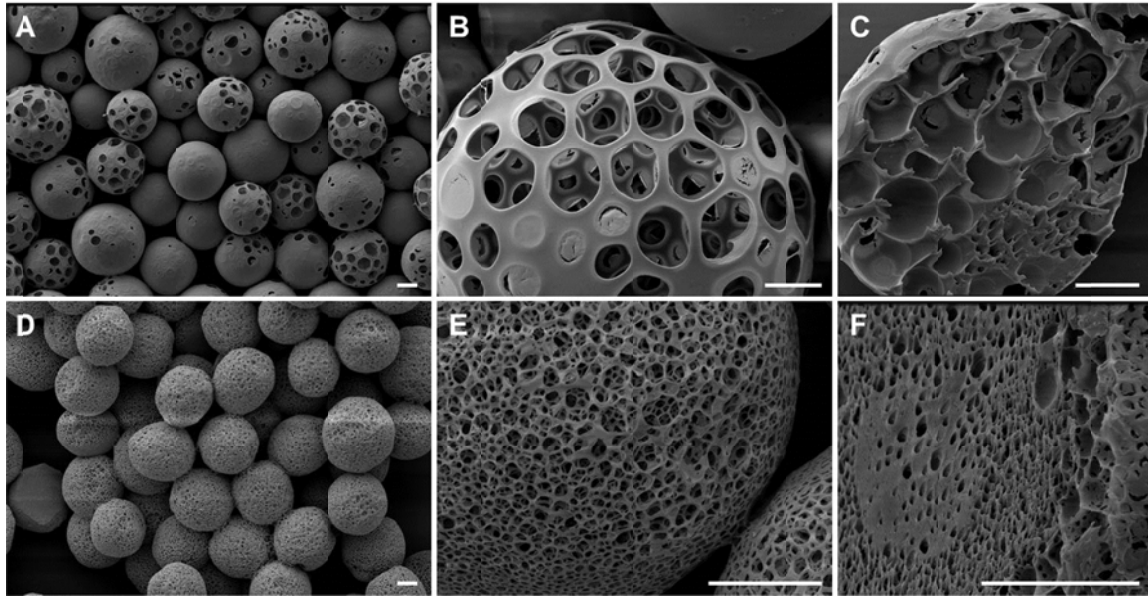
Figure 6-7. Shape-shifting of PLGA microcylinders (20 µm in diameter x 70 µm in length) into porous microspheres in a boiling aqueous solution. (A-C) The microcylinders after stirring in boiling 1 v/v% Tween 20/DI water for 2 min. B is a zoomed-in image of A, and C is a cross-sectional view of B. (D-F) The microcylinders after stirring in boiling 1 v/v% Tween 20/DI water at pH 10 for 5 min. E is a zoomed-in image of D, and F is a cross-sectional view of E. Scale bars are all 10 µm.
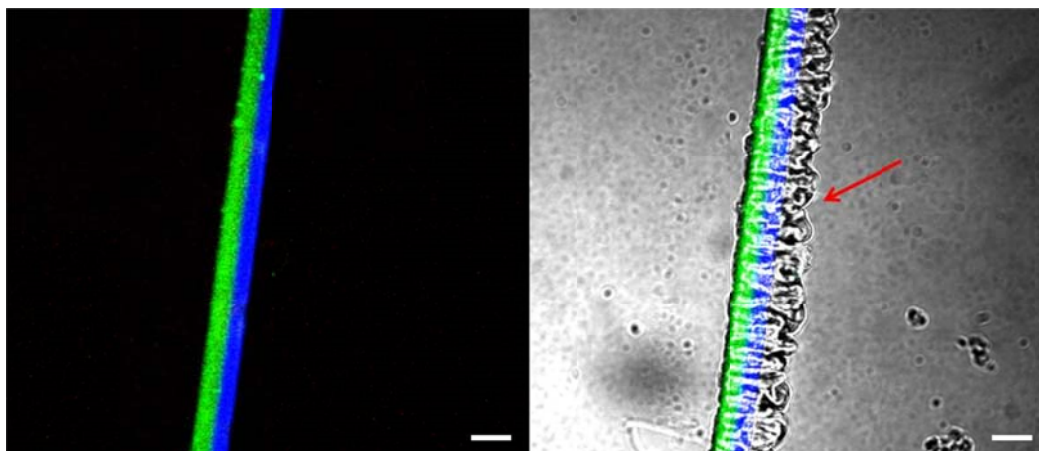
Figure 6-8. CLSM images of the selective growth of PEGMA brushes (where the red arrow is pointing) on alkyne-functionalized bicompartmental PLGA microfibers via ATRP for 1 hr. Scale bars are all 20 μm.
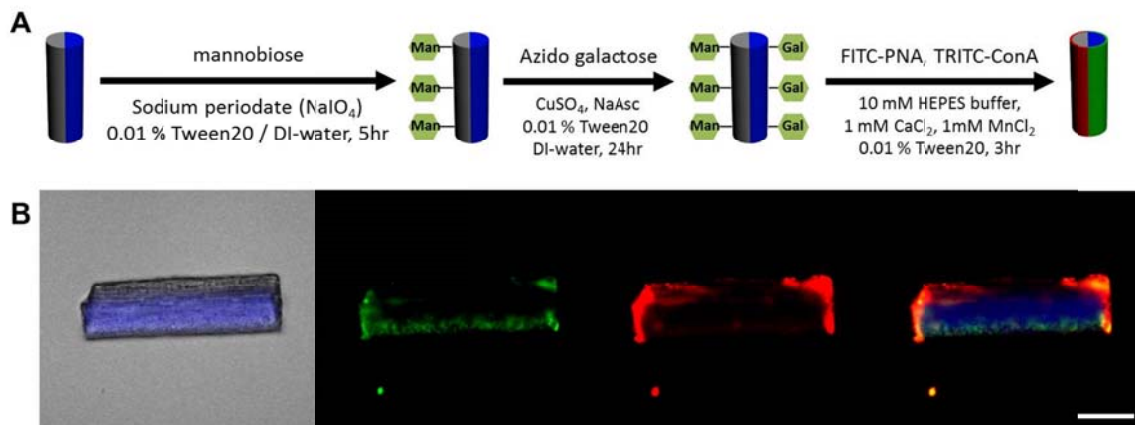
Figure 6-9. Bicompartmental PLGA microcylinders having alkyne and hydrazide groups in each side. Two different functional groups are used for the selective immobilization of mannobiose (hydrazide – aldehyde) and galactose (alkyne – azide), respectively. (A) The scheme showing selective surface modification of each compartment with two different carbohydrates bound with specific lectins (i.e., mannobiose – ConA and galactose – PNA). (B) CLSM images of the microcylinder displaying lectin-carbohydrate recognitions. The green and red fluorescence indicate successful binding of PNA with galactose, and the binding of ConA with mannobiose, respectively. Scale bar is 20 μm.
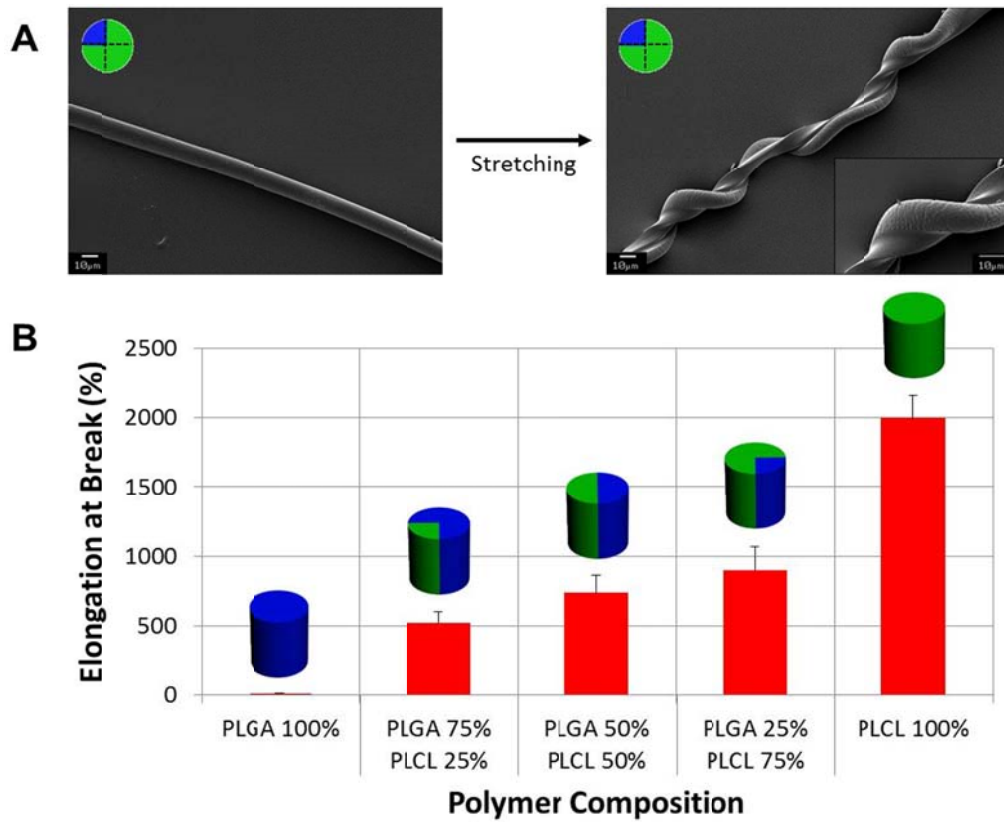
Figure 6-10. Mechanical tests of multicompartmental PLGA/PLCL fibers. (A) SEM images before and after stretching of tetracompartmental PLGA/PLCL fibers. (B) Elongation at break for fibers of various polymer compositions, measured by pulling each fiber to rupture.

6.6. References

1. Roh, K.-H.; Martin, D. C.; Lahann, J. Triphasic Nanocolloids. *Journal of the American Chemical Society* **2006**, 128, 6796-6797.
2. Bhaskar, S.; Lahann, J. Microstructured Materials Based on Multicompartmental Fibers. *Journal of the American Chemical Society* **2009**, 131, 6650-6651.
3. Lee, K. J.; Yoon, J.; Rahmani, S.; Hwang, S.; Bhaskar, S.; Mitragotri, S.; Lahann, J. Spontaneous Shape Reconfigurations in Multicompartmental Microcylinders. *Proceedings of the National Academy of Sciences* **2012**, 109, 16057-16062.
4. Xie, J.; Lim, L. K.; Phua, Y.; Hua, J.; Wang, C.-H. Electrohydrodynamic Atomization for Biodegradable Polymeric Particle Production. *Journal of Colloid and Interface Science* **2006**, 302, 103-112.
5. Chen, Y.-z.; Zhang, Z.-p.; Yu, J.; Guo, Z.-X. Poly(Methyl Methacrylate)/Silica Nanocomposite Fibers by Electrospinning. *Journal of Polymer Science Part B: Polymer Physics* **2009**, 47, 1211-1218.
6. Greiner, A.; Wendorff, J. H. Electrospinning: A Fascinating Method for the Preparation of Ultrathin Fibers. *Angewandte Chemie International Edition* **2007**, 46, 5670-5703.
7. Bhardwaj, N.; Kundu, S. C. Electrospinning: A Fascinating Fiber Fabrication Technique. *Biotechnology Advances* **2010**, 28, 325-347.
8. Bhaskar, S.; Hitt, J.; Chang, S.-W. L.; Lahann, J. Multicompartmental Microcylinders. *Angewandte Chemie International Edition* **2009**, 48, 4589-4593.
9. Saha, S.; Copic, D.; Bhaskar, S.; Clay, N.; Donini, A.; Hart, A. J.; Lahann, J. Chemically Controlled Bending of Compositionally Anisotropic Microcylinders. *Angewandte Chemie International Edition* **2012**, 51, 660-665.
10. Xu, Q.; Rioux, R. M.; Dickey, M. D.; Whitesides, G. M. Nanoskiving: A New Method to Produce Arrays of Nanostructures. *Accounts of Chemical Research* **2008**, 41, 1566-1577.
11. Lipomi, D. J.; Martinez, R. V.; Whitesides, G. M. Use of Thin Sectioning (Nanoskiving) to Fabricate Nanostructures for Electronic and Optical Applications. *Angewandte Chemie International Edition* **2011**, 50, 8566-8583.
12. Tawfick, S.; De Volder, M.; Copic, D.; Park, S. J.; Oliver, C. R.; Polsen, E. S.; Roberts, M. J.; Hart, A. J. Engineering of Micro- and Nanostructured Surfaces with Anisotropic Geometries and Properties. *Advanced Materials* **2012**, 24, 1628-1674.
13. Stevens, M. M.; George, J. H. Exploring and Engineering the Cell Surface Interface. *Science* **2005**, 310, 1135-1138.
14. Discher, D. E.; Janmey, P.; Wang, Y.-l. Tissue Cells Feel and Respond to the Stiffness of Their Substrate. *Science* **2005**, 310, 1139-1143.
15. Mitragotri, S.; Lahann, J. Physical Approaches to Biomaterial Design. *Nat Mater* **2009**, 8, 15-23.
16. Deng, X.; Eyster, T. W.; Elkasabi, Y.; Lahann, J. Bio-Orthogonal Polymer Coatings for Co-Presentation of Biomolecules. *Macromolecular Rapid Communications* **2012**, 33, 640-645.
17. Mandal, S.; Bhaskar, S.; Lahann, J. Micropatterned Fiber Scaffolds for Spatially Controlled Cell Adhesion. *Macromolecular Rapid Communications* **2009**, 30, 1638-1644.

18.   Nandivada, H.; Chen, H.-Y.; Lahann, J. Vapor-Based Synthesis of Poly[(4-Formyl-P-Xylylene)-Co-(P-Xylylene)] and Its Use for Biomimetic Surface Modifications. *Macromolecular Rapid Communications* **2005**, 26, 1794-1799.

APPENDIX

Theoretical Models of Selective Shape-Shifting

In Chapter 2, the changes in particle morphologies of the experimentally obtained shape-shifted particles were compared with that of the theoretical models. Here, the selective shape-shifting of bicompartmental microcylinders was studied.

The theoretical models of bicompartmental microcylinders were created through Surface Evolver software. In this model, two separate rectangular boxes were defined as body 1 and body 2 representing each compartment, with one face touching each other (from now on, face X will refer to this interface). First, the vertices and edges that are defining the face X were constrained to lie in the plane z = 0. The rest of the facets in the body 1 and body 2 were set to have surface tension of PMMA (γ_{PMMA} = 35.4 mN/m) and PLGA (γ_{PLGA} = 50 mN/m), respectively. Next, the interfacial energy between the two bodies was estimated by using the Owens-Wendt approach.[1]

$$\gamma_{12} = \left[(\gamma_1^d)^{1/2} + (\gamma_2^d)^{1/2}\right]^2 + \left[(\gamma_1^p)^{1/2} + (\gamma_2^p)^{1/2}\right]^2 \tag{1}$$

Here γ_1^d and γ_2^d are the dispersive components of the surface tension of substances 1 and 2, while γ_1^p, and γ_2^p are the polar components of the surface tension of substances 1 and 2.

Thus, in the case of PLGA (γ_{PLGA}^d = 37 mN/m, γ_{PLGA}^p = 13 mN/m) and PMMA

(γ_{PMMA}^d = 26.2 mN/m, γ_{PMMA}^p = 9.2 mN/m) of which γ_1 and γ_2 are known, we can

estimate the interfacial energy between PLGA and PMMA as 1.257 mN/m. Upon running

the software, the Surface Evolver seeks the optimal scale factor to minimize energy by

iterations and refinements, which means we can continue evolving the objects as long as

there is enough memory and time. Figure A-1 displays the equilibrium envelopes of the

PLGA/PMMA microcylinder (A-D) with increasing number of iterations and refinements.

From the intermediate state C, it is clear that the PLGA compartment evolved more than

the PMMA compartment due to the higher surface tension of PLGA. For comparison,

PLGA/PTFE microcylinder (E-H) was also evolved, and after a number of runs, the two

compartments showed a dramatic difference in shapes. (The known values for the surface

energy of PTFE are γ_{PTFE}^d = 1.5 mN/m, γ_{PTFE}^p = 12.5 mN/m, and γ_{PTFE} = 14 mN/m, and

from the Eq. (1), we get the interfacial energy between PLGA and PTFE as 23.6 mN/m.)

However, the limitation associated with these models is that the Surface Evolver

does not take account of temperature effect. In reality, the PMMA compartment will not

evolve into a spherical shape even with multiple runs because our shape-shifting process

is depending on the Tg of polymers. In order to resemble the shape-shifted particles in

Chapter 2, the facets of the PMMA compartment were set to have surface tension of '0'

such that it was extraneous to the calculations and no external force (surface energy) was

affecting the shape of the body. While having other values such as the surface energy of

PLGA and the interfacial energy between PLGA and PMMA same as the previous model,

we obtained a new model (Figure A-2, top) that is more close to the experimental

obtained particles. Moreover, the effect of changes in the interfacial energy between the

two bodies on particle morphologies was simulated (Figure A-2, bottom), and we prepared PLGA/PTFE microcylinder with the interfacial energy of 23.6 mN/m. As the surface was simulated toward the minimal energy, the shape of the PLGA changed to a sphere, which was different form the PLGA/PMMA microcylinder where the PLGA evolved into a flattened shape. Here, we also need to note that the interfacial energy depends on the temperature, and there may be a mismatch of interfacial surface tension between the actual particles and theoretical models. Although further studies are needed to develop model systems that have more control over the temperature, the present work suggested that the changes in shapes of particles can be predicted by varying their surface tensions of the material used.

Reference

1. Owens, D. K.; Wendt, R. C. Estimation of the Surface Free Energy of Polymers. Journal of Applied Polymer Science 1969, 13, 1741-1747.
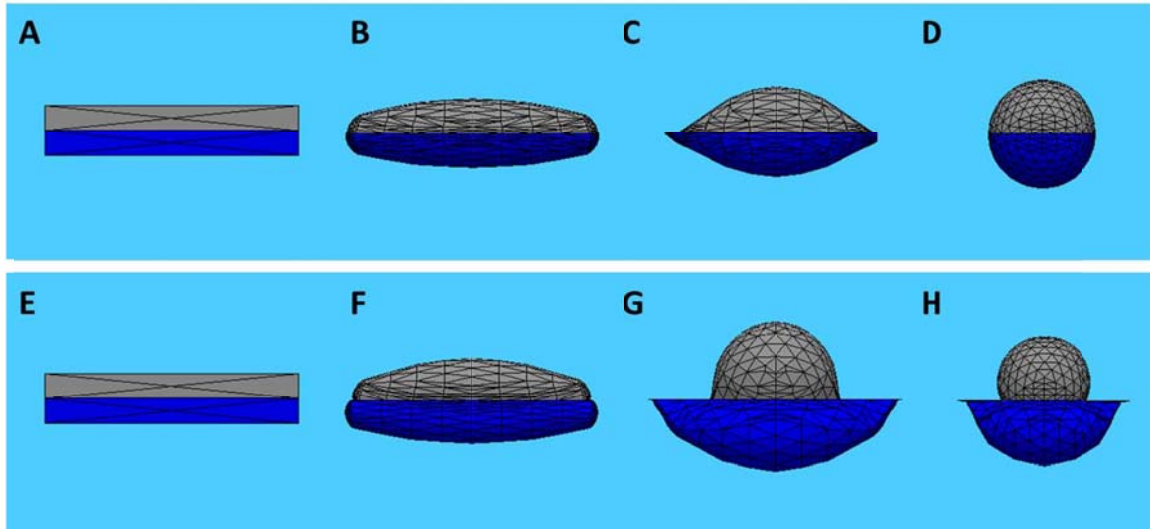
Figure A-1. The effect of surface tensions on the equilibrium morphology of bicompartmental microparticles after selective shape-shifting. The constraints were applied to the vertices and edges of the interface (face X) of the two bodies. A-D and E-H describe PLGA/PMMA, and PLGA/PTFE microcylinders, respectively, with increasing the number of interactions and refinements.
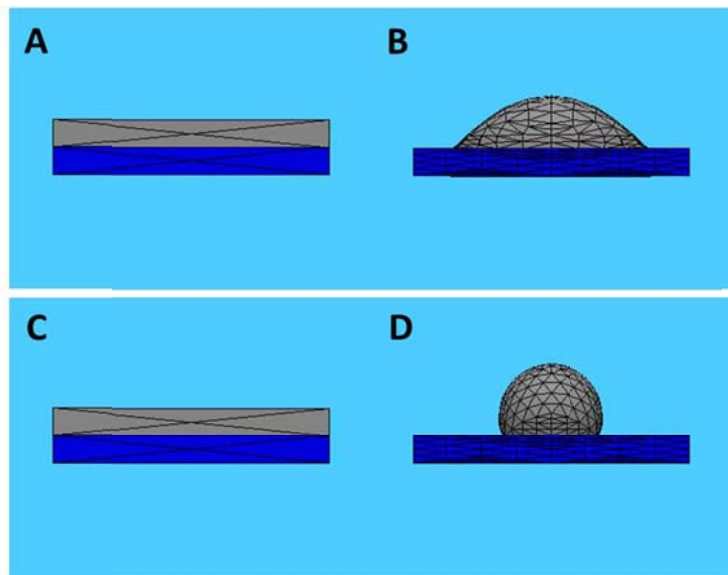

Figure A-2. Computational models of PLGA/PMMA and PLGA/PTFE bicompartmental microparticles before (A, C) and after (B, D) selective shape-shifting. Only one of the compartments (gray) was given with surface energy, and the interfacial tensions between the two compartments were varied from 1.257 mN/m to 23.6 mN/m. To demonstrate the effect of interfacial energy on the equilibrium shapes of each particle, the number of iterations and refinements were kept constant during the simulations.